PRODUCTION OF ACTIVATED CARBON FIBERS AND CARBON NANOTUBES FROM ION EXCHANGE RESINS

MSc RESEARCH DISSERTATION

Prepared by

Masedi Mmonatau (456653)

Submitted to:

School of Chemical and Metallurgical Engineering, Faculty of Engineering and the Built Environment, University of the Witwatersrand, Johannesburg, South Africa

Supervisor(s): Prof G. S. Simate and Prof S. Ndlovu

20 September 2018

DECLARATION

I, the undersigned, hereby declare that the work contained in this thesis is my own unaided original work. It is being submitted to the degree of Master of Science in Engineering to the University of Witwatersrand, Johannesburg, South Africa. I declare that I have not previously in its entirety or in any part submitted it for any other degree or examination in any university.

_____

Masedi M. M. Mmonatau

20 September 2018

ABSTRACT

Adsorption has proven to be successful in the recovery of metal ions from dilute solutions. It is a simple, effective, economical and versatile technique, and of late, activated carbon (AC) has been of great interest. The ACs are well known nano-porous carbonaceous materials which have received great attention in recent times due to their relatively high kinetics and adsorption capacity. AC is a universal adsorbent available in a variety of physical forms such as powdered activated carbon (PAC), granular activated carbon (GAC) and activated carbon fiber (ACF). The main structural difference between AC and ACF is in the smaller diameter of the pores in ACF; the ACF mainly have micropores allowing for a greater adsorption rate. For this reason, this study assessed the use of ion exchange resins in the production of ACF, in order to provide a probable solution in the disposal of ion exchange resins (IER). Furthermore, the production of carbon nanotubes (CNTs) from IER was investigated, as they too have unique electrical, mechanical, chemical and physical properties.

The ACF were synthesized by chemical activation conducted at varying temperatures between 600 ˚C and 1000 ˚C, and NaOH concentration between 8 and 40 wt%. The produced ACFs were characterized by nitrogen adsorption fitted to the Brunauer-Emmet-Teller (BET) equation, scanning electron microscopy (SEM), thermogravimetric analysis (TGA) and fourier transform infrared spectroscopy (FTIR). The BET analysis showed that mesoporous ACMs produced possessing pore sizes in the range of 2.29 to 20.06 nm. Thermally stable, microporous and mesoporous activated carbon fiber (ACF) with a maximum surface area of 217.41 m^2/g, were achieved from samples produced at an activation temperature of 800 ˚C using 40 wt% NaOH. The FTIR results showed that no functional groups were present on the ACF surface.

The produced CNTs were synthesized through chemical vapour deposition (CVD), in which iron was used as the catalyst and different catalyst supports were investigated (unsupported iron, magnesium oxide, aluminium oxide and calcium carbonate) using different carrier gases (nitrogen and argon). For the characterization of the synthesized CNTs, SEM, BET, TGA and Raman spectroscopy techniques were employed. The Raman spectroscopy showed development of single walled carbon nanotubes (SWCNTs) in the case where aluminium oxide was used as a support and multi walled carbon nanotubes (MWCNTs) for the rest of the other supports. The greatest surface area of 70.54 m^2/g was achieved by using calcium carbonate as a support and nitrogen as a carrier gas. The use of argon as a carrier gas yielded a greatest G band intensity of 1050.00 a.u, thus suggesting the greatest amount of amorphous carbon formed.

The ACF synthesized with 40 wt % NaOH at a temperature of 800 °C were used for the adsorption experiments. The ACF had a high initial adsorption rate, however, a low adsorption capacity of 0.62 mg/g. The adsorption isotherms indicated that the Langmuir model was a better fit in comparison to the Freundlich model, therefore suggesting that monolayer adsorption of platinum ions on the ACF occurred.

PUBLICATIONS

Conference Presentation – Poster

1. Production of activated carbon and activated carbon fiber from ion exchange resins. 1 – 3 August 2016. *SAIMM Hydrometallurgy 2016 conference, Sustainable Hydrometallurgical Extraction of Metals, Cape Town, South Africa.*

Journal Publication – Submitted for publication

1. Masedi M. M. Mmonatau, Geoffrey S. Simate, Sehliselo Ndlovu, Aoyi Ochieng, 2018. Synthesis and characterization of activated carbon fibers from ion exchange resins. *Chemical Engineering Journal.*

DEDICATION

To anyone who is constantly accepting the challenges offered by the universe in aspiration to grow into a better version of themselves and to those who have and/or who are contributing knowledge of any magnitude into conserving, preserving and making the world a better place.

ACKNOWLEDGEMENTS

My first note of thanks undoubtedly goes to my supervisors, Prof Geoffrey S. Simate and Prof Sehliselo Ndlovu for their continuous guidance, motivation and the knowledge that they have imparted unto me. I believe that my mind has been transformed by the numerous questions they have thrown my way in making this research more meaningful and shaping my writing.

I would also like to thank the National Research Foundation (NRF) of South Africa for funding this project, as well as The School of Chemical and Metallurgical Engineering and the School of Chemistry from the University of the Witwatersrand, this research would have not been possible without the facilities and guidance offered.

"Great works are performed not by strength but by perseverance." *-Samuel Johnson*

"Perseverance is the hard work you do after you get tired of doing the hard work you already did." *-Newt Gingrich*

More than anything, the writing of this dissertation has taught me to preserve, to endure, and that there are more opportunities than we could ever imagine, for this I thank my mentors John, Graeme and Brian for encouraging me and teaching me to see life in a positive light, always.

I am eternally thankful for my greatest and constant support system, my parents, Yvonne and Kagiso Rrerre Mmonatau, who add value and bring meaning to my life. My deepest gratitude is also extended to my friends and colleagues, Gaosi, Kamogelo, Tapiwa, Lyroyce, Ayo, Aliki, Alan, and Ike for their encouragement.

For all of this, God in all your grandeur, beauty, love and infinite intelligence, I thank you.

TABLE OF CONTENTS

LIST OF FIGURES

LIST OF TABLES

1

INTRODUCTION

1.1 GENERAL INTRODUCTION

The platinum group metals (PGMs) are 6 precious metals comprising of palladium (Pd), platinum (Pt), rhodium (Rd), iridium (Ir), ruthenium (Ru) and osmium (Os). Of these PGMs, platinum and palladium are the most abundant and have the highest economic importance. Furthermore, these two metals are currently used as investment commodities (Fujiwara et al., 2007; Mavhungu et al., 2013). These metals are known for their extraordinary physical and chemical properties such as high resistance to corrosion, tarnishing and degradative effects of chemical attack. In academia and industry, these metals have gained popularity for their stable electrode properties, excellent catalytic properties and very high melting points (Jones, 2005; Mavhungu et al., 2013). Due to these unique properties, aforementioned metals have immense technological importance (Nikoloski and Ang, 2014) making them essential for numerous modern day industrial applications (Jones, 2005).

Platinum is used for numerous applications such as production of jewelry, fuel cells and as a catalysts driving several chemical processes. Platinum's contribution in the reduction of

greenhouse gases as an emission control catalysts in automobile exhaust systems cannot be overemphasized (Jones, 2005; Nikoloski and Ang, 2014). Table 1.1 indicates the yearly supply, demand and amount of platinum recovered through recycling from 2014 to 2016.

Table 1.1: The supply and demand for platinum from 2014 – 2016 (Matthey, 2016).

PLATINUM SUPPLY AND DEMAND (tons)			
	Supply		
	2 014	**2 015**	**2 016**
South Africa	124 762	161 164	151 252
Russia	24 691	23 633	23 951
Others	30 723	29 524	32 875
Total Supply	**180 176**	**214 321**	**208 078**
	Gross Demand		
Autocatalyst	114 321	121 093	123 351
Jewellery	102 187	99 718	103 316
Industrial	61 905	61 693	67 690
Investment	9 771	15 908	11 711
Total Gross Demand	**288 183**	**298 413**	**306 067**
Recycling	-73 051	-60 847	-67 619
Total Net Demand	**215 132**	**237 566**	**238 448**
Movement in stock	-34 956	-23 245	-30 370

As can be seen from Table 1.1, the total gross demand of platinum is rapidly growing and it increases on an annual basis, yet there is still a deficit in stock movement. The rise in demand of platinum in myriads of industries leads to intensive PGM mining from known deposits and expansion in the recovery of PGMs through recycling of the secondary raw materials such as automotive catalysts (Nikoloski and Ang, 2014). This study will focus on the recovery of platinum from dilute solutions in order to contribute in providing an additional solution in meeting platinum demands.

Whilst a number of techniques have proven to be successful in the recovery of platinum in concentrated solutions, adsorption has proven to be the most effective recovery technique in the recovery of metals in dilute solutions (Mavhungu et al., 2013). Recent studies have shown

that adsorption techniques are considered to be the most promising techniques for removal of contaminants and metals in solution because adsorption is a highly effective method with a simple design, and low investment costs (Barakat, 2011; Fujiwara et al., 2007; Kyzas and Kostoglou, 2014; Rashed, 2013). Thus a wide range of adsorbents have been investigated such as minerals, clays and waste materials (Sharma et al., 2009). Undoubtedly, over the years, the most common and widely used adsorbent has been activated carbon (AC) (Bhatnagar and Minocha, 2006; Sharma et al., 2009).

The AC, commonly termed as a universal adsorbent, exhibits a variety of physical forms such as granules known as granular activated carbon (GAC), powders known as powdered activated carbon (PAC), and fibers known as activated carbon fiber (ACF) (Al-Qodah and Shawabkah, 2009; Dyk and Doreen, 2000; Lozano-Castello et al., 2002; Osmond, 2000). As a result of its high porosity and great thermal stability, AC is mainly used on an industrial scale as an adsorbent in the purification and/or the separation of liquid and gases (Hesas et al., 2013; Sharififard et al., 2012; Suzuki, 1993; Yakout and Sharaf El-Deen, 2011), and as a catalyst to control nitrogen oxides (NOx) emission from stationary and mobile sources (Ahmed et al., 1993; Rubel and Stencel, 1996). Furthermore, it has also been used in a range of other applications including removal of dyes, ions, heavy metals, volatile organic compounds, air pollution control and water purification (Giraldo et al., 2007; Ioannidou and Zabaniotou, 2007; Lakherwal, 2014; Yakout and Sharaf El-Deen, 2011). In the case of heavy metal remediation and recovery of precious metals, adsorption by AC has been viewed as the preferred method due to its simplicity, easy scale-up, high adsorption capacity, high adsorption rate, good resistance to abrasion and its ability to recover the metals with a high efficiency (Sharififard et al., 2012; Zaini et al., 2010).

In recent years, considerable interest has been shown to a new category of AC in the form of fiber known as ACF (Brasquet and Le Cloirec, 1997; Suzuki, 1993). The ACF is a novel material with abundant micropores (Fu et al., 2003), known to possess high packing density and excellent volumetric capacity (Lee et al., 2014; Lozano-Castello et al., 2002). In comparison to the ordinary GAC and PAC, ACF has a higher adsorption capacity, surface area, more rapid adsorption and desorption rate and it can be easily fabricated (Lee et al., 2014; Suzuki, 1993).

The ACF is normally produced from carbon containing materials such as coal, petroleum pitches, rayon, polyacrylonitrile (PAN) and phenolic polymers through high temperature gasification in steam or carbon dioxide (Bajaj and Dhawan, 1997; Sittig, 1980; Zaini et al., 2010). However, the main challenges related to the commercial manufacturing of ACF, is partially due to manufacturing ACFs from synthetic polymers such as rayon, PAN and phenolic polymers, which results in high production and regeneration costs (Hesas et al., 2013; Lin and Juang, 2009; Mavhungu et al., 2013). Therefore, locally available material such as agricultural wastes and industrial wastes should be utilized as low-cost precursor so as to minimize the production cost of ACFs (Crini, 2005; Rashed, 2013).

Recently, research has been focused on various other materials, in an effort to find economical and renewable types of precursors for the production of ACF (Ma et al., 2014). This study proposes the use of low cost precursors such as spent ion exchange resins (IER). The IER are used in numerous industries such as industrial water treatment, food and beverage, pharmaceuticals, petrochemical, hydrometallurgy and nuclear power plants (Deventer, 2011) thus, they are found abundantly. However, the disposal and storage of spent IERs has proven to be problematic over the years as they require special approach and precautions during their conditioning in order to meet the acceptable criteria for disposal (Braet et al., 2012; Gan et al.,

2008). Therefore, the best way to mitigate the environmental concerns related to IERs would be to produce an intermediate stable product which could be further used in alternative applications.

Furthermore, the use of carbon nanotubes (CNTs) for gas adsorption has received a sprouting interest in research (Ding et al., 2006; Zhao et al., 2002). The CNTs were discovered in 1991 by Sumio Iijima (Iijima, 1991) and since then they have received much attention in research due to their unique electrical, mechanical, chemical and physical properties such as chemical stability, electrical conductivity, high mechanical structure and specific surface area, to name a few (Manocha et al., 2005; Shukrullah et al., 2016). These nanostructures of graphitic filaments, having a length to diameter ratio greater than 1 000 000, have a vast variety of potential applications in electric devices, nanotechnological tools, novel nanoscale materials, drug delivery systems field emission applications, magnetic field applications, hydrogen adsorption, textile, etc. (Manocha et al., 2005; Saifuddin et al., 2013; Tekkaya and Karatepe, 2011).

The three generally known methods for CNTs production are arch discharge, laser ablation and chemical vapor deposition (CVD). From research, the CVD method has been the most common method for CNT production as it has benefits including it being a simple method allowing for better control over the growth parameters, relatively lower production temperatures and cost, and the most suitable technique for mass production. In addition to the aforementioned benefits of the preferred use of CVD in CNT synthesis, the CVD method was chosen in this research as this method involves the deposition of a hydrocarbon gas as a carbon precursor (e.g. acetylene, methane, benzene) onto a metal catalyst (e.g. Fe, Co, Ni, etc.) at temperatures between 500 and 1200 °C (Li et al., 2004; Saifuddin et al., 2013; Tekkaya and Karatepe, 2011). This study investigates the use of gas emitted from the IER pyrolysis on the growth of CNT

and the associated growth parameters such as the catalyst support, carrier gas and reaction temperature, in the production of CNT from IER.

1.2 RESEARCH PROBLEM

From literature, it is noted that the disposal of spent IER is becoming increasingly problematic. The current disposal and storage techniques for spent IERs has a major drawback which is lack of volume reduction, therefore, there is a need to research new disposal methods. A worthwhile spent ion disposal method is one that would produce an intermediate stable product which could further be used. Hence, to start with, this study investigated the use of unused IER for the production of ACF and/or CNTs.

Multiple studies have shown that phenolic resins are known to be one of the precursors of AC and ACFs, it was, therefore, theorized that if phenolic resins and spent ion exchange materials have similar chemical compositions, then ACFs can be synthesized from IER.

It can also be seen from past research that other carbon species such as acetylene, benzene, xylene, toluene and so forth, have been used as a carbon feedstock in the production of CNTs (Saifuddin et al., 2013). The IER used in this study was Amberlite XAD4, which has an aromatic nature on its surface. Therefore, if the pyrolysis of the IER in this study can produce an aromatic gas, then this gas can be used as a carbon precursor in the production of CNTs.

These are the conceptual theories upon which this research was based. Consequently, the various questions that need to be addressed to support the basis of this research are as follows:

i). Can ACFs be produced from IER?

ii). Can CNTs be produced from IER?

iii). What are the optimal conditions for the production of ACFs and CNTs from IER?

iv). Can the produced ACFs and/or CNTs be used for platinum adsorption?

1.2.1. Aim

The overall aim of this research is to synthesize and characterize ACF and/or CNTs from IERs and subsequently use them for the removal of platinum from dilute solutions.

1.2.2. Objectives

For this study, the specific sets of objectives are:-

i). To examine the feasibility of producing ACFs from IERs.

ii). To examine the feasibility of producing CNTs from IERs.

iii). To evaluate the effectiveness of ACFs and/or CNTs on the adsorption of platinum from the potassium tetrachloroplatinate solutions.

1.2.3. Research Approach

In order to examine the feasibility of synthesizing ACFs from spent IER, ACFs will be made from unused IER in this study. The ACFs will then be analyzed and characterized by the use of a scanning electron microscope (SEM), thermogravimetric analysis (TGA), Fourier Transform Infrared Spectroscopy (FTIR) and nitrogen adsorption isotherms which will help in determining the Brunauer-Emmet-Teller (BET) surface area, pore volume and pore size. After production of ACFs, batch adsorption experiments were conducted using varying concentrations of potassium tetrachloroplatinate solutions in order to determine adsorption capacity and adsorption isotherms of the produced ACF from IER. For the production of CNTs, a gas chromatography and mass spectroscopy (GC-MS) was used to identify the gases emitted from the pyrolysis of the IER and further deduce if the gas could be used as a carbon source in the synthesis of CNTs. The produced CNTs were then analysed and characterized by the use of the SEM, TGA, Raman Spectroscopy and BET surface area.

1.3 DISSERTATION STRUCTURE

The dissertation is presented in five chapters as follows:

Chapter 1 - Introduction. The current chapter provides background information on the problem. A comprehensive purpose of the study is presented, in which the research problem, aim and objectives of the study at hand are given.

Chapter 2 - Literature Review. The given literature review provides relevant information on which the investigation at hand is based on. This includes the use of adsorption as an alternative process for removal of platinum ions from dilute solutions as opposed to the usual platinum recovery methods. A review on the synthesis of ACF and CNTs is also presented in order to investigate how the production of these materials could be used as a mean to mitigate problems associated with the disposal of IER.

Chapter 3 – Experimental Techniques. All the experimental techniques used for this study are explained in detail in this chapter. This chapter highlights the production of ACF produced from unused ion exchange materials and the production of CNTs. There was an evolution of gas during the production of the ACF. This gas was analysed by means of GC-MS and it was therefore proposed to investigate the use of this gas in the production of CNTs so as to determine if the CNTs can be used to increase the surface area of the synthesized ACF or as an alternative adsorbent for platinum in dilute solutions. For this study, the produced ACF and CNTs are characterized by means of analytical techniques such as SEM, BET, TGA, FTIR and Raman spectroscopy. Lastly, the methodology used for the batch adsorption experiments of platinum from potassium tetrachloroplatinate solutions using ACF is outlined.

Chapter 4 – Result and discussion. The experimental results, thereof, of the synthesis of ACF, and CNTs are presented and thoroughly discussed in this chapter. The produced ACF and

CNTs are characterized and compared. Thereafter, the kinetics, adsorption capacity and adsorption isotherms of the produced ACF are investigated and discussed.

Chapter 5 – Conclusion and recommendations. This final chapter summarizes the experimental findings and evaluates the success of the produced ACFs relative to the platinum adsorption capacity. The chapter also includes suggestions for improvements of the production of the adsorbents and adsorption process.

1.4 REFERENCES

Ahmed, S.N., Stencel, J., Derbyshire, F., Baldwin, B., 1993. Activated carbon for the removal of nitric oxides. Fuel Process. Technol. 34, 123–136.

Al-Qodah, Z., Shawabkah, R., 2009. Production and characterization of granular activated carbon from activated sludge. Braz. J. Chem. Eng. 26, 1678–4383.

Bajaj, P., Dhawan, A., 1997. PAN - based activated carbon fibers: Production, characterization and applications. Indian J. Fiber Text. Res. 22, 222–235.

Barakat, M.A., 2011. New trends in removing heavy metals from industrial wastewater. Arab. J. Chem. 4, 361–377.

Bhatnagar, A., Minocha, A.K., 2006. Conventional and non-conventional adsorbents for removal of pollutants from water – A review. Indian J. Chem. Technol. 13, 203 - 217.

Braet, J., Charpentier, D., Centner, B., Vanderperre, S., 2012. Radioactive Spent Ion-Exchange Resins Conditioning by the Hot Supercompaction Process at Tihange NPP - Early Experience - 12200, in: Waste Management 2012 Conference on Improving the Future in Waste Management. Phoenix, Arizona, USA, p. 10.

Brasquet, C., Le Cloirec, P., 1997. Adsorption onto Activated Carbon Fibers: Application to Water and Air Treatments. Carbon 35, 1307–1313.

Crini, G., 2005. Recent development in polysaccharide-based materials used as adsorbents in wastewater treatment. Prog. Polym. Sci. 30, 38–70.

Deventer, J. van, 2011. Selected Ion Exchange Applications in the Hydrometallurgical Industry. Solvent Extr. Ion Exch. 29, 695–718.

Ding, Y., Yang, X., Ni, J., 2006. Adsorption on the carbon nanotubes. Front. Phys. China 1, 317–322.

Dyk, V., Doreen, L., 2000. The production of granular activated carbon from agricultural waste products (Thesis). Stellenbosch : Stellenbosch University.

Fu, R., Zheng, B., Liu, J., Weiss, S., Ying, J.Y., Dresselhaus, M.S., Dresselhaus, G., Satcher, J.H.J., Baumann, T.F., 2003. Fabrication of activated carbon fibers/carbon aerogels composites by gelation and supercritical drying in isopropanol. Mater. Res. Soc. 18, 2765–2773.

Fujiwara, K., Ramesh, A., Maki, T., Hasegawa, H., Ueda, K., 2007. Adsorption of platinum (IV), palladium (II) and gold (III) from aqueous solutions onto l-lysine modified crosslinked chitosan resin. J. Hazard. Mater. 146, 39–50.

Gan, X., Lin, M., Bao, L., Gao, Y., Zhang, Z., 2008. Investigation of the Immobilization of the Radioactive Ion Exchange Resins into Specific Cement Using the Mixture Response Surface Approach. J. Nucl. Sci. Technol. 45, 1084–1090.

Giraldo, L., Ladino, Y., Pirajánc, J.C.M., Rodríguez, M.P., 2007. Synthesis and characterization of activated carbon fibers from Kevlar. Electica Quimica 32, 55–62.

Hesas, R.H., Arami-Niya, A., Daud, W.M.A.W., Sahu, J.N., 2013. Preparation and Characterization of Activated Carbon from Apple waste by Microwave-Assisted Phosphoric Acid Activation: Application in Methylene Blue Adsorption. BioResource 8, 2950–2966.

Iijima, S., 1991. Helical microtubules of graphitic carbon. Nature 354, 56–58.

Ioannidou, O., Zabaniotou, A., 2007. Agricultural residues as precursors for activated carbon production - A review. Renew. Sustain. Energy Rev. 11, 1966–2005.

Jones, R.T., 2005. An Overview of Southern African PGM smelting, in: Nickel and Cobalt 2005: Challenges in Extraction and Production. Presented at the 44th Annual Conference of Metallurgists, Calgary, Alberta, Canada, 147–178.

Kumar, M., Ando, Y., 2010. Chemical Vapor Deposition of Carbon Nanotubes: A Review on Growth Mechanism and Mass Production. J. Nanosci. Nanotechnol. 10, 3739-3758

Kyzas, G.Z., Kostoglou, M., 2014. Green Adsorbents for Wastewaters: A Critical Review. Materials 7, 333–364.

Lakherwal, D., 2014. Adsorption of Heavy Metals: A Review. Int. J. Environ. Res. Dev. 4, 41–48.

Lee, T., Ooi, C.-H., Othman, R., Yeoh, F., 2014. Activated Carbon Fiber - The Hybrid of Carbon Fiber and Activated Carbon. Rev. Adv. Mater. Sci. 36, 118–136.

Li, Q., Yan, H., Zhang, J., Liu, Z., 2004. Effect of hydrocarbons precursors on the formation of carbon nanotubes in chemical vapor deposition. Carbon 42, 829–835.

Lin, S.-H., Juang, R.-S., 2009. Adsorption of phenol and its derivatives from water using synthetic resins and low-cost natural adsorbents: A review. J. Environ. Manage. 90, 1336–1349.

Lozano-Castello, D., Cazorla-Amoros, D., Linares-Solano, A., 2002. Powdered Activated Carbons and Activated Carbon Fibers for Methane Storage: A Comparative Study. Energy Fuels 16, 1321–1328.

Ma, X., Yang, H., Yu, L., Chen, Y., Li, Y., 2014. Preparation, Surface and Pore Structure of High Surface Area Activated Carbon Fibers from Bamboo by Steam Activation. Materials 7, 4431–4441.

Manocha, L.M., Valand, J., Manocha, S., 2005. Role of metal catalyst and substrate site for the growth of carbon nanomaterials. Carbon Sci. 6, 79–85.

Matthey, J., 2016. Summary of Platinum Supply and Demand in 2015. 1st ed. [pdf] Available at: http://www.platinum.matthey.com/ [Accessed 18 Aug. 2016].

Mavhungu, A., Mbaya, R.K.K., Moropeng, M.L., 2013. Recovery of Platinum and Palladium Ions from Aqueous Solution Using Grape Stalk Waste. Int. J. Chem. Eng. Appl. 4, 354–358.

Nikoloski, A.N., Ang, K.-L., 2014. Review of the Application of Ion Exchange Resins for the Recovery of Platinum-Group Metals From Hydrochloric Acid Solutions. Miner. Process. Extr. Metall. Rev. 35, 369-389.

Osmond, N.M., 2000. Activated Carbon Fiber Adsorbent Materials. Adsorpt. Sci. Technol. 18, 529–539.

Rashed, M.N., 2013. Adsorption Technique for the Removal of Organic Pollutants from Water and Wastewater. In Tech. 167-194.

Rubel, A.M., Stencel, J.M., 1996. Effect of Pressure on NOx Adsorption by Activated Carbons. Energy Fuels 10, 701–708.

Saifuddin, N., Raziah, A.Z., Junizah, A.R., 2012. Carbon Nanotubes: A Review on Structure and Their Interaction with Proteins. J. Chem. 2013, 1-18.

Sharififard, H., Soleimani, M., Ashtiani, F.Z., 2012. Evaluation of activated carbon and bio-polymer modified activated carbon performance for palladium and platinum removal. J. Taiwan Inst. Chem. Eng. 43, 696–703.

Sharma, Y. c., Srivastava, V., Singh, V. k., Kaul, S. n., Weng, C. h., 2009. Nano-adsorbents for the removal of metallic pollutants from water and wastewater. Environ. Technol. 30, 583–609.

Shukrullah, S., Mohamed, N.M., Shaharun, M.S., Naz, M.Y., 2016. Parametric study on vapor-solid growth mechanism of multiwalled carbon nanotubes. Mater. Chem. Phys. 176, 32 43.

Sittig, M., 1980. Carbon and Graphite Fibers: Manufacture and Applications, Carbon and Graphite Fibers. Noyes Data Corporation, Park Ridge.

Suzuki, M., 1993. Activated Carbon Fiber: Fundamentals and Applications. Carbon 32, 577–586.

Tekkaya, E.D., Karatepe, N., 2011. Production of carbon nanotubes by iron. Int. J. Chem. Mol. Nucl. Mater. Metall. Eng. 5, 541–547.

Yakout, S.M., Sharaf El-Deen, G., 2011. Characterization of activated carbon prepared by phosphoric acid activation of olive stones. Arab. J. Chem. 1, 1878–5352.

Zaini, M.A.A., Amano, Y., Machida, M., 2010. Adsorption of heavy metals onto activated carbons derived from polyacrylonitrile fiber. J. Hazard. Mater. 180, 552–560.

Zhao, J., Buldum, A., Han, J., Lu, J.P., 2002. Gas molecule adsorption in carbon nanotubes and nanotube bundles. Nanotechnology 13, 195–200.

2

LITERATURE REVIEW

2.1 GENERAL INTRODUCTION

In past times, the separation of platinum from solution has been achieved through a series of precipitation reactions up until the 1970s. This method had an overall efficiency of 95 % and could only be achieved through the use of multiple unit operations and recycle streams, making the processes highly labour intensive. Techniques such as cementation, crystallization, distillation and sublimation, have also been employed, however, they too are complex methods requiring a number of process steps. Nonetheless, the demand for platinum is increasing despite its relatively low abundance in the earths' crust. Much attention has been focused on recycling secondary raw materials such as the automotive catalyst, however, it is worth noting that recycling is not a closed loop, only a fraction of PGMs produced can be recovered. Therefore, this study investigated the recovery of platinum from dilute solutions through the use adsorption.

This chapter is a review of the literature that was used to provide the basis of this research. The chapter begins with a brief description on the history of platinum refining methods (section 2.2), incorporating how the adsorption technique can be an alternative solution in the recovery

of platinum from dilute solutions. The following section (section 2.3), gives an introduction to activated carbon fibers (ACFs), as ACF have received much appraisal from research and industry across, and why ACF are the chosen adsorbent for the study. The third section (section 2.4) is the ACF synthesis, describing the general ACF preparation methods - physical and chemical activation. Following this is section 2.5, giving an introduction to carbon nanomaterial (CNM), more specifically so, the carbon nanotubes (CNTs). Section 2.6 and 2.7 further review the CNT synthesis and the parameters involved in CNT preparation, respectively. The last section in this chapter (section 2.8), is an introduction on the adsorption technique, highlighting adsorption isotherms to be used.

2.2 GENERAL RECOVERY OF PLATINUM

The classical separation of platinum group metals (PGMs) from solutions, with more emphasis on platinum, has largely been achieved by a series of precipitation reactions, up until the mid-1970s (Nikoloski and Ang, 2014). Due to the numerous number of precipitation steps, each with poor selectivity towards the PGMs, the classical refining method was relatively inefficient. For this process to be considered cost effective, an overall efficiency greater than 95% had to be achieved. Therefore, the process required many recycling and intermediate steps. The use of precipitation reactions for recovery of platinum with an overall efficiency of 95% could only be achieved with a number of unit operations and recycle streams thus having lengthy labour intensive refining operations (Nikoloski and Ang, 2014). The other techniques that have been employed are cementation, electrolysis, crystallization, distillation and sublimation, however these techniques are quite complex and also involve numerous steps (Renner, 1992).

During the mid-1970s, it was of great importance to develop new technologies for the effective recovery and separation of PGMs from industrial effluents (Nikoloski and Ang, 2014). Part of

the development criteria was to design separation processes with high efficiency and minimal loss of noble metals (Renner, 1992). At this point in time, techniques such as liquid-liquid extraction, solid-phase extraction and selective photocatalytic reduction were introduced as powerful and promising techniques. In comparison to precipitation reactions and other classical methods, these techniques had a higher selectivity and a higher metal purity. For this reason, the separation of PGMs from chloride solutions, with reference to solvent extraction and ion exchange resins have been widely explored (Nikoloski and Ang, 2014). As promising as solvent extraction may have been for the recovery of PGMs from low concentrated solutions and with numerous solvent extractants being studied, some operations have reported practical drawbacks. To name a few, production costs including cost of solvents can be quite high due to solute losses and from handling and storage of the organic solvents. Solvent extraction equipment can be quite complex, difficult to operate and there is a possibility of encountering problems with reagent losses or disengagement of phases. Using solvent extraction for PGM recovery in dilute solutions results in relatively low recovery yield and slower kinetics (Nikoloski and Ang, 2014).

In recent past, the demand of precious metals is rapidly growing in myriads of industries leading to rigorous mining from platinum reserves and in the case of expansion in the recovery of platinum through recycling of the secondary raw materials such as automotive catalysts (Nikoloski and Ang, 2014). Unfortunately the recycling of PGMs, where most of the PGMs are expected to come from is not a closed loop; only a fraction of the PGMs that are produced can be recycled (Ryan et al., 2010).

Subsequently, over the past years, the rise in demand has induced a decline in mineral stock and thus increased the scarcity and price of PGMs including platinum. For this reason, the increasing demand is of great economical interest in the recovery of these precious metals

(Ramesh et al., 2008). It is noted that the accumulation of these valuable metals in residue and waste streams represents a significant loss of unclaimed water and valuable metals. Therefore, it is essential to look into the methods which can effectively process and/or recycle PGMs from aqueous or waste solutions in order to increase metal recovery and reduce the detrimental impact on the environment (Deventer, 2011; Oke et al., 2014). In other words, the accumulation of valuable metals in residue and discharge waste streams has prompted the need to develop efficient and cost effective methods of recovering platinum from primary and secondary sources. Therefore, over the years, various methods such as ion exchange, liquid-liquid extraction, membrane filtration and adsorption (Fujiwara et al., 2007; Mavhungu et al., 2013; Ramesh et al., 2008) have been developed/investigated for the recovery of platinum from low grade ores and industrial waste streams of low concentrations (Parodi et al., 2008).

Whilst a number of techniques have proven to be successful for the recovery of platinum in concentrated solutions, as mentioned previously, with regards to the recovery of metals in dilute solutions, adsorption has proven to be the most effective recovery technique (Mavhungu et al., 2013). With reference to Table 2.1, it can be seen that adsorption is the only technique able to work with concentrations less than 10mg/l (dilute solution) of desired metal to be recovered.

Table 2.1: Performance characteristics of heavy metal removal and recovery technologies (Crundwell et al., 2011)

	Adsorption	Electrochemical	Ion Exchange	Precipitation as hydroxide	Solvent extraction	Ion membrane technology
pH change	Limited tolerance	Tolerant	Limited Tolerance	Tolerant	Some system tolerant	Limited tolerance
Metal selectivity	Moderate	Moderate	Chelate resins can be selective	Non-selective	selective if extractant available	Moderate
Working concentration range (mg/l)	< 10	> 10	< 100	> 10	> 100	>10

In fact, adsorption processes have proven to be very simple, economical, effective and versatile, making them the most preferred and cost effective method for removal of toxic contaminants, recycling precious metal; ions and hence wastewater treatment (Lakherwal, 2014; Ramahali and Mahlangu, 2010).

Thus, a range of adsorbents such as activated carbon (AC), synthetic resins and low cost natural adsorbents have been investigated and/or are being used. Currently, AC, more specifically ACF, has been of great interest as an adsorbent (Lin and Juang, 2009; Mavhungu et al., 2013).

2.3 ACTIVATED CARBON FIBER

2.3.1 Activated Carbon Fiber

"Activated carbon fibers (ACF) are porous carbon materials produced from a variety of fibrous carbonaceous precursors" (Ma et al., 2014).

The ACF is normally produced from carbon fiber (CF). The activation of the carbon fiber includes an additional thermal treatment step under oxidising atmosphere at a temperature of 700°C to 1000°C (Lee et al., 2013). To activate carbon fibers means to process the material such that the material is made extremely porous. In doing so, the formed pores and pockets increase the surface area for adsorption and chemical reactions to take place. Pores found within the ACF can be classified into three groups. These groups are distinguished by the pore diameter or slit widths as follows (Engber, 2005):

- Micropores 8 – 100 Å
- Mesopores 100 – 500 Å
- Macropores 500 – 20000 Å

2.3.2 Activated Carbon VS Activated Carbon Fiber

The difference between AC and ACF is the pore structures. The type of pores found within ACFs are mainly micropores whereas in AC, complex structures are formed consisting of micropores, mesopores and macropores. Because of the smaller diameter of the pores within ACFs in comparison to granular activated carbon (GAC) and powdered activated carbon (PAC), the adsorption rate of ACFs tends to be greater (Giraldo et al., 2007). In order for adsorbate gas molecules to reach micropores in AC molecules, the adsorbate gas molecules have to first pass through macropores and mesopores. In the case of ACF, large amounts of

micropores can be reached by adsorbate gas as the micropores are directly exposed to the fiber surface (Lee et al., 2013).

The high adsorption rate of ACF in comparison to that of CF is also due to the greater bulk volume that ACF have (Zaini et al., 2010) and their small fiber diameter (Bikshapathi et al., 2011). What makes ACF advantageous is the ability to control the distance between the fibers in order for the ACF to be packed in fixed bed adsorbents. This distance is controlled through choice in precursor materials (Giraldo et al., 2007). Due to the small fiber diameter, diffusional resistance is minimized. Other prominent advantages of ACF include abrasion resistance, ease of handling, various choice in fibers design i.e. creating fiber forms such as felt, paper and nonwovens; ACFs are amenable to surface functionalization and regeneration (Bikshapathi et al., 2011). What makes ACFs exceptional adsorbents is their high contact efficiency and flexibility, low pressure fell, lightness and malleability (Giraldo et al., 2007).

2.3.3 Production History of Activated Carbon Fiber

ACF can be seen as the hybrid between AC and CF. Commercially, as stated by Lee et al (2013), ACFs are produced by the pyrolysis of fiber-forming materials in an inert atmosphere (Sittig, 1980). Preparation of ACF can be done using different fibrous materials of varying compositions. The types of raw materials used for CF production is very similar to materials used for the preparation of ACFs. In 1966, the first ACFs were produced from viscose and acetate cloth; their production was at low yield. Later in 1970, ACF produced from lignin, polyvinylchloride and phenolic resin, had a high yield and good mechanical properties. Since then, many companies have been commercializing ACFs from phenolic resin, followed by polyacrylonitrile (PAN) and pitch-based ACFs in 1985 (Giraldo et al., 2007). ACF precursor materials are usually of low crystallinity. A few of these feedstock materials are viscose rayon, polyacrylonitrile and coal tar pitch. The production costs of ACFs from these synthetic

polymers and phenolic resin are high and thus it is crucial for studies to be performed to reduce processing cost. In addition to this, most synthetic fibers are usually derived from petroleum products (Lee et al., 2013; Ma et al., 2014; Sittig, 1980). Unfortunately these resources are in shortage and are in high demands in other industries. Recently research has been focused on various natural materials, in order to find cheap and renewable types of precursors (Ma et al., 2014). Some of the natural materials include cotton stalk, coconut shell, wood and paper just to name a few. One of the cost effective research performed is the production of ACF through the use of agricultural by-products in biomass form. However, the use of biomass is an emerging technology; there is limited existing literature on its use for ACF production.

2.4 ACTIVATED CARBON FIBERS SYNTHESIS

The activation method plays a very important role in the porosity of the structure generated. The activation process is carried out in order to remove material/atoms that block the pores in the activated carbon. Activation helps increase the number of pores and also expands the size of the existing pores, thus producing porous carbon with readily accessible pore structure and large internal surface area leading to a high adsorption capacity. The two methods that can be used to synthesize ACFs are physical activation and chemical activation (Abdallah, 2004; Lee et al., 2013).

2.4.1 Physical Activation

The physical activation process for the preparation of ACFs initially involves carbonization of carbonaceous material followed by the activation of the char under oxidising gases such as carbon dioxide, steam, air or their mixtures at temperatures between 800 – 1000 °C (Lee et al., 2013). The main objective of carbonization is to lower the volatile content of the precursor in order to convert the material to a form suitable for activation (Abdallah, 2004). During the carbonization process, there is elimination of the non-carbon elements such as oxygen,

hydrogen, and nitrogen, through the thermal decomposition of the raw materials. Carbonization leads to a carbon skeleton (char) possessing a primary pore structure (Lee et al., 2013). Carbonization is performed mostly by pyrolysing carbonaceous material in an inert atmosphere at high temperatures using nitrogen gas (Montoya et al., 2012). Other carbonization processes are carried out by combustion under an air/ambient atmosphere at much lower temperatures. The carbonization process creates small pores which are usually partially blocked by other elements (Lee et al., 2013). After carbonization, the development and unblocking of the pores is established by a second thermal treatment for the activation process, known as physical activation.

2.4.2 Chemical Activation

In chemical activation, the carbonization and activation steps occur simultaneously. The chemical activation process treats the raw material using an activation agent such as zinc chloride, phosphoric acid, sodium hydroxide and other chemicals (Lee et al., 2013; Montoya et al., 2012). The chemical agents used are strong dehydrating agents, and they are added to free the pores after carbonization and can be recovered for reuse. Their addition influence the pyrolytic process by restriction of tar formation (Abdallah, 2004). The activating agent is combined with the raw material through impregnation or physical mixing and the resulting precursor is heat-treated under an inert atmosphere between temperatures of 400 – 800 °C. The chemicals are then removed through exhaustive washing with water and then dried and separated from the slurry (Lee, et al., 2013). Given that the temperature required for pyrolysis with chemical activation is slower than that of physical activation, this promotes development of porous structure and crystallites of smaller dimensions (micropores) are formed (Abdallah, 2004).

2.4.3 Physical versus Chemical

High quality ACFs are obtained from both the physical and chemical activation methods. The choice in either method is dependent on the purpose in which the ACFs will be used. It is important to know the properties, advantages and disadvantages of ACF produced from both methods. Table 2.2 and Table 2.3 list the advantages and disadvantages of chemical and physical activation methods respectively.

Table 2.2: The advantages and disadvantages of using chemical activation (Montoya et al., 2012)

Advantages	Disadvantages
Activation obtained in one step	Corrosiveness of the process
Shorter activation times	Requires a washing stage
Lower pyrolysis temperatures (600°C -800°C)	Inorganic Impurities
Better control of textural properties	More expensive
High yield	
High surface area	
Well-developed microporosity	
Narrow micropore size distributions	
Reduction of mineral matter content	

Table 2.3: The advantages and disadvantages of using physical activation (Montoya et al., 2012)

Advantages	Disadvantages
Avoids incorporation of impurities coming from the activating agent	ACFs are obtained in two steps
Process is not corrosive	Higher activation temperature (800°C-1000°C)
No washing stage required	Poorer porosity control
Cheaper	

For this research, chemical activation technique was employed in the production of activated carbon fibers from the ion exchange materials. The chemical activation was chosen over the physical activation because chemical activation is known to have a higher porosity development than the physical activation (Montoya et al., 2012; Moore and Maciá-Agulló, 2004). Furthermore, chemical activation maintains the fiber morphology better and produces a higher yield. In addition, the equipment used in chemical activation was easily attainable locally.

2.5 CARBON NANOMATERIALS

The ion exchange resin used (Amberlite xad-4) in this research was used for the production of ACFs and carbon nanotubes (CNTs). Substances with at least one dimension being less than 100 nanometers are known as nanomaterials. There are various nanomaterials ranging from carbon nanotubes, carbon onions, nanoscale diamonds and diamondoids, having different classes and occurring naturally or produced through synthesis (Krueger, 2014). Nanomaterials are of great interest in the research community due to their exceptional electrical, optical and mechanical properties. Thus they are used in multiple industries such as electronics, energy storage, sensors, biotechnology and also an emerging interest has been shown in the application of adsorption using single- walled carbon nanotubes (SWCNT) (Çınar et al., 2012; Ding et al., 2006; Zhao et al., 2002).

The CNTs are defined as graphitic filaments with diameters ranging from 0.4 to 500 nm and have lengths ranging from several micrometres to millimetres. Ideally, the structure of CNTs consists of a graphite sheet wrapped into a cylinder - essentially a rolled up sheet of hexagonally bonded carbon atoms taking a cylindrical form (Gay et al., 2005; Wu, 2006). A basic characteristic of a single nanotube is that a fullerene hemisphere may cap the cylinder. In addition, the nanotube walls may consist of one to many hundreds of concentric cylindrical

graphitic shells. Synthesized CNTs can take one of two forms, the single-walled carbon nanotubes (SWCNTs) or the multi-walled carbon nanotubes (MWCNTs). As per the name, SWCNTs comprise of one cylindrical hollow graphitic shell and the MWCNTs are concentric cylinders which are two or more in number (Koziol et al., 2010). For the purpose of this research, the synthesis of SWCNT from the pyrolysis of IER will be examined to determine if the synthesized CNTs can be used for adsorption purposes and further beneficiate spent IER.

2.6 CARBON NANOTUBE SYNTHESIS

2.6.1 Growth mechanisms

The growth mechanisms for CNTs have been debatable and currently up to date there is no single well established growth mechanisms for CNTs (Khurshed and Bilal, 2016; Kumar, 2011; Shifrina, 2011). The widely accepted most-general catalytic decomposition model as described by Kumar (2011) will be used. When a hydrocarbon vapour comes into contact with a “hot” metal nanoparticle, it decomposes into carbon and hydrogen species, having the hydrogen flying away and the carbon dissolving into the metal. Once the metal reaches its carbon-solubility limit in the metal at the specific temperature, the dissolved carbon starts to precipitate out and crystallizes in the form of a cylindrical network, having no dangling bonds and hence it is energetically stable. The exothermic hydrocarbon decomposition process releases heat to the metal exposed zone and the carbon crystallization process is an endothermic process which absorbs heat from the metal precipitation zone causing a thermal gradient within the metal particles resulting in the process to go on. There are two types of growth mechanisms that can result from this, tip and base growth, both depending on the catalyst support interactions (Kumar, 2011; Kumar and Ando, 2010). Figure 2.1 illustrates these two mechanisms.

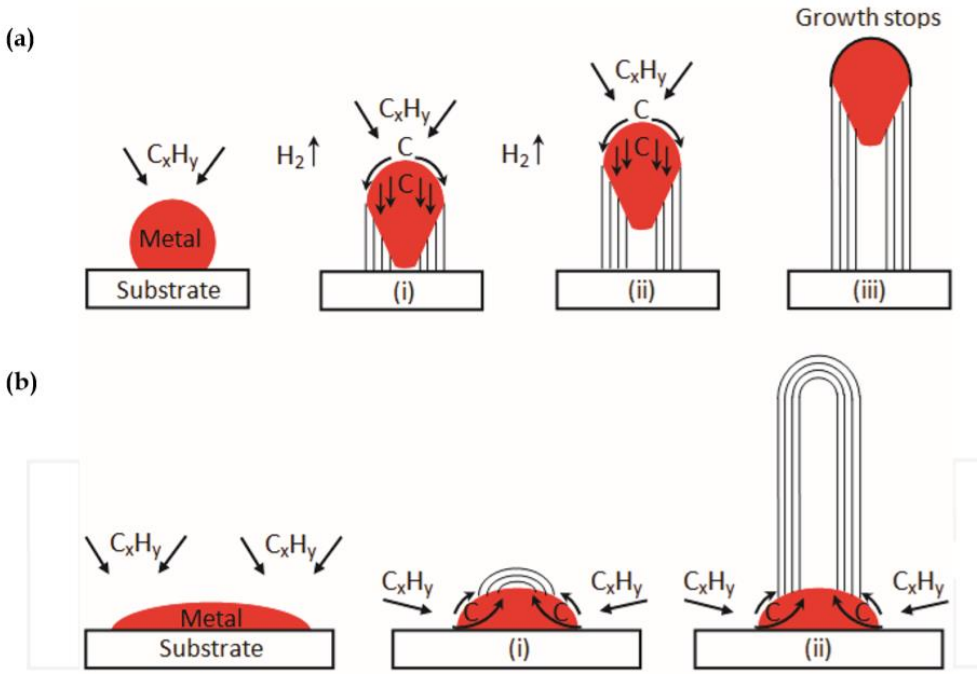

Figure 2.1: The growth mechanisms for CNTs; a) tip-growth model and, b) the base-growth model (Kumar, 2011).

- **Tip growth**

Figure 2.1 (a) shows the tip- growth model, in which the catalyst-substrate interaction is weak. The metal has an acute contact angle with the substrate. The hydrocarbon will decompose on top of the surface of the metal particle; the carbon diffuses down through the metal and the CNT precipitates out across the bottom, pushing the whole metal particle off the substrate. The CNT will continue to grow if the metal surface is open for fresh hydrocarbon decomposition and the concentration gradient still exists in the metal, allowing for carbon diffusion. The CNT production only stops once the metal is fully covered with excess carbon and the catalytic activity ceases to stop the CNT growth (Khurshed and Bilal, 2016; Kumar, 2011).

- **Base growth**

The other growth model can be seen in Figure 2.1 (b) called the base-growth model. In this case, the catalyst-substrate interaction is strong and the metal has an obtuse angle with the

substrate. Initially the hydrocarbon decomposition and carbon diffusion occurs as in the tip-growth model. In the base growth, however, the precipitation cannot push the metal off the substrate and so the CNT is compelled to emerge out from the metal's apex (the point which is furthest from the substrate, having minimal interaction with the substrate). Therefore, the CNT grows up with the catalyst particle rooted on its base (Khurshed and Bilal, 2016; Kumar, 2011).

It is important to note that the discord associated with the above generalized growth mechanisms is the lack of assurance in knowing certainly if the metal in question is in solid or liquid state, if whether or not the carbon diffusion in metal is volume diffusion or surface diffusion and whether or not the catalyst for growth is the pure metal or metal carbide (Kumar, 2011).

2.6.2 Carbon Nanotube Synthesis Methods

The three prevalent methods used for the synthesis of CNTs or nanomaterials, are Arc Discharge, Laser Ablation and Catalytic Chemical Vapour Deposition (CCVD or CVD). Arc Discharge and Laser Ablation fall under the classification of high temperature (> 2700 °C) and very short reactions times (microseconds to milli seconds). The use of the CVD method, however, involves the decomposition of a hydrocarbon vapour achieved in the presence of a metal catalyst at medium temperatures (426 – 1126 °C) and long reaction times (minutes to hours), relative to the aforementioned methods (Kumar and Ando, 2010).

In this research, CVD was the method of choice as the use of CVD in the synthesis of CNT is simple and economical, producing CNTs with a high yield and purity at low temperatures and at ambient pressure. A more predominant reason why CVD was the method of choice in this research is its versatility; CVD allows one to control the formation/structure of the CNT, it can harness a number of hydrocarbons in any state (solid liquid or gas), it enables the use of different substrates and allows for the growth of CNTs in various forms such as powders, thin

or thick films, aligned or entangled, straight or coiled nanotubes with an added advantages of a better control on the CNT growth parameters (Dikio et al., 2013; Kumar and Ando, 2010).

The CVD method makes use of a reactor setup in order to synthesize the CNTs. There are two main reactor configurations which exist to accomplish this are: a vertical reactor configuration and a horizontal reactor configuration.

2.6.3 Catalytic Chemical Vapour Deposition: Horizontal furnace

The use of a horizontal furnace is the most commonly used configuration for CNT synthesis. As can be seen in Figure 2.2 below, this setup allows for catalysts/support (substrate) to be placed in a removable ceramic boat in the centre of the furnace, within the quartz tube, allowing for the reactant gas and inert gas to flow across the catalyst (Chhowalla et al., 2005).

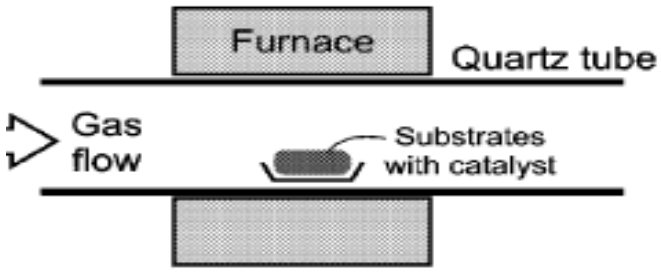

Figure 2.2: CVD horizontal setup (Chhowalla et al., 2005)

The use of the horizontal reactor configuration is more common as it makes for easy handling of the catalyst support as the support is kept in a fixed position allowing the majority of the nanostructures to be formed on the support (Szabó et al., 2010)

2.6.4 Catalytic Chemical Vapour Deposition: Verttical furnace

The vertical furnace is usually used in cases where the CNT synthesis is continuous. As can be seen in Figure 2.3 below, the catalyst and carbon source are fed at the top of the reactor and

the resultant filaments grow as the catalyst and the carbon source flow to the bottom of the reactor, where they are collected.

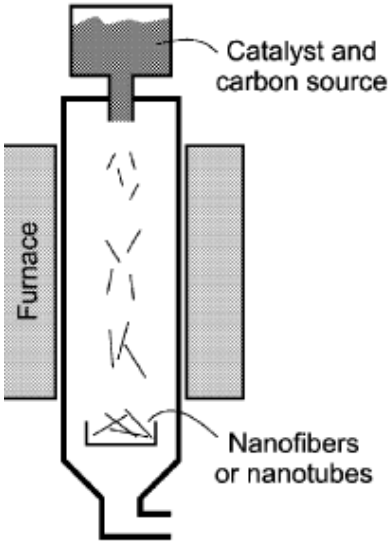

Figure 2.3: CVD vertical setup (Chhowalla et al., 2005)

The main advantages of this setup is that continuous CNTs of high purity are produced as there is no purification or removal of the nanostructures from the substrate after production (Chhowalla et al., 2005). However, the vertical flow reactor presents problems when attempting to suspend a substrate inside it. This is overcome by employing gas-phase CVD, in which the catalyst is allowed to flow into the reactor in some vapour phase. One of the reasons that make using a vertical flow reactor desirable is the ability to control the feed gas (Young et al., 1992).

The CVD method in general allows for a variety of different nanostructures to be formed. A large part of this is due to the parameters that are controlled during the synthesis process (Koziol et al., 2010).

2.7 PARAMETERS FOR CHEMICAL VAPOUR DEPOSITION

The growth and formation of CNTs is affected by many parameters, such as the carbon source, catalyst, catalyst support materials, carrier gas and synthesis temperature.

2.7.1 Carbon Source

A very wide variety of carbon sources may be used for CVD, such as hydrocarbon gases like ethylene, acetylene; other carbon sources like carbon monoxide or carbon polymers (Koziol et al., 2010); and natural carbon sources such as camphor, turpentine oil, eucalyptus oil and castor oil. However, it is worth noting that the carbon source greatly affects the morphology of the CNTs produced. Linear hydrocarbons such as methane and acetylene are thermally decomposed into atomic carbons or linear dimers/trimmers or carbons resulting in producing straight hollow CNTs. In the instances when cylindrical hydrocarbons are used, benzene, xylene and fullerene to name a few, curved CNTs are produced having bridged tube walls inside. The carbon source together with the carrier gas play a vital role in controlling the amount of tube layers. The carbon source with low carbon content at the appropriate feed rate is required for efficient synthesis of SWCNTs and MWCNTs since it simplifies control of the layer number (Endo et al., 2006). As stated above, the carbon source are required in gaseous form, if not, they are vapourized before being fed into the reactor chamber and the reactor is kept free of any oxygen in order to prevent the carbon from oxidation (Szabó et al., 2010).

2.7.2 Catalyst

The transition metal nanoparticles are required in the formation of SWCNT. The metals such as Co, Ni and Fe are mostly employed as they are able to form metastable carbides, unlike those that form very stable carbides (Mo and others from group IV and VI) or those that do not form carbides at all (Pt, Pd and Rh to name a few) (Manocha et al., 2005; Szabó et al., 2010). These catalysts may be present as organometallic compounds such as ferrocene and cobaltocene (which may be used in gas-phase CVD) or exist as compounds such as nitrates (for supported CVD). The catalyst decomposes the hydrocarbons and that the size of the particle dictates the tube diameter (Endo et al., 2006; Koziol et al., 2010).

2.7.3 Catalyst Support

The catalyst support/substrate plays a vital role in the dispersion and catalytic activity of the metal present on it. The metal characteristics on the supported catalyst depend on the metal-support interaction, which in turn depends on the nature of the support (Adams et al., 2012). The catalyst needs a suitable support material for quality and yield of CNTs. The material of the support, its surface morphology and texture properties affect the yield and quality of the grown CNTs. A strong metal-support interaction must give high metal dispersion and have high density of catalytic sites on the support. The strong interaction helps in preventing metal species accumulation forming large particles resulting in graphitic particles and defects. The control over the diameter of the catalyst particle is the key factor in controlling the diameter and number of layers of the tube, thus, supporting a catalyst on a substrate is a method applied to control the diameter of the CNTs. The substrates include quartz substrate and the use of ceramic particles such as aluminum oxide ($Al_2O_{3)}$, magnesium oxide (MgO) and zeolites. The particle's size ranges from ~100 nm to ~100 μm and the particles are mixed with a metal solution in order prepare ceramic-supported catalysts (Endo et al., 2006).

2.7.4 Carrier Gas

The role of the carrier gas in CVD is to transport the carbon source to the substrate supported catalyst (Menzel et al., 2012). The gases most commonly used as carriers, or most commonly used to provide an inert atmosphere within the reactor are: helium, argon and nitrogen (Szabó et al., 2010). The type of carrier gas in CVD can affect the structure, growth rate and densities of synthesised nanotubes as well as cause the carbon source to decompose faster or slower (Yap et al., 2004). It is important for the atmosphere within the reactor, or for the carrier gas, to be inert so as to not incite undesirable reactions (Koziol et al., 2010). Changing the conditions of the gas within the reactor will influence the quality of the product formed, as well as the quantity of product formed. The carrier gas flow plays a large part in the transfer

mechanisms occurring within the CVD reactor. The relationship between the carrier gas flow and its pressure affect the rate of diffusion in distribution of the growing substances (Menzel et al., 2012).

2.7.5 Temperature

Synthesizing CNTs at low temperatures (600 - 900°C) favours the production of MWNTs, while synthesis occurring at high temperatures (900 - 1200°C) yield SWNTs. The exact temperature ranges depend upon the choice of carbon source and catalyst support. The morphologies of the resulting carbon nanostructures via CVD synthesis change as temperature is increased. Lower temperatures may produce nanotubes while at higher temperatures other carbonaceous structures form (Koziol et al., 2010; Szabó et al., 2010).

2.8 ADSORPTION

The phenomenon in which a solid substance attaches other substances to its surface without covalent binding is known as adsorption. It is the adhesion of a chemical substance, known as the adsorbate, onto the surface of a solid, the adsorbent (Desta, 2013). Adsorption can be classified into two general types, namely physical adsorption (physisorption) and chemical adsorption (chemisorption). Physisorption is the force of attraction that exist between the adsorbent and the adsorbate molecules, also known as the Vander Waal's forces. The Vander Waal's forces have a weak forces of interaction, therefore, adsorption of this type can be reversed by heating or reducing the pressure. In the case of chemisorption, the forces of attraction that exist between the adsorbent and the adsorbate are of similar strength as that of chemical bonds, this type of adsorption cannot be easily reversed.

2.8.1 Adsorption isotherms

The adsorption isotherms are empirical relationships used to predict how much solute can be adsorbed by the adsorbent in question. The isotherms are graphical representation illustrating

the relationship between the amount adsorbed by a unit weight of adsorbent and the amount of adsorbate remaining in the test medium at equilibrium. The adsorption isotherms also shows the distribution of adsorbable solute between the liquid and solid phases at various equilibrium concentrations (Desta, 2013). The assumption basis of the adsorption isotherms are in relation to heterogeneity/homogeneity of the solid surface as well as the type of coverage and likelihood of interaction between the adsorbate species (Et and Shahmohammadi-Kalalagh, 2011). There are a number of adsorption isotherms which have been developed to understand the adsorption process. These models include a one-perameter isotherm such as Henry's Isotherm; two parameter isotherms such as, Hill-Deboer Model, Fouwler-Guggenheim, Langmuir Isotherm and Freundlich just to name a few. However, in this research, the two most well-known isotherms, Freundlich and Langmuir will be used.

- **Langmuir adsorption isotherm**

The Langmuir model is a semi – empirical isotherm derived from a proposed kinetic model. It is based on the following four assumptions:

i. The adsorbent surface is uniform, i.e. all adsorption sites are equivalent.
ii. The adsorbent molecules do not interact.
iii. All adsorption occurs through the same mechanism.
iv. A monolayer is formed at the maximum adsorption where molecules of the adsorbate do not deposit on each other as they are already adsorbed. The molecules of the adsorbate adsorb only on the free surface of adsorbent, i.e. once the site is filled no further sorption can take place on that site.

From this, it can be deduced that the surface reaches a saturation point where the maximum adsorption of the surface will be achieved. The isotherm is represented by the following linear equation (Desta, 2013; Et and Shahmohammadi-Kalalagh, 2011):

$$\frac{C_e}{q_e} = \frac{1}{q_m K_L} + \frac{C_e}{q_m}$$ **Equation 2.1**

Where:

$q_e = amount\ adsorbed\ \left(\frac{mg}{g}\right)$

$C_e =\ \ equillibrium\ concentration\ of\ metal\ ion\ \left(\frac{mg}{L}\right)$

$q_m = maximum\ amount\ of\ adsorbed\ metal\ ion\ per\ unit\ mass\ of\ sorbent\ \left(\frac{mg}{g}\right)$

$K_L = Langmuir\ constant\ related\ to\ the\ energy\ of\ adsorption\ \left(\frac{L}{mg}\right)$

- **Freundlich adsorption isotherm**

The Freundlich adsorption isotherm is an empirically derived model based on the adsorption of a heterogeneous surface. The premise of this model is that each adsorption site has its own energy of adsorption and having a heterogeneous surface implies that not all adsorption sites are equal. This model mathematically indicates that infinite loading is possible. However, practically speaking, there is a finite adsorption capacity for each adsorbent. The linear form of the Freundlich equation may be expressed as:

$$\boldsymbol{Ln\ q_e = Ln\ K_f + \frac{1}{n} Ln\ C_e}$$ **Equation 2.2**

Where:

$K_f = Freundlich\ constant\ indicating\ relative\ adsorption\ capacity\ of\ adsorbent\ \left(\frac{L}{g}\right)$

$n = Freundlich\ equation\ exponent, a\ parameter\ representing\ the\ quasi$

$- gaussian\ energetic\ heterogeneity\ of\ the\ adsorption\ surface.$

2.9 REFERENCES

Abdallah, W., 2004. Production and Characterization of Activated Carbon from Sulphonated Styrene Divinylbenzene Copolymer. MSc. Middle East Technical University.

Adams, T., Duong, B., Seraphin, S., 2012. Effect of catalyst components on carbon Nanotubes grown by Chemical Vapor Deposition. J. Undergrad. Res. Phys. 1, 1–7.

Bikshapathi, M., Verma, N., Singh, R.K., Joshi, H.C., Srivastava, A., 2011. Preparation of Activated Carbon Fibers from Cost Effective Commercial Textile Grade Acrylic Fibers. Carbon Lett. 12, 44–47.

Chhowalla, M., Milne, W.I., Teo, K.B., Singh, C., 2005. Catalytic synthesis of carbon nanotubes and nanofibers. Encycl. Nanascience Nanotechnol. 5, 1–22.

Çınar, N., Yuca, N., Karatepe, N., 2012. Effect of Hydrogen Reduction on Carbon Nanotube Synthesis. Online J. Sci. Technol. 2, 20–25.

Crundwell, F., Moats, M., Ramachandran, V., Robinson, T., Davenport, W.G., 2011. Extractive Metallurgy of Nickel, Cobalt and Platinum Group Metals. Oxford: Elsevier.

Desta, M.B., 2013. Batch Sorption Experiments: Langmuir and Freundlich Isotherm Studies for the Adsorption of Textile Metal Ions onto Teff Straw (Eragrostis tef) Agricultural Waste [WWW Document]. J. Thermodyn. https://doi.org/10.1155/2013/375830

Deventer, J. van, 2011. Selected Ion Exchange Applications in the Hydrometallurgical Industry. Solvent Extr. Ion Exch. 29, 695–718.

Dikio, E.D., Shooto, N.D., Thema, F.T., Farah, A.M., 2013. Raman and TGA study of carbon nanotubes synthesized over Mo/Fe catalyst on aluminium oxide, calcium carbonate and magnesium oxide support. Chem. Sci. Trans. 2, 1160–1173.

Ding, Y., Yang, X., Ni, J., 2006. Adsorption on the carbon nanotubes. Front. Phys. China 1, 317–322.

Endo, M., Hyasli, T., Kim, Y.A., Muramatsu, H., 2006. Development and Application of carbon nanotubes. Jpn. J. Appl. Phys. 45, 4883–4892.

Engber, D., 2005. How Does Activated Carbon Work? [online] Slate. Available at: http://www.slate.com/articles/news_and_politics/explainer/2005/11/how_does_activated_carbon_work.html [Accessed 20 August 2018].

Et, A., Shahmohammadi-Kalalagh, S., 2011. Isotherm and Kinetic Studies on Adsorption of Pb, Zn and Cu by Kaolinite. Casp. J. Environ. Sci. 9, 243–255.

Fujiwara, K., Ramesh, A., Maki, T., Hasegawa, H., Ueda, K., 2007. Adsorption of platinum (IV), palladium (II) and gold (III) from aqueous solutions onto l-lysine modified crosslinked chitosan resin. J. Hazard. Mater. 146, 39–50.

Gay, T., Kaufman, J., McGuigan, M., 2005. Stronger than steel: Carbon Nanotubes. [WWW Document]. Boston Univ. URL http://www.bu.edu/gk12/marc/Lessons/cnt/cnt_talk.pdf

Giraldo, L., Ladino, Y., Pirajánc, J.C.M., Rodríguez, M.P., 2007. Synthesis and characterization of activated carbon fibers from Kevlar. Eclética Quím. 32, 55–62.

Khurshed, A.S., Bilal, A.T., 2016. Synthesis of carbon nanotubes by catalytic chemical vapour deposition:A review on carbon sources,catalysts and substrates. Mater. Sci. Semicond. Process. 1, 97–82.

Koziol, K., Boskovic, B.O., Yahya, N., 2010. Synthesis of Carbon Nanostructures by CVD Method. Adv. Struct. Mater. 5, 23–48.

Krueger, A., 2014. Carbon nanomaterials. Beilstein J. Org. Chem. 10, 1785–1786. https://doi.org/10.3762/bjoc.10.186

Kumar, M., 2011. Carbon Nanotube Synthesis and Growth Mechanism.

Kumar, M., Ando, Y., 2010. Chemical Vapor Deposition of Carbon Nanotubes: A Review on Growth Mechanism and Mass Production.

Lakherwal, D., 2014. Adsorption of Heavy Metals: A Review. Int. J. Environ. Res. Dev. 4, 41–48.

Lee, T., Ooi, C.-H., Othman, R., Yeoh, F., 2013. Activated Carbon Fiber - The Hybrid of Carbon Fiber and Activated Carbon.

Lin, S.-H., Juang, R.-S., 2009. Adsorption of phenol and its derivatives from water using synthetic resins and low-cost natural adsorbents: A review. J. Environ. Manage. 90, 1336–1349.

Ma, X., Yang, H., Yu, L., Chen, Y., Li, Y., 2014. Preparation, Surface and Pore Structure of High Surface Area Activated Carbon Fibers from Bamboo by Steam Activation. Materials 7, 4431–4441.

Manocha, L.M., Valand, J., Manocha, S., 2005. Role of metal catalyst and substrate site for the growth of carbon nanomaterials. Carbon Sci. 6, 79–85.

Mavhungu, A., Mbaya, R.K.K., Moropeng, M.L., 2013. Recovery of Platinum and Palladium Ions from Aqueous Solution Using Grape Stalk Waste. Int. J. Chem. Eng. Appl. 4, 354–358.

Menzel, A., Goldberg, R., Burshtein, G., Lumelsky, V., Subannajui, K., Zacharias, M., Lifshitz, Y., 2012. Role of Carrier Gas Flow and Species Diffusion in Nanowire Growth from Thermal CVD. J. Phys. Chem. 116, 5524–5530.

Montoya, V.H., Servin, J.G., López, J.I.B., 2012. Thermal Treatments and Activation Procedures Used in the Preparation of Activated Carbons, in: Lignocellulosic Precursors Used in the Synthesis of Activated Carbon - Characterization Techniques and Applications in the Wastewater Treatment. InTech. 19-38.

Moore, B.C., Maciá-Agulló, J.A., 2004. Activation of coal tar pitch carbon Fibers: Physical activation vs. chemical activation. Carbon 42, 1367–1370.

Nikoloski, A.N., Ang, K.-L., 2014. Review of the Application of Ion Exchange Resins for the Recovery of Platinum-Group Metals From Hydrochloric Acid Solutions. Miner. Process. Extr. Metall. Rev. 35, 369-389.

Oke, D., Ndlovu, S., Sibanda, V., 2014. Removal of platinum group metals from dilute process streams: Identification of influential factors using DOE approach. J. Environ. Chem. Eng. 2, 1061–1069.

Parodi, A., Vincent, T., Pilsniak, M., Trochimczuk, A.W., Guibal, E., 2008. Palladium and platinum binding on an imidazol containing resin. Hydrometallurgy 92, 1–10.

Ramahali, T., Mahlangu, T., 2010. Effluent treatment: what role can modified waste/biomass play in the local platinum industry - a review. South Afr. Inst. Min. Metall. 239-246.

Ramesh, A., Hasegawa, H., Sugimoto, W., Maki, T., Ueda, K., 2008. Adsorption of gold (III), platinum(IV) and palladium(II) onto glycine modified crosslinked chitosan resin. Bioresour. Technol. 99, 3801–3809.

Renner, H., 1992. Platinum group metals and compounds, Ullmann's Encyclopedia of Industrial Chemistry. VCH Publishers, Weinheim, Germany.

Ryan, A., Clarke, B., Atilan, O., Watts, J., Trickey, S., 2010. Recycling: volume, momentum and consequences for PGMs [WWW Document]. URL http://www.saimm.co.za/Conferences/Pt2010/383-386_Ryan.pdf (accessed 3.20.16).

Shifrina, P., 2011. Synthesis of Carbon Nanotubes. 1-5. Available at: http://www.physik.fu-berlin.de/einrichtungen/ag/ag-reich/lehre/Archiv/ss2011/docs/Polina_Shifrina-Handout.pdf

Sittig, M., 1980. Carbon and Graphite Fibers: Manufacture and applications. Noyes, Park Ridge, NJ.

Szabó, A., Perri, C., Csató, A., Giordano, G., Vuono, D., Nagy, J.B., 2010. Synthesis Methods of Carbon Nanotubes and Related Materials. Materials 3, 3092–3140.

Wu, C., 2006. Chemical Vapor Deposition of Carbon Nanostructures and Carbon Nanotubes-Reinforced Composites. MSc. University of Rochester.

Yap, Y.K., Kayastha, V., Hackney, S., Dimovski, S., Gogotsi, Y., 2004. Effect of Carrier Gas on the Growth Rate, Growth Density, and Structure of Carbon Nanotubes. Mater. Res. Soc. Symp. Proc. 818, 31.1-31.6.

Young, G.W., Hariharan, S.I., Carnahan, R., 1992. Flow Effects in a Vertical CVD Reactor. SIAM J. Appl. Math. 52, 1509–1532.

Zaini, M.A.A., Amano, Y., Machida, M., 2010. Adsorption of heavy metals onto activated carbons derived from polyacrylonitrile fiber. J. Hazard. Mater. 180, 552–560.

Zhao, J., Buldum, A., Han, J., Lu, J.P., 2002. Gas molecule adsorption in carbon nanotubes and nanotube bundles. Nanotechnology 13, 195–200.

3

EXPERIMENTAL TECHNIQUES

3.1 INTRODUCTION

The materials and experimental procedures used in the synthesis of activated carbon fiber (ACF), synthesis of carbon nanotubes / nanomaterials (CNT / CNT) and the adsorption of platinum are described in this Chapter. This Chapter is made up of three main sections, the first section being material acquisition and preparation (section 3.2). All materials used in the study and necessary material preparations are described in this section. The second section is the experimental techniques (section 3.3), in which all methods and laboratory work conducted are described. The last section (section 3.4) describes the analytical techniques used to characterize the ACF and CNT, and the determination of metal concentration in solution. At all times prior to and during the experiments, safety was considered.

3.2 MATERIAL ACQUISITION AND PREPARATION

The ion exchange resins (IER) used in this study was Amberlite xad-4, a non-ionic cross-linked polymer, purchased from Sigma Aldrich, South Africa. The gases used were nitrogen (N_2) baseline 99 %, hydrogen (H_2) and Argon (Ar). All the gases used were purchased from AFROX, South Africa. All chemicals iron (III) nitrate ($Fe(NO_3)_3.9H_2O$), sodium hydroxide (NaOH), hydrochloric acid (HCl), aluminium oxide (Al_2O_3), calcium carbonate ($CaCO_3$), magnesium oxide (MgO) and potassium tetrachloroplatinate (II) (K_2PtCl_4) were provided by Merck and Sigma-Aldrich, South Africa.

3.2.1 Activated carbon fiber synthesis preparation: resin impregnation

Before the activation was carried out, approximately 16 g of the IER was impregnated with NaOH solutions of varying concentrations, i.e., 8, 16, 24, 32, and 40 wt%. The amount of NaOH solution used was just adequate to cover the resins in the crucibles. The impregnated IERs were placed and dried at 120 ˚C in a vacuum furnace for 24 hours so as to ensure sufficient saturation of the resins with NaOH whilst having minimal water.

3.2.2 Determination of gases produced from the pyrolysis of resins

One of the key parameters in the synthesis of CNT is the carbon source. It is important to know the carbon source as it has an effect on the choice of the catalyst used and thus the growth of the nanotubes. In order to determine the gas emitted from the pyrolysis of the resin in this study (amberlite XAD4), 2 – 3 g of the resin was weighed onto a quartz boat and was placed in a tubular furnace. One end of the furnace was connected to an inlet flow of nitrogen gas, which was used as a carrier gas and also to create an inert atmosphere. The other end of the furnace (outlet) was connected to a gas collector. Both ends of the furnace were well sealed and made airtight using correct fitting, grease sealant and parafilm.

The gas produced from the pyrolysis of resins at a temperature of 450 ˚C, 500 ˚C, 600 ˚C, 700 ˚C, 800 ˚C and 900 ˚C was collected. Once the gas was collected, it was analysed using a gas chromatography and mass spectroscopy (GC – MS). The GC – MS procedure used is in section 3.4.

3.2.3 Carbon nanotube synthesis preparation: catalyst preparation

For the preparation of the catalyst support for CNT synthesis, 13 g of iron (III) nitrate ($Fe(NO_3)_3.9H_2O$) was weighed into 250 mL conical flask and dissolved with 45 mL of distilled water measured using 50 mL volumetric flask. About 10 g of the various supports (Al_2O_3/ $CaCO_3$/ MgO) were weighed separately into 250 mL crucibles. The dissolved $Fe(NO_3)_3.9H_2O$ mixture was added drop-wise onto the chosen metal-supports. Thereafter, the catalyst metal-support mixtures were stirred in an incubator at speed of 120 rpm and temperature of 25 ˚C for 30 minutes. Afterwards the mixtures were dried in an oven at 120 ˚C for 12 hours, then ground into powder using a pestle and motor and then calcined in a furnace for 16 hours at 400 ˚C. Once the calcined mixture had cooled, it was placed in a crucible for storage before use in the synthesis of the CNT.

3.3 EXPERIMENTAL TECHNIQUES

The main experiments that were conducted are described in detail in this section. Firstly the production of ACF, then the production of the CNT and lastly, metal adsorption using ACF.

3.3.1 Production of Activated Carbon Fiber

The two methods that can be used to synthesize ACFs are physical activation and chemical activation (Abdallah, 2004; Lee et al., 2014). For this study, the chemical activation technique was employed in the production of ACF from ion exchange materials. The activation process was carried out in order to remove disorganized carbons that close the pores in the ACF.

Basically, activation helps increase the number of pores and also expands the size of the existing pores, thus producing porous carbon with readily accessible pore structure and large internal surface area leading to a high adsorption capacity of adsorbent.

The chemical activation technique was chosen over the physical activation method because chemical activation is known to have a higher porosity development than the physical activation (Montoya et al., 2012; Moore and Maciá-Agulló, 2004). Furthermore, in the case of activated carbon fibers (ACF), chemical activation maintains the fiber morphology better and produces a higher yield. In comparison to physical activation, chemical activation has shorter activation times and carbonization and activation process are able to be conducted in one step (Montoya et al., 2012; Moore and Maciá-Agulló, 2004). A horizontal tube furnace was used for the production of ACF to allow a cross flow of gases in an inert atmosphere.

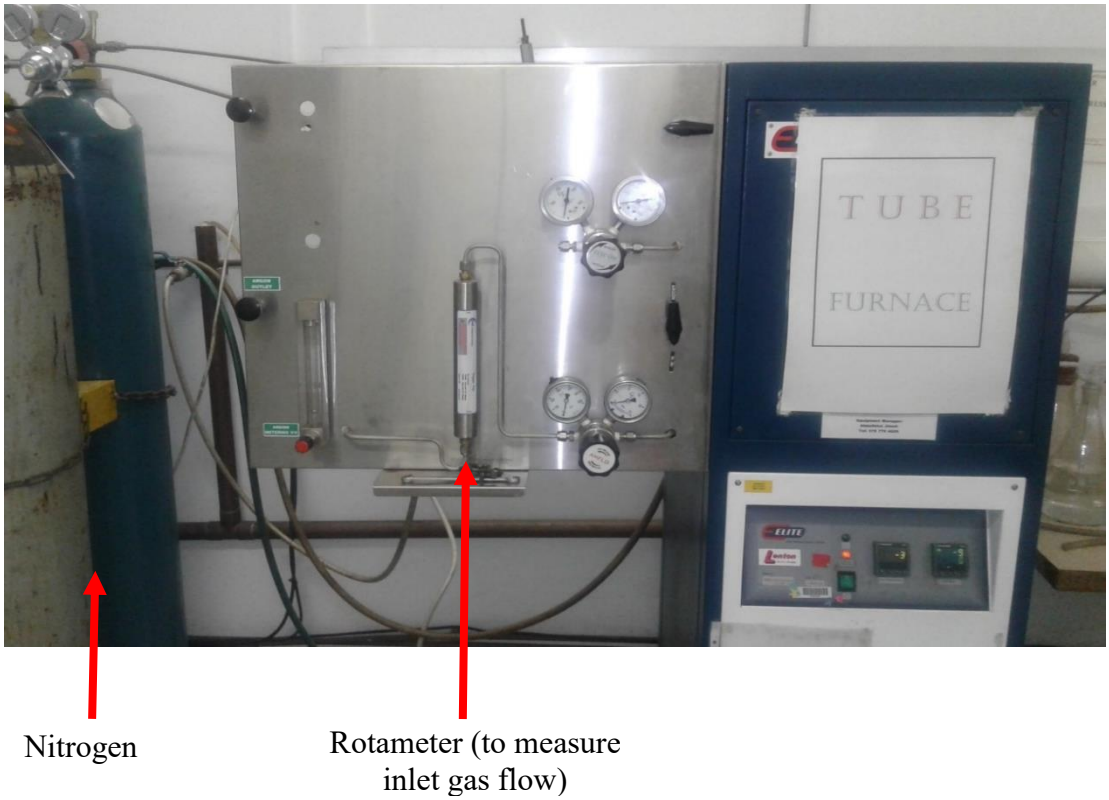

Figure 3.1: Experimental setup for the production of ACF.

After the NaOH impregnated samples were dried (as already discussed in section 3.2.1), the mixtures were activated in a tube furnace in the presence of nitrogen gas in order to create an inert atmosphere. The mixtures were heated in the tube furnace in Figure 3.1 above, at a rate of 6 ˚C/min from room temperature to the desired activation temperature, ranging from 600 ˚C – 1000 ˚C for an hour. Once activation was completed, samples were allowed to cool to room temperature before being removed from the furnace. Thereafter, the samples were washed with HCl (to neutralized the samples) and then thoroughly rinsed with distilled water before filtering and drying in a vacuum furnace at 120 ˚C for 24 hours. A total of 25 experiments were conducted as can be seen in Table 3.1. This table indicates the various activation temperatures used and the corresponding concentration of NaOH.

Table 3.1: Experimental runs for the activated carbon fiber synthesis.

Run	Temperature	NaOH WT %
1	600	40
2	700	40
3	800	40
4	900	40
5	1000	40
6	600	32
7	700	32
8	800	32
9	900	32
10	1000	32
11	600	24
12	700	24
13	800	24
14	900	24
15	1000	24
16	600	16
17	700	16
18	800	16
19	900	16
20	1000	16
21	600	8
22	700	8
23	800	8
24	900	8
25	1000	8

3.3.2 Production of CNT

The three most common methods for synthesis of CNT are arch discharge, laser ablation and chemical vapour deposition (CVD) (Eatemadi et al., 2014; Prasek et al., 2011; Soutter, 2012). For the production of CNT in this study, the CVD methodology was used to grow the nanomaterial as it has a high production yield and quality, lower production cost and easily attainable equipment for the experiments. Of the CVD methods, the fixed catalyst method was chosen, as the residence time could be easily controlled in order to promote growth of CNTs.

Based on the aforementioned reasons, a horizontal tube furnace was used for the production of CNT as can be seen in Figure 3.2. A water bubbler was used to verify that the gas outlet flow was purged out into the atmosphere.

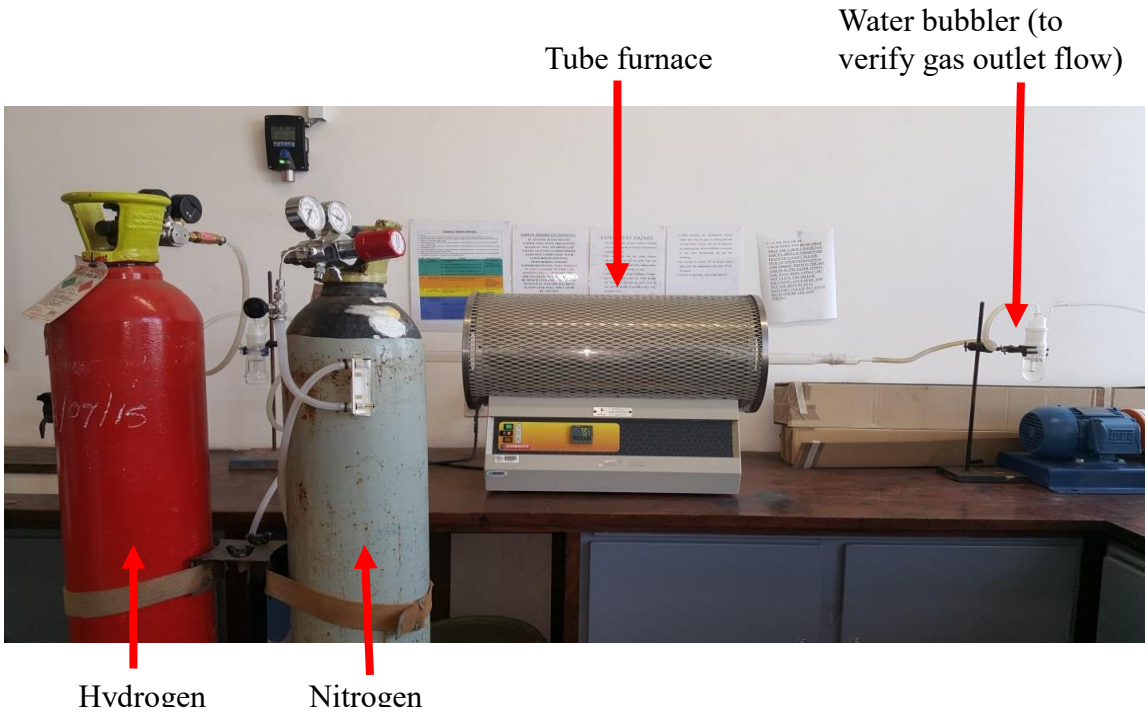

Figure 3.2: Picture of the experimental setup for the production of carbon nanotubes.

For each run, 3g of resin and 0.2g of iron in the respective catalyst support were measured using a gravimetric scale and placed in quartz boats. The catalyst material was placed first inside the front end of the tube followed by the resin so that the carbon source would be released by the resin and allowed to flow over the catalyst. The ends of the tube were sealed using Parafilm® in order to prevent gas leakage. The system was then purged with nitrogen for 10 minutes to evacuate the system of any other gases and to create an inert atmosphere. After 10 minutes, the nitrogen flow was set at 0.2 litres per minute (LPM). Thereafter, the hydrogen flow was introduced and set at about 0.12 LPM. The furnace was then switched on and allowed to reach the setpoint temperature of 800˚C. Each run then took place for 30 minutes at the setpoint temperature. After the required time, the hydrogen gas was switched off and the

furnace was allowed to cool to room temperature before collecting and storing the catalyst support samples. Table 3.2 shows the experimental design for the production of CNT's in which the effect of type of catalyst support and unsupported catalyst support was investigated.

Table 3.2: Experiments conducted to determine the effect of varying metal support on the production of CNTs

Run	Catalyst support	Carrier gas (200 mL/min)	Reducing agent (114 mL/min)	Temperature	Time (minutes)
1	Unsupported Fe (0.20g)	Nitrogen	Hydrogen	800	30
2	Fe - MgO (1.33g)	Nitrogen	Hydrogen	800	30
3	Fe - Al_2O_3 (1.65g)	Nitrogen	Hydrogen	800	30
4	Fe - $CaCO_3$ (10.67g)	Nitrogen	Hydrogen	800	30

Table 3.3 shows the experimental design of the second set of experiments conducted in the synthesis of CNT's. In this set of experiments, the effect of carrier gas on the production of CNT's was investigated.

Table 3.3: Experiments conducted to determine the effect of carrier gas and transition metal support on the production of CNTs.

Run	Catalyst support	Carrier gas (200 mL/min)	Reducing agent (114 mL/min)	Temperature	Time (minutes)
1	Unsupported Fe (0,20g)	Nitrogen	Hydrogen	800	30
2	Fe - MgO (1,33g)	Nitrogen	Hydrogen	800	30
3	Unsupported Fe (0,20g)	Argon	Hydrogen	800	30
4	Fe - MgO (1,33g)	Argon	Hydrogen	800	30

Table 3.4 shows the design of experiments method used in order to determine the relationship between the carrier gas flow rate and the difference in temperature when using a 2-staged furnace for resin pyrolysis and CNT formation.

Table 3.4: Effect of carrier gas flow rate and change in temperature for each of the furnaces in the double staged furnace.

Run	Catalyst support	Argon Flowrate (mL/min)	Hydrogen Flowrate (mL/min)	Stage 1 Temp (˚C)	Stage 2 Temp (˚C)	Time (minutes)
1	Fe - MgO (1,33g)	266	90	500	950	10
2	Fe - MgO (1,33g)	266	90	700	950	10
3	Fe - MgO (1,33g)	266	90	700	750	10
4	Fe - MgO (1,33g)	266	90	500	750	10
5	Fe - MgO (1,33g)	266	150	500	750	10
6	Fe - MgO (1,33g)	266	150	700	750	10
7	Fe - MgO (1,33g)	266	150	700	950	10
8	Fe - MgO (1,33g)	266	150	500	950	10

3.3.3 Metal Adsorption Using Activated Carbon Fibers

Analytical techniques outlined in detail in section 3.4 of this chapter were employed to characterize the synthesized ACF and the CNF. After the characterization the synthesized ACF were used in batch adsorption experiments to generate adsorption isotherms in order to determine and investigate the adsorption mechanisms and also to calculate the maximum adsorption capacity.

For the adsorption experiments, 0.1g of ACF was placed in a 100 mL conical flask which contained 30 mL of potassium tetrachloroplatinate solution of three different concentrations of 100, 10 and 0.1 ppm of platinum. The pH was adjusted to 2.0, using HCl and NaOH solutions. The mixtures were placed in a shaker and then shaken at 100 rpm at a temperature of 30 ˚C. Solutions samples were collected at various time intervals (20, 40, 60, 90 and 150 minutes) and

analyzed for platinum concentration using inductively coupled plasma mass spectrometry (ICP- MS).

3.4 ANALYTICAL TECHNIQUES

Various analytical techniques were used to characterize the synthesized ACF and CNT. The details of the procedures of the various analytical techniques used in the present study are discussed in this section.

3.4.1 Surface Topography and Morphological analysis

The surface topography and morphology of the ACF and CNT samples were determined after drying and cooling of the synthesized samples, using Carl-Zeiss Sigma Scanning Electron Microscope (SEM) equipped with an energy-dispersive X-ray spectroscopy (EDX) mechanism, and operated under vacuum between $7.23x10^{-10}$ –$1.7x10^{-9}$ Torr (Zeiss AG, 2016). The samples used for the SEM analysis were prepared by depositing the synthesized ACF/CNT onto the specimen-stubs which were covered with conductive double sticky carbon tape. Prior to the examination, the samples were sputter-coated with Au-Pd in order to prevent electrical charging during the SEM analysis. The imaging was conducted in the high vacuum mode under an accelerating voltage of 5 kV using the SEM seen in Figure 3.3.

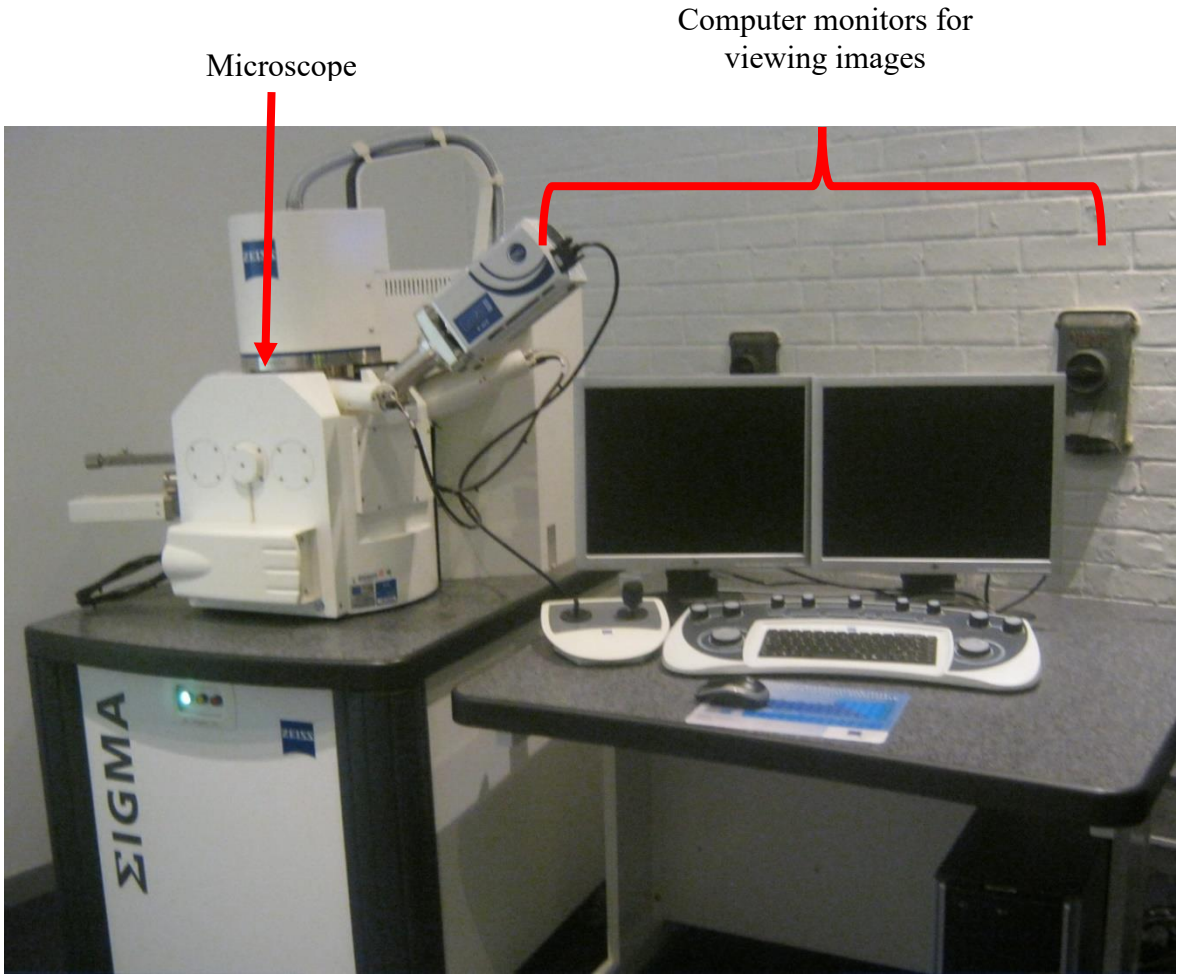

Figure 3.3: Picture of the SEM (Carl Zeiss Sigma model, manufactured from Germany), picture taken at the School of Chemical and Metallurgical Engineering, University of the Witwatersrand, used in this study.

3.4.2 Surface area, porosity and adsorption isotherm analysis

A Micromeritics TriStar 3000 Surface Area and Porosity Analyser, as can be seen in Figure 3.4 below, was used to determine the surface areas and porosities of the materials. A sample with a mass of 0.2 g was degassed in nitrogen at 150 ˚C for 5 hrs prior to analysis using a Micromeritics flow Prep 060, sample degas system (Micromeritics Instrumentation Corporation, 2007). The analysis adsorptive gas used was N_2 and the analysis bath temperature was -195.80 ˚C. Using the equation developed by Brunauer – Emmett- Teller (BET), the

specific surface area, pore volume and pore sizes of the produced ACF and CNT were determined.

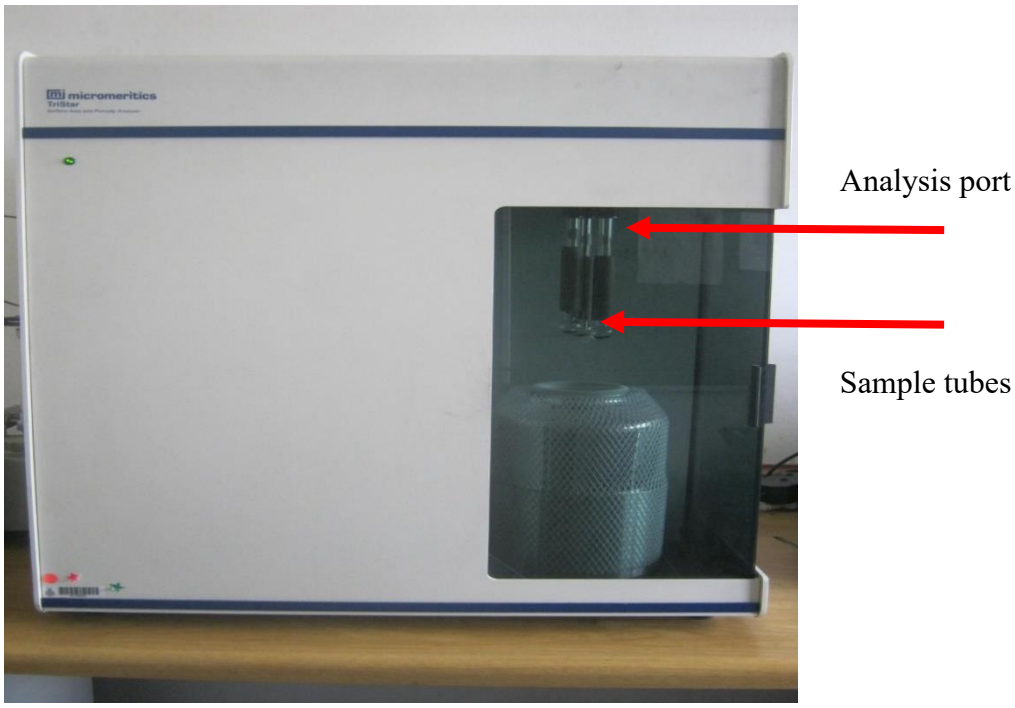

Figure 3.4: Picture of the BET analyser (Micromerotics Tristar 3000, manufactured by Micromeritics in the United Stated of America) picture taken at the School of Chemistry, University of the Witwatersrand, used in this study.

3.4.3 Thermal stability and material purity analysis

The thermogravimetric analysis (TGA) was used to study the thermal stability of carbon deposits and also to distinguish the forms of carbon species formed according to their combustion temperatures, therefore giving an indication in the purity of the carbon material produced (Li et al., 2004). The TGA was conducted using a Perkin Elmer STA 6000 to measure the change in weight in relation to the change in annealing temperature of the ACF and the CNT. The TGA was also used to determine the purity of the synthesized CNTs. Approximately 5 mg of each sample was placed inside a crucible, mounted on a stage and then placed inside the furnace (Figure 3.5 below). Once the sample was place in the furnace, Nitrogen gas was

used to purge the system of any contaminants then the material (ACF/CNT) was heated at a heating rate of 10 ˚C/min from 30 to 900 ˚C, in air at a flow rate of 50 mL/min (PerkinElmer, 2016).

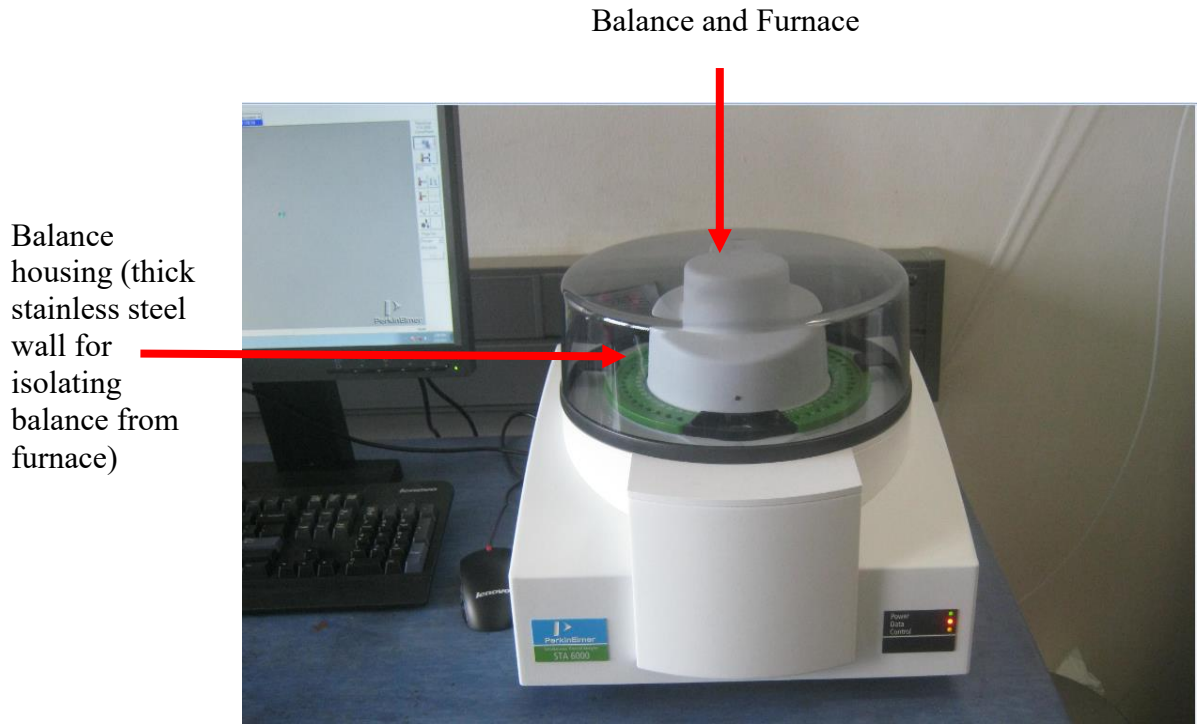

Figure 3.5: Picture of the TGA (Perkin Elmer STA 6000, manufactured by PerkinElmer Inc. in the USA), picture taken at the School of Chemistry, University of the Witwatersrand, used in this study.

3.4.4 Functional group determination

In order to determine the functional groups present on the surface of the ACF, the Fourier Transform Infrared Spectroscopy (FTIR) was used. The FTIR used in this study can be seen in Figure 3.6. The FTIR spectra was measured directly using the Bruker Tensor device in the range 500 cm^{-1} to 4000 cm^{-1}. From the FTIR analysis, an absorbance spectra is generated in which each wavelength on the spectra represents different types of bonds and functional groups.

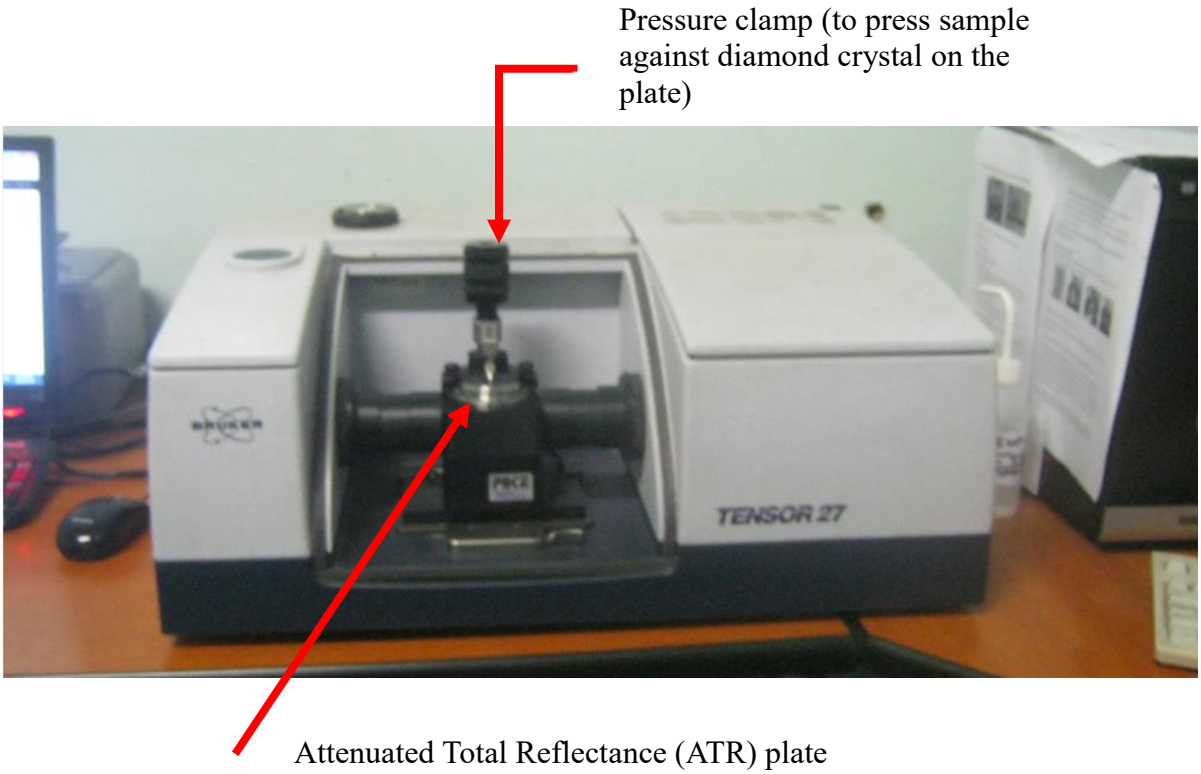

Figure 3.6: Picture of the FTIR (Bruker Tensor 27, manufactured by Bruker in Germany), picture taken at the School of Chemistry, University of the Witwatersrand, used in this study.

3.4.5 Carbon form analysis

In order to ascertain the form of carbon formed during the synthesis of the CNT, the Raman spectroscopy was used. The Raman (model Jobin-Yvon LabRAM HR) spectrometer equipped with an Olympus BX41 microscope attachment was used (Figure 3.7) to determine if single-walled CNTs (SWCNTs) or multi-walled CNTs (MWCNTs) were formed, and also to assess the quality of the CNTs. Approximately 5 mg of the synthesized CNTs was inserted in 1.5 μm diameter of the equipment's chamber. In order to minimize heat, the power was set to 1.2MW.

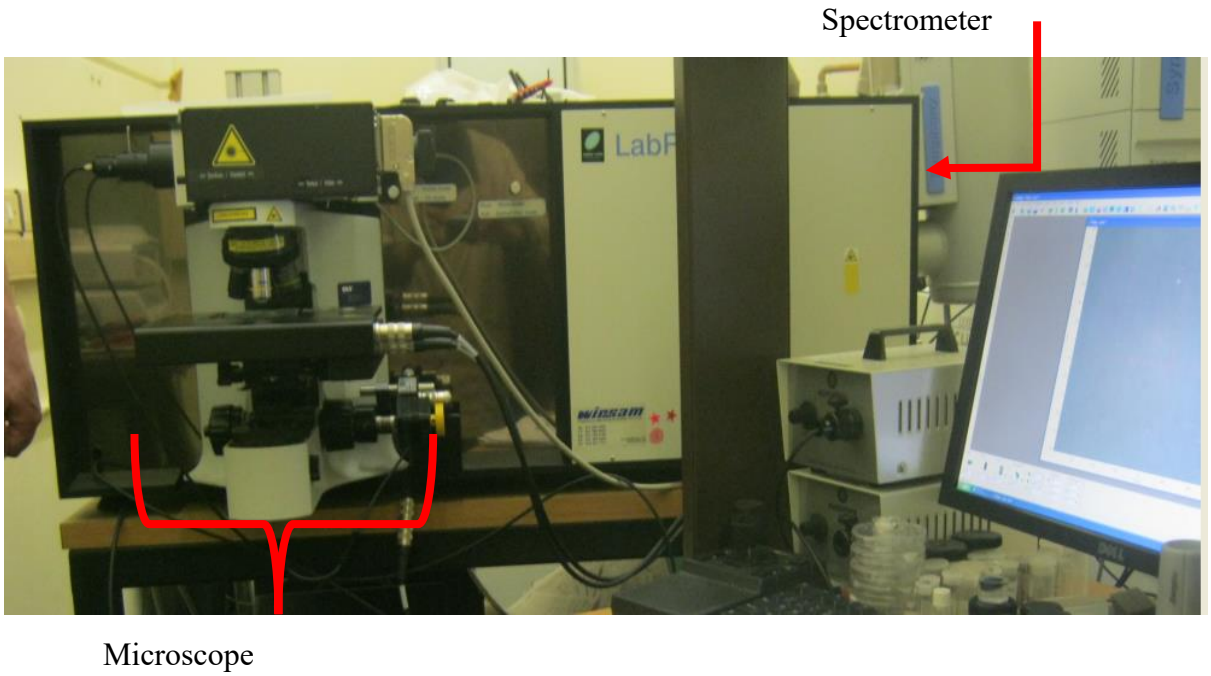

Figure 3.7: Picture of the Raman (Jobin – Yvon LabRAM HR), picture taken at the School of Biology, University of the Witwatersrand, used in this study.

3.4.6 Identification of gas from the pyrolysis of resin

In order to determine the gases that were emitted from the pyrolysis of the resin, the gas was collected in a gas collector instrument and manually injected into a gas chromatography – mass spectroscopy (GC-MS). The GC Agilent© 7890B and MS Pegasus 4D GCXGC from Leco was used, as can be seen in Figure 3.8. About 0.5 mL of the collected gas was injected into the injection port of the GC-MS.

- **The gas chromatography method used for manual gas injection**

Column type (Rxi-5SilMS), with an internal diameter of 250 µm and film thickness of 0.25 µm with a maximum temperature of 350 ˚C was used. Carrier gas was helium; front inlet type was split/splitless with a split mode of 50:1. The flow rate was 1 mL/min at constant flow while front inlet temperature was 250 ˚C. The initial oven temperature of 50 ˚C was maintained for

0.5 min and ramped at 10 ˚C /min to 100 ˚C and ramped again at 15 ˚C /min to 250 ˚C. Transfer line temperature was 225 ˚C.

- **The MS method used**

Acquisition delay of 0 min, mass range of between 5 to 450 m/z, with acquisition rate of 10 spectra/second and electron energy (ionization energy) of -70 eV was used. The ion source temperature was 250 ^{o} C.

- **Data processing method**

The base line offset of 1 (just above the noise) was used, with a peak width of 4 seconds and signal to noise (S/N) ratio of 100. The library search mode was normal and forward. The number of library hit was 10, while the minimum molecular weight allowed was 5 and maximum molecular weight was 450. Mass threshold was 2% and minimum similarity before name was assigned was 50%. The library used was Replib and mainlb from the national institute of standards and technology (NIST).

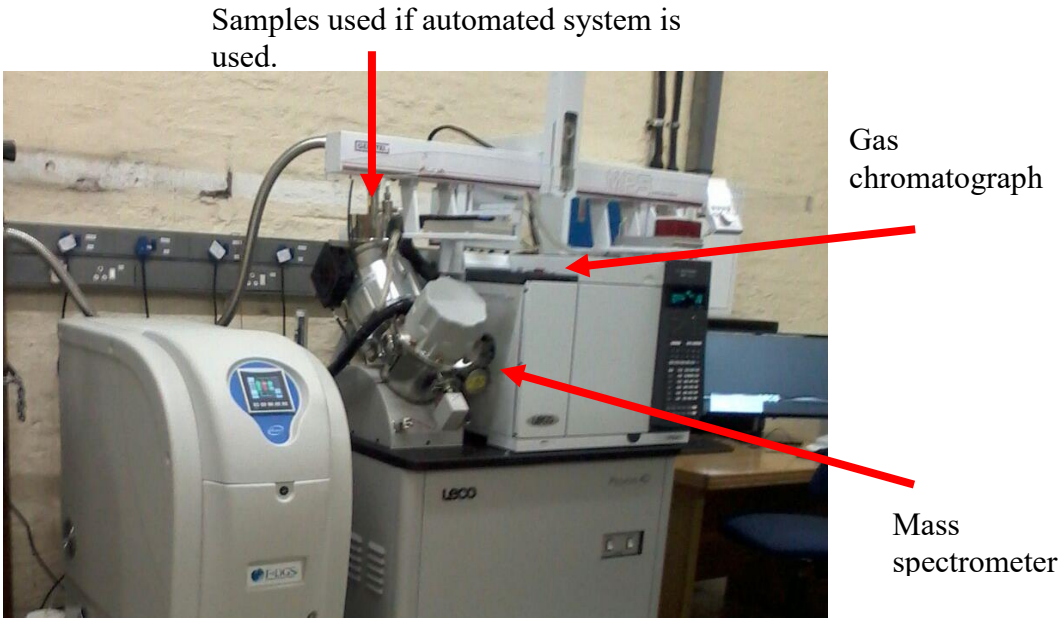

Figure 3.8: Picture of the GC – MS (GC Agilent© 7890B and MS Pegasus 4D GCXGC from Leco) taken at the School of Chemistry, University of the Witwatersrand, in this study.

3.5 REFERENCES

Abdallah, W., 2004. Production and Characterization of Activated Carbon from Sulphonated Styrene Divinylbenzene Copolymer (Thesis). Middle East Technical University, Ankara, Turkey.

Eatemadi, A., Daraee, H., Karimkhanloo, H., Kouhi, M., Zarghami, N., Akbarzadeh, A., Abasi, M., Hanifehpour, Y., Joo, S.W., 2014. Carbon nanotubes: properties, synthesis, purification, and medical applications. Nanoscale Res. Lett. 9, 393.

Lee, T., Ooi, C.-H., Othman, R., Yeoh, F., 2014. Activated Carbon Fiber - The Hybrid of Carbon Fiber and Activated Carbon. Rev. Adv. Mater. Sci. 36, 118–136.

Li, Q., Yan, H., Zhang, J., Liu, Z., 2004. Effect of hydrocarbons precursors on the formation of carbon nanotubes in chemical vapor deposition. Carbon 42, 829–835.

Micromeritics Instrumentation Corporation, 2007. TriStar 3000 Operators Manual. Micromeritics Instrumentation Corporation, USA.

Montoya, V.H., Servin, J.G., López, J.I.B., 2012. Thermal Treatments and Activation Procedures Used in the Preparation of Activated Carbons, in: Lignocellulosic Precursors Used in the Synthesis of Activated Carbon - Characterization Techniques and Applications in the Wastewater Treatment. InTech.

Moore, B.C., Maciá-Agulló, J.A., 2004. Activation of coal tar pitch carbon Fibers: Physical activation vs. chemical activation. Carbon 42, 1367–1370.

Prasek, J., Drbohlavova, J., Chomoucka, J., Hubalek, J., Jasek, O., Adam, V., Kizek, R., 2011. Methods for carbon nanotubes synthesis—review. J. Mater. Chem. 21, 15872–15884.

Soutter, W., 2012. Synthesis of Carbon Nanotubes [WWW Document]. AZoNano.com. URL https://www.azonano.com/article.aspx?ArticleID=3029 [accessed 1.16.18].

Zeiss AG, C., 2016. Scanning Electron Microscopes (SEM) Manual. Zeiss, Germany.

4

RESULTS AND DISCUSSION

4.1 INTRODUCTION

The characterization techniques used in this research have all been described in the previous chapter (Chapter 3). This chapter presents results and discussions of the aforesaid characterization techniques used to characterize the synthesized activated carbon fibers (ACFs) and carbon nanomaterial (CNTs), and also, to determine the adsorptivity of platinum from dilute solutions using the synthesized ACF. The Results and Discussion Chapter comprises of 3 main sections, firstly the results and discussion of the production of the activated carbon fiber (section 4.2), then the results and discussion of the production of the carbon nanotubes (section 4.3), and lastly, the results and discussion pertaining to the adsorption of platinum (section 4.4).

4.2 PRODUCTION OF ACTIVATED CARBON FIBER

The synthesized ACF characterized through the use of analyzing the surface morphology using SEM; surface area and pore size determination by the Brunauer – Emmett – Teller equation;

thermal stability and carbon purity through the use of TGA; the functional group determination through the use of FTIR; the carbon form analysis of the CNTs through the use of the Raman Spectroscopy: and the pyrolysis gas analysis through using the GC-MS.

4.2.1 Surface Topography and Morphological Characterization of the Activated Carbon Fiber

The topography and morphology of the activated carbon (AC – fiberous and non fiberous) activated at different NaOH concentrations and at a temperature of 1000 °C are presented in Figure 4.1.

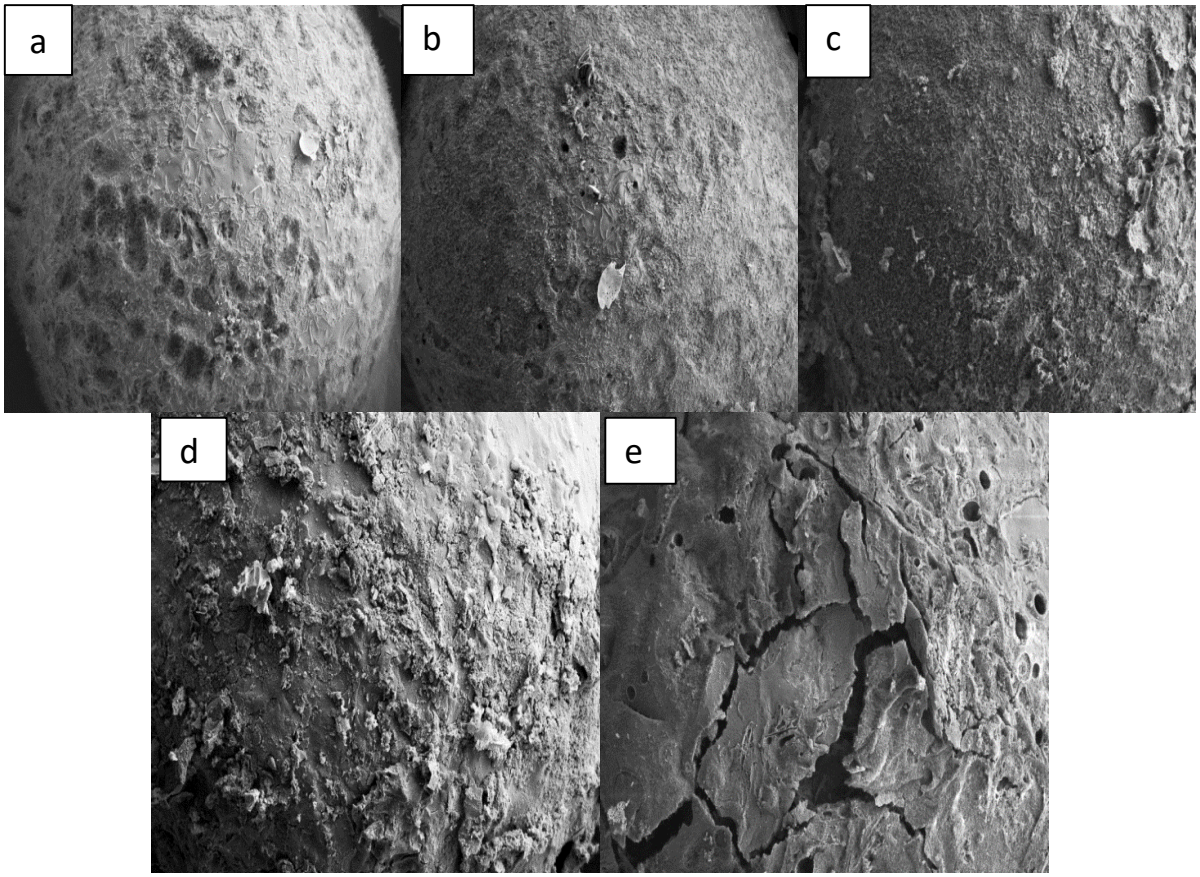

Figure 4.1: SEM images at 1000X magnification of ion exchange resin (IER) activated at 1000 °C using different NaOH concentrations: (a) 8 wt% NaOH, (b) 16 wt% NaOH, (c) 24 wt% NaOH, (d) 32 wt% NaOH, and (e) 40 wt% NaOH.

The figure 4.1 (e) shows that at higher concentrations of activation agent results in greater development of pores and also a significant change to the texture of the resin surface, as can be seen from the raptures and cracks on the surface. Lower NaOH concentrations resulted in minimal defects to the ion exchange resin (IER) surface (Figure 4.1-a). From the ACF point of view, greater micropore development provides an additional surface area for adsorption. The production of ACF using the higher concentration of NaOH is, therefore, the preferred condition.

The effect of temperature on the texture and physical form of the prepared ACF is shown in Figure 4.2. The figure shows samples activated with 40 wt% NaOH at temperatures ranging from 600 to 1000 °C.

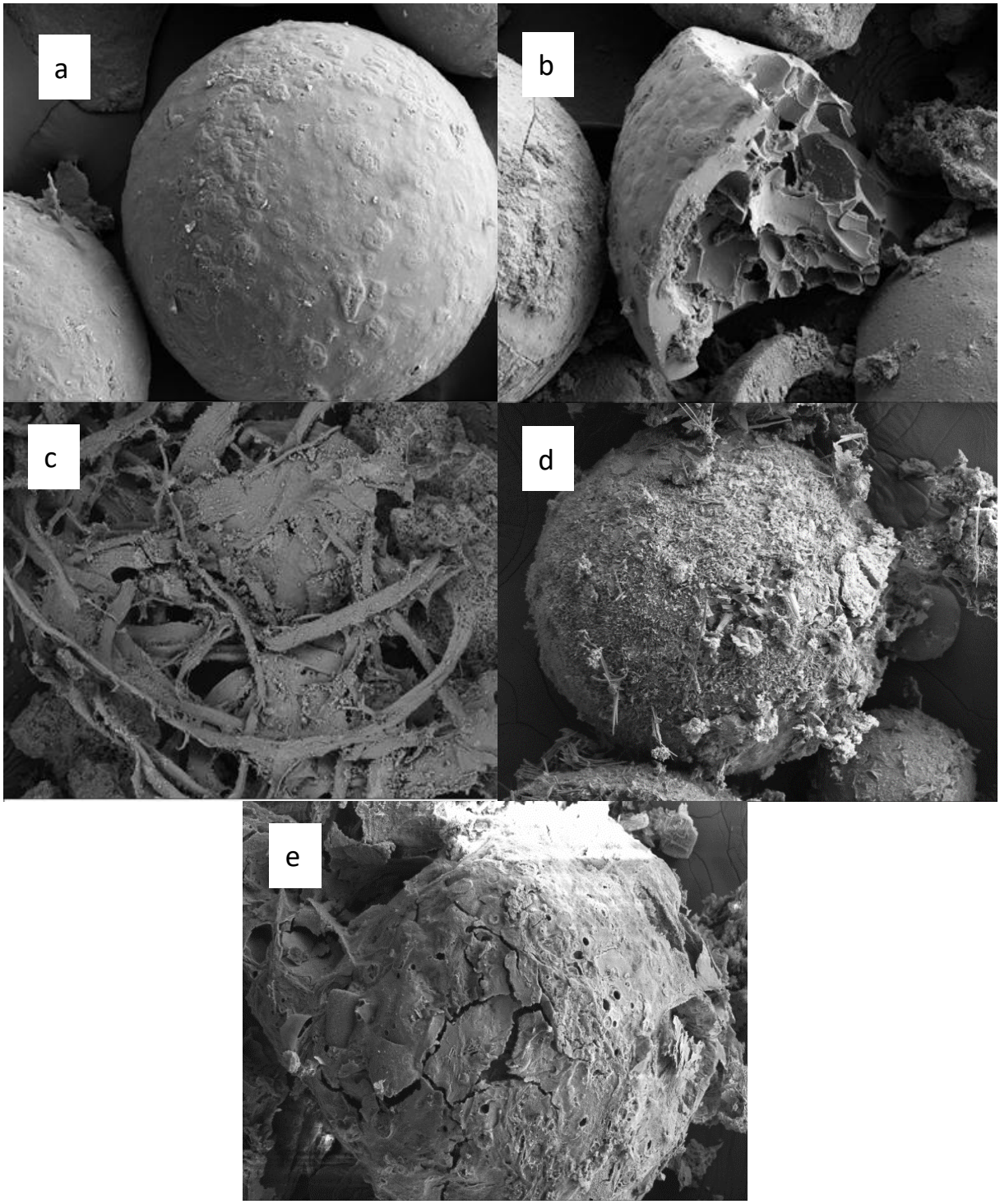

Figure 4.2: SEM images at 500X magnification of IER activated with 40 wt% NaOH and at different temperatures: (a) 600 °C, (b) 700 °C, (c) 800 °C, (d) 900 °C, and (e) 1000 °C.

The results show that increasing temperature resulted in some of the resins decomposing and having their spherical shape dismantled. The disintegration of the activated material is probably due to the removal of volatiles and disorganized carbons as the temperature increases.

The IER activated at 600 °C (Figure 4.2-a) has an uneven surface while activation carried out at 700 °C (Figure 4.2-b) results in broken up activated material revealing micropores and hollow spaces/cavities within the resin structure. At temperatures from 800 °C - 1000 °C (Figure 4.2-c, Figure 4.2-d and Figure 4.2-e), there is development of fibers on the surface of the activated material at a micro scale, whereas for the IER activated at temperatures below 800 °C no formation of fibers were found. In Figure 4.3 shows well-developed fibers were produced at higher activating temperatures of 800 to 1000 °C.

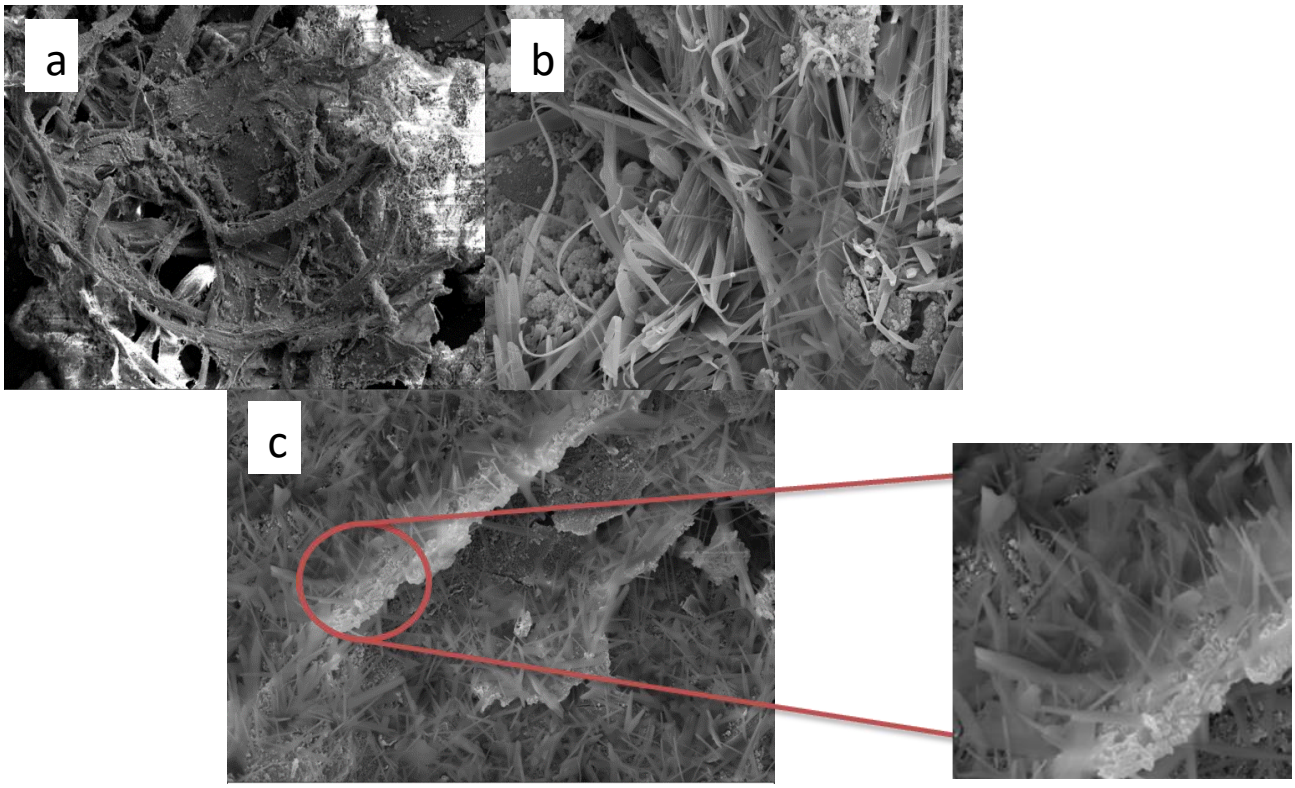

Figure 4.3: SEM images of ACF activated with 40 wt% NaOH at three different temperatures: (a) 800 °C, at a magnification of 15000X, (b) 900 °C, at a magnification of 15000X, and (c) 1000 °C, at a magnification of 15000X

Fibers produce at an activation temperature of 800 °C were visible from a resolution of 500X, fibers produced at an activation temperature of 900 and 10 000 °C were visible from a magnification of 15 000X. This indicates that there was a development of smaller fibers formed at activation temperatures greater than 900 °C in comparison to fibers formed at an activation temperature of 800 °C. However, at the highest temperature of 1000 °C (Figure 4.3-c), the fibrous structures showed signs of weathering, resulting in shorter fibrils on the ACF surface. The reduction in the fiber size at higher temperatures can be attributed to sintering, in which the adjacent fibrils partially coalesce and form a single fibril strand (Bhatia et al., 1997).

4.2.2 Surface Area Analysis

The single point surface area AC activated at temperatures ranging from 600 to 1000 °C, using NaOH of concentrations ranging from 8 to 40 wt%, is presented in a form of a contour plot in Figure 4.4, in which surface area ranges are represented by different colors as can be seen by the scale on the graph.

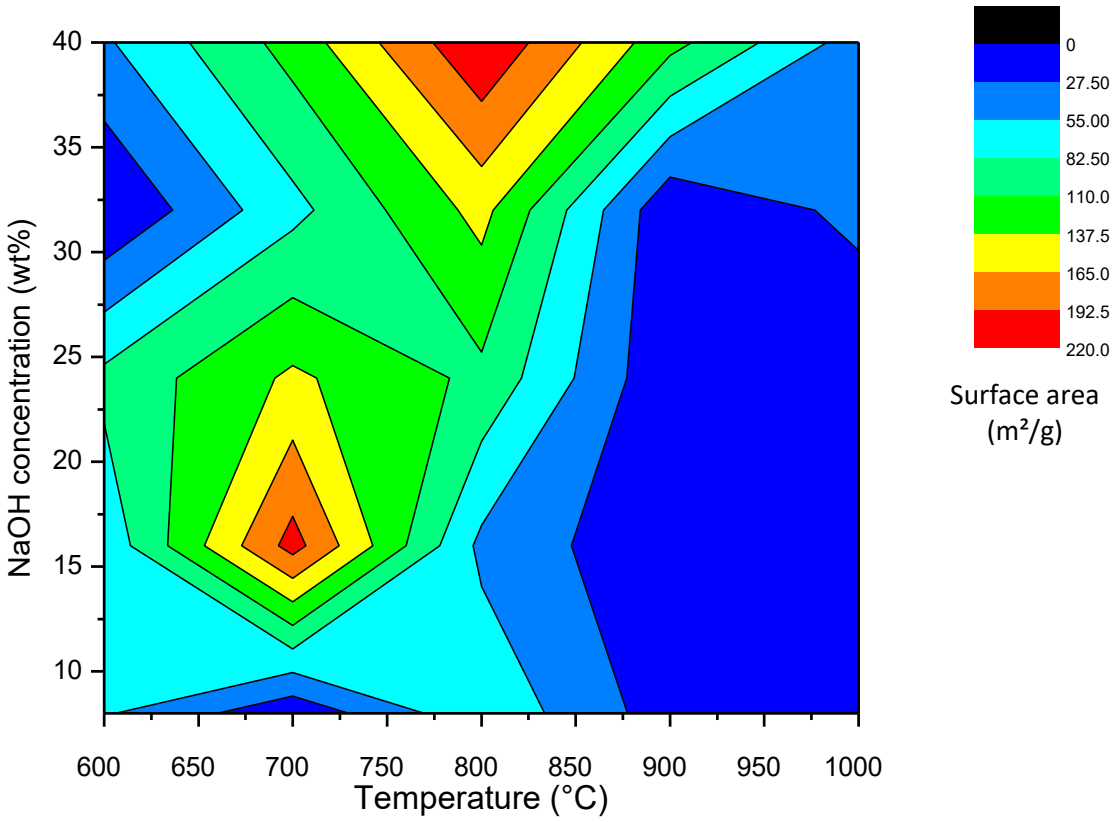

Figure 4.4: Contour plot of the single point surface area of AC (fibrous and non fiberous) activated at temperatures ranging from 600 – 1000 °C and using NaOH concentration ranging from 8 – 40 wt%.

The region of interest on the contour plot is the red zone. This is the region where the greatest single point surface area is attained. As shown in the figure, the single point surface area ranged from 192.5 – 220.0 m²/g, achieved at temperatures of 700 and 800 °C. The greatest surface area, of 217.4 m²/g, was achieved at 800 °C with 40 wt% NaOH. Figure 4.4 also further shows that in order for a high surface area to be reached at lower temperatures of around 700 °C, a lower concentration of NaOH (16 wt%) should be used.

With a higher concentration of activating agent used, there are more pores produced and there is also a higher probability of expanding the existing pores. Ideally, increasing the concentration of the activating agent increases the amount of matter present. Therefore, a

greater amount of energy, and thus, a higher temperature is required to achieve optimum activation of the resin. However, operation at 800 °C is preferable because the probability of achieving a higher surface area at this temperature, where there is a wider red zone, is higher than that at 700 °C.

It is evident that as the temperature increases beyond 800 °C, there is a significant decline in the surface area showing lower carbon activity. The low carbon activity, which results in the formation of smaller surface area, is confirmed by the SEM images in Figure 4.2 and Figure 4.3, showing less disorder in the AC structure at activation carried out at temperatures beyond 800 °C. Figure 4.3, in particular shows that the fibers on AC surface at higher temperatures are of smaller length and size. This is because at the higher temperatures, beyond 800 °C, the fibril particles tend to agglomerate and in turn decrease the surface area (Zdravkov et al., 2007). Furthermore, as a result of sintering at high temperatures, the spherical shape of the activated carbon material (ACM) collapses and shrinks, closing up some pores and thus significantly reducing the surface area. In addition, the charred particles realign, and shrink, resulting in the formation of narrower ACF particles (Guo and Chong Lua, 1998) with lower pore volume and thus reduced surface area available for adsorption to take place.

4.2.3 Pore Size Classification

There are several ways of pore size classification described in literature (Zdravkov et al., 2007). In this work, the International Union of Pure and Applied Chemistry (IUPAC) pore size classification is used (Table 4.1). The IUPAC is a classification based on different mechanisms such as multilayer adsorption relating to macropores, capillary condensation relating to mesopores, and micropore filling relating to micropores.

Table 4.1: IUPAC pore size classification, where d is the diameter

Specified types of pores, d (nm)		
Macro-	**Meso-**	**Micro-**
d > 50	2 < d < 50	d < 2

Table 4.2 shows the pore size range of the produced ACMs. It is evident from Table 4.2 that the synthesized ACMs (at the different temperatures used) mostly fall within mesoporous size range, according to the IUPAC pore size classification (Table 4.1). However, of the produced ACMs, micropores were produced in the instance when activation was carried out at 800 °C, it can therefore be concluded that the micropores were identified only in the fiberous material.

Table 4.2: Diameter pore size range of the AC (nm)

Temperature (°C)	Diameter pore size range (nm)
600	2.39 – 20.06
700	2.60 – 4.40
800	1.66 – 6.72
900	5.01 – 11.87
1000	2.29 – 7.70

The pores in ACMs are generally divided into two categories, vis-à-vis, transport pores (macropores with diameter greater than 50 nm) and adsorbing pores that are further classified as mesopores, micropores and sub-micro-pores. The produced ACM have pore diameters less than 50 nm, therefore, it can be deduced that the produced pores are only for adsorption (Zdravkov et al., 2007) and that no transport pores were generated.

4.2.4 Adsorption Isotherm Analysis

In this study, the nitrogen adsorption isotherm of ACF activated at 800 °C using 40 wt% NaOH was used as a representative adsorption isotherm of the ACMs produced. The results of an adsorption isotherm of ACM which was obtained is presented in Figure 4.5.

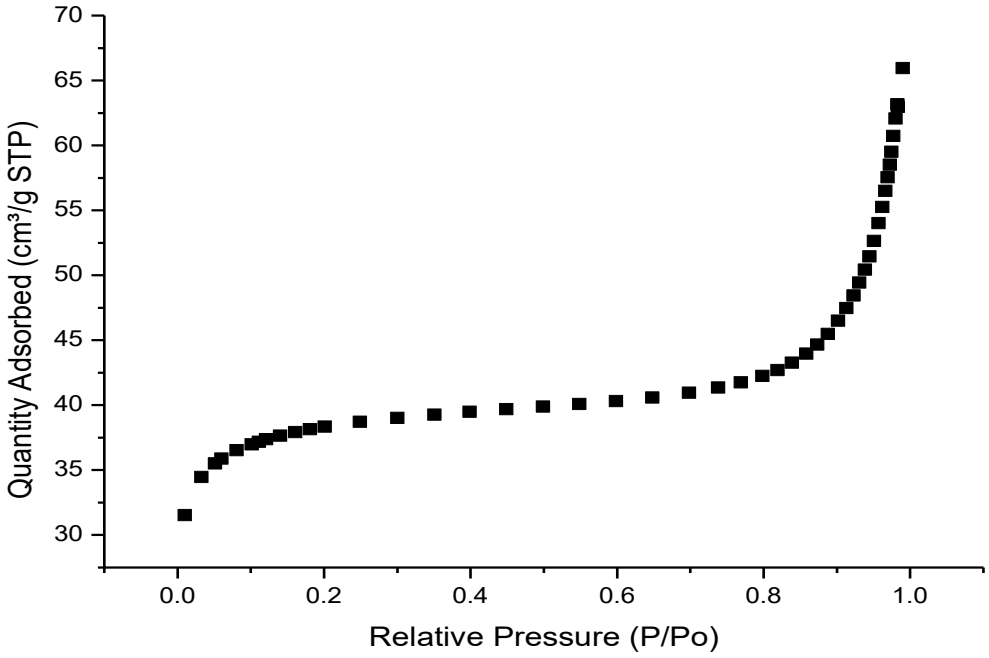

Figure 4.5: A graph showing the adsorption isotherms of ACM activated at 800 ˚C with 40wt% NaOH

Of the five general types of adsorption isotherms, the graph in Figure 4.5 shows type II adsorption isotherm. This type of isotherm is known to deviate significantly from the Langmuir isotherm. The flat region in Figure 4.5 (at the relative pressure between 0.2 and 0.8) suggests the occurrence of monolayer adsorption of the gas adsorbate molecules. Monolayer adsorption implies that once the pores are filled with adsorbate, there is little or no external surface for further adsorption. However, the point of inflection (at the relative pressure of 0.8) on the graph indicates the completion of the first adsorbed monolayer, and as the relative pressure increases other layers of adsorption are formed (Lowell et al., 2004). Therefore, the produced ACF possess more than one adsorption layer. This implies that the adsorption capacity is not solely based on the exposed surface area of the ACF, but also on the additional adsorption layers that are formed when the relative pressure increases.

4.2.5 Thermal Stability Analysis

TGA was conducted on the produced ACF, which was at the optimum temperature of 800 °C, in order to analyse the effect of the activating agent on the thermal stability and purity of the produced ACF. The TGA graphs of ACF activated at 800 °C with NaOH concentration of 8, 24 and 40 wt% are presented in Figure 4.6.

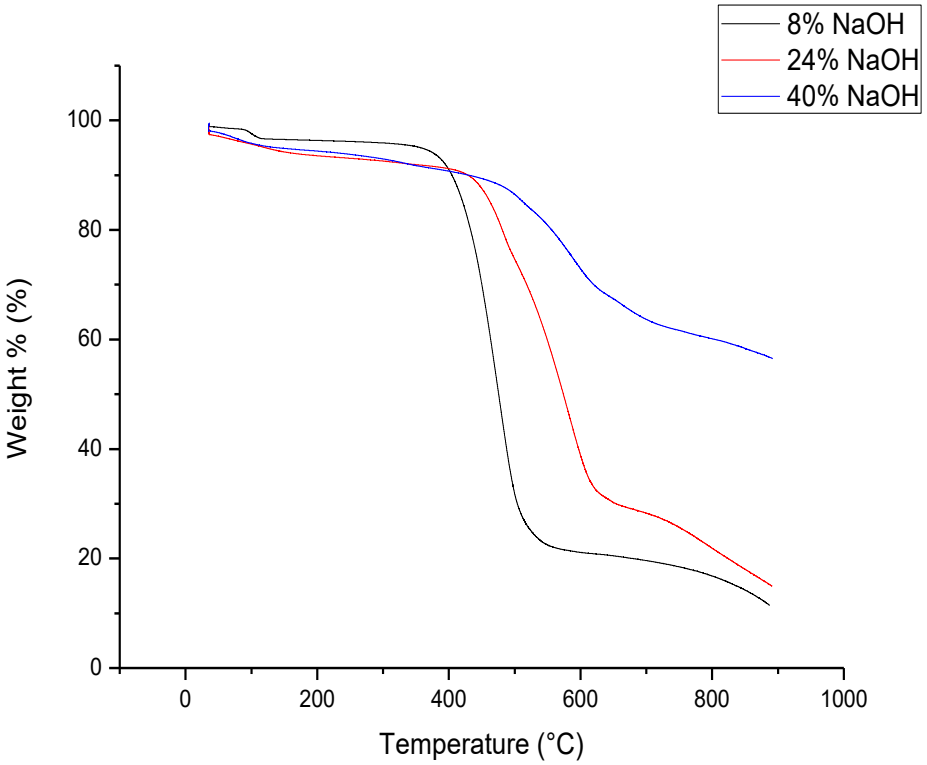

Figure 4.6: Shows the TGA graphs of ACF activated at 800 ˚C with 8, 24 and 40 wt% NaOH

The TGA results of ACF shown in Figure 4.6 indicate a sharp decrease in sample weight occurring in the temperature range of 400 - 500 °C, for the sample activated with 8 wt% NaOH. In contrast, the sample activated with 40 wt% shows a more gentle decrease, signifying more weight retention. The purpose of the activating agent is to dehydrate the carbon precursor, therefore, the addition of activating agent frees the pores in the carbon precursors during carbonization (Abdallah, 2004). For this reason, the use of a highly concentrated activating

agent results in a greater extent of dehydration and thus, a greater loss of volatiles during carbonization and activation. Therefore, the sharp decrease in weight loss in samples activated with 8 wt% NaOH may be ascribed to the volatization of the remnant of volatile material which was not removed during carbonization and activation steps.

4.2.6 Functional group determination

The adsorption capacity of any material is dependent on the porosity of the material and the chemical reactivity of the functional groups at the surface of the adsorbent (Joshi and Pokharel, 2014). FTIR was obtained (Figure 4.7) and used to determine the functional groups on the surface of the ACF synthesized with 40 wt % NaOH at 800 ˚C, and thus the type of bonds on the ACF. Knowing the various functional groups present on the surface of the ACF will enable one to determine if there is a preferential uptake of molecules by the synthesized ACF.

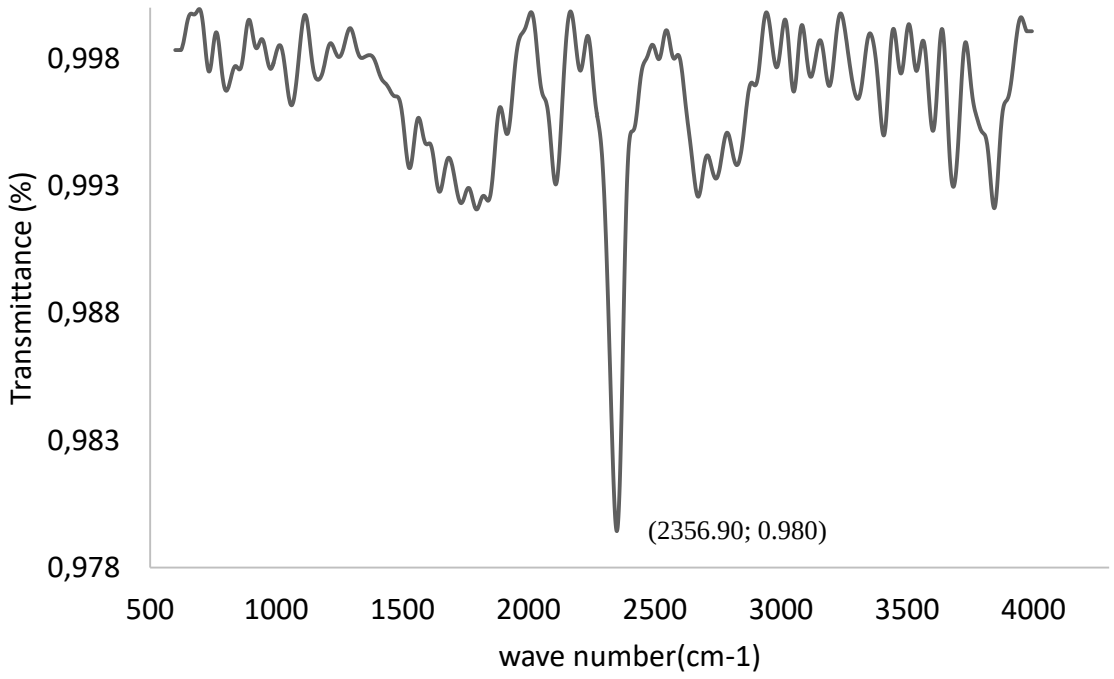

Figure 4.7: FTIR of ACF activated with 40 wt % NaOH at 800 ˚C

A high percent transmittance of 100% indicates that no absorption took place, therefore with reference to the FTIR spectra in Figure 4.7, for any given wave number, a high transmittance is indicative of no photons being absorbed and thus the specific bond at that frequency does not exist in the molecule. Table 4.3 lists the main IR frequencies/wave number, their respective functional groups and the peak description to expect if that functional group is present in the molecule. Looking at Figure 4.7, the most prominent peak can be seen at a wave number of 2356.90 cm^{-1} and it has a transmittance of 98.00 %. With reference to Table 4.3 below, this wave number does not fall into any of the functional group wave number ranges in the table below, and its transmittance is very high indicating minimal absorption of light taking place at that frequency. Therefore, it can be concluded that the synthesized ACF at 800 °C using 40 wt % NaOH, do not have any functional group on their surface.

Table 4.3: Indicates the Main IR Frequencies (Solomons et al., 2011)

Wavenumber cm^{-1}	**Functional group**	**Peak Description**
3300 - 3600	$O-H$ (alcohol)	Strong and broad
2500 - 3000	$O-H$ (carboxylic acids)	Very Broad (over - 500 cm^{-1}), often looks like distorted baseline, above 3000 cm^{-1}
3200 - 3500	$N-H$	Doublet in case of NH2 group of a primary amine or amide
3300	$\equiv C-H$ terminal alkyne	Usually Sharp and strong
3000 - 3100	$=C-H$ alkene or arene	Often weak, overlaps with CH alkane absorption
2800 - 3000	$C-H$	Strong, broad and multi-banded
2250 - 2220	$C \equiv N$	Medium intensity
2100 - 2260	$C \equiv C$ alkyne	Medium intensity for terminal alkynes, very weak for internal
1680 -1820	$C=O$ amides, ketones, aldehydes, carboxylic acid, esters	Very strong, lower frequency for amides and when C=O is conjugated
1600 - 1650	$C=C$ alkene, aromatic ring	Check to see if you have C-H unsaturated > 3000 cm^{-1} (if not, it's completely substituted)
~ 1600	$-NH_2$	Only if you have corresponding N-H peak at 3200 3500 cm^{-1} (this peak may be mistaken for C=C otherwise)
1200	$Ar-O$	Strong (look for =C-H and C=C first)
1050 - 1150	$C-O$	
690 & 750	Phenyl group	Strong (look for =C-H and C=C first)

4.3 PRODUCTION OF CARBON NANOTUBES

The morphology of the CNTs produced is largely dependent on the molecular structure of the carbon source used in its production (Shah and Tali, 2015). This research investigated the use of gases resulting from the pyrolysis of IER in the production of CNTs. The synthesized nanomaterials were characterized by means of analyzing the carbon form using the Raman spectroscopy; the morphology of species using the SEM; the surface areas, pore size and pore volume determination using the BET method and the carbon purity using TGA.

4.3.1 Gas Chromatography and Mass Spectrometry

The IER used in this study was amberlite xad- 4, a polymeric adsorbent purchased from Sigma-Aldrich. These white insoluble beads are non-ionic cross linked polymers of high surface area with an aromatic nature of its surface, as can be seen in Figure 4.8 below. One can, therefore, assume to expect aromatic compounds to evolve from the pyrolysis of the resin.

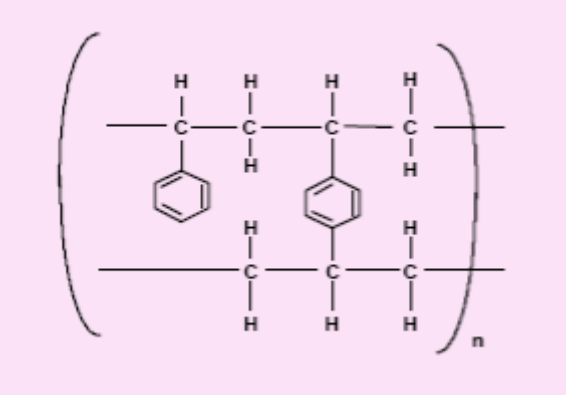

Figure 4.8: Chemical structure of amberlite xad-4 polymeric adsorbent (Lenntech, 2003)

The GC-MS was used in order to analyze which gases evolved during the pyrolysis of the amberlite xad-4 resin at temperatures ranging from 500 – 900 °C. Figure 4.9 shows one of the GC-MS chromatogram obtained from the gases evolving from resin pyrolysis at 800 °C. Figure 4.9 shows the very same chromatogram with labelled peaks of the gas identified. Generally, the spectral peaks should be symmetrical, narrow, separate (not overlapping), and made with

smooth lines, however, the peaks obtained are more drawn out, this may indicate traces of water.

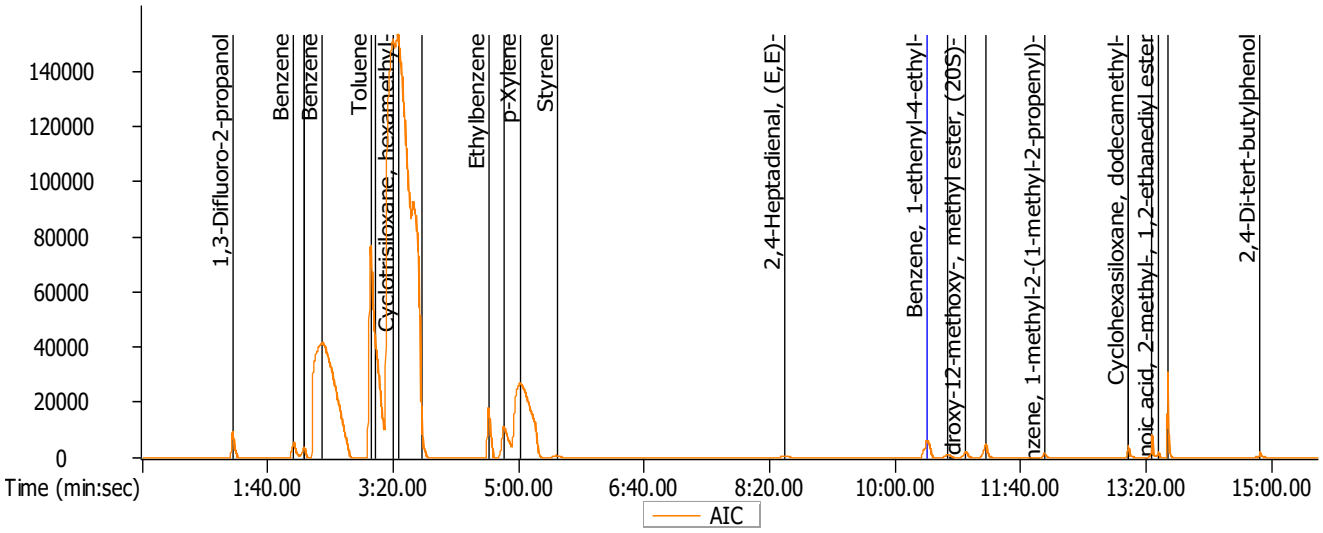

Figure 4.9: GC – MS chromatogram of gas evolved from the pyrolysis of amberlite xad4 at 800 °C, indicating the substances identified at the relative peaks.

Nonetheless, these results were used for the identification of gases evolved as they had high mass spectral similarity. Based on similarity and volume % of the results obtained from the GC-MS, the top 3 most abundant gases from resin pyrolysis occurring at 500, 600, 700, 800 and 900 °C were identified and can be seen in Figure 4.10. Figure 4.11 shows the chemical structures of some compounds that were identified.

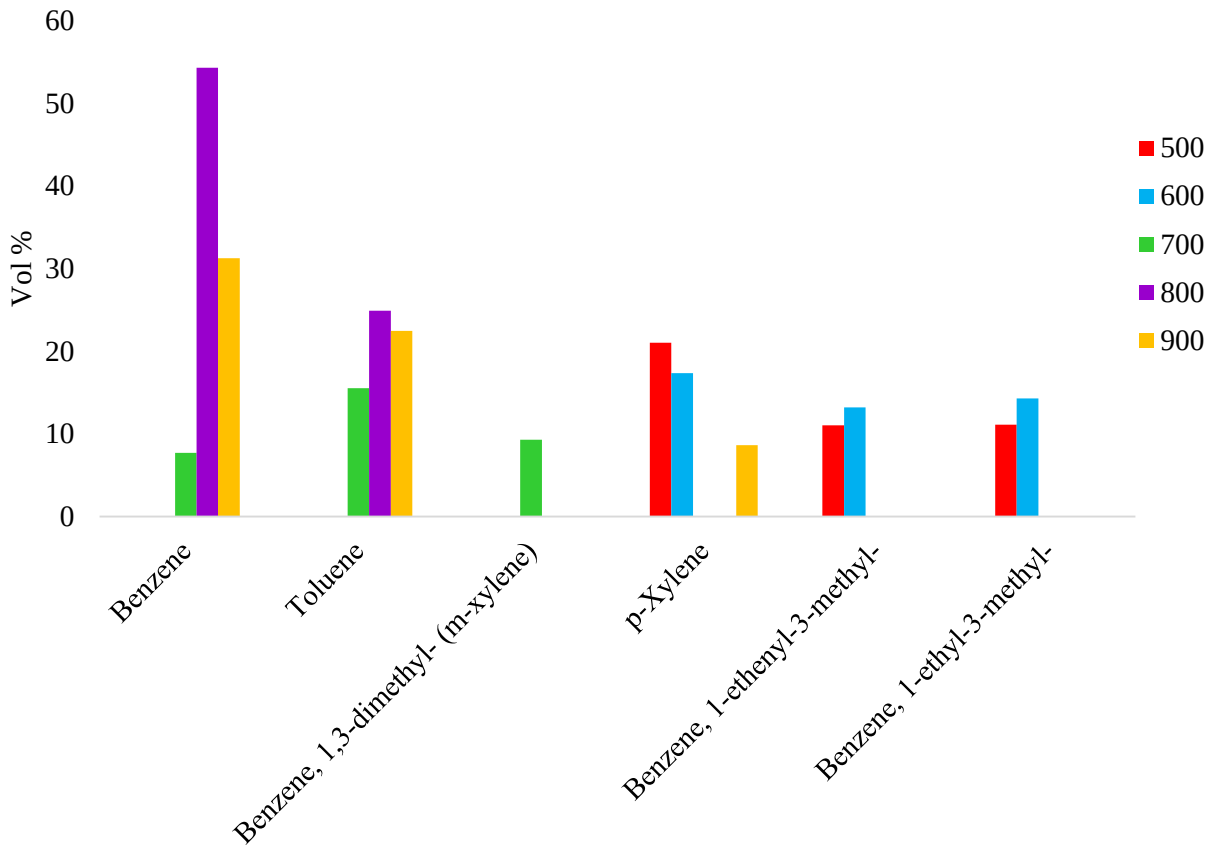

Figure 4.10: The top 3 most abundant gases that were identified at IER resin pyrolysis occurring at 500, 600, 700, 800 and 900 °C.

The gas pyrolysis experiment was for a duration of 10 minutes. The gas at different pyrolysis temperatures was collected after the 10 minutes and then analyzed. As shown in Figure 4.10, the greatest concentration of one compound is that of benzene produced at pyrolysis occurring at 800 °C. The GC-MS results also included an identification of compound by name and chemical formula. It can be seen that lower pyrolysis temperature resulted in production of aromatics with great molecular weights such as benzene 1,3-dimethyl. For the pyrolysis that took place at higher temperatures, the GC-MS analysis identified aromatics with smaller molecular weight such as benzene and toluene.

The chemical structure of these compounds were determined and used to classify the most abundant gases from the resin pyrolysis. Figure 4.11 shows the chemical structures of some of the more prominent gases, it can be seen that these gases are aromatics because they all contain the conjugated planar ring. It is expected to find these compounds given that the amberlite is a polymer made up of aromatic compounds.

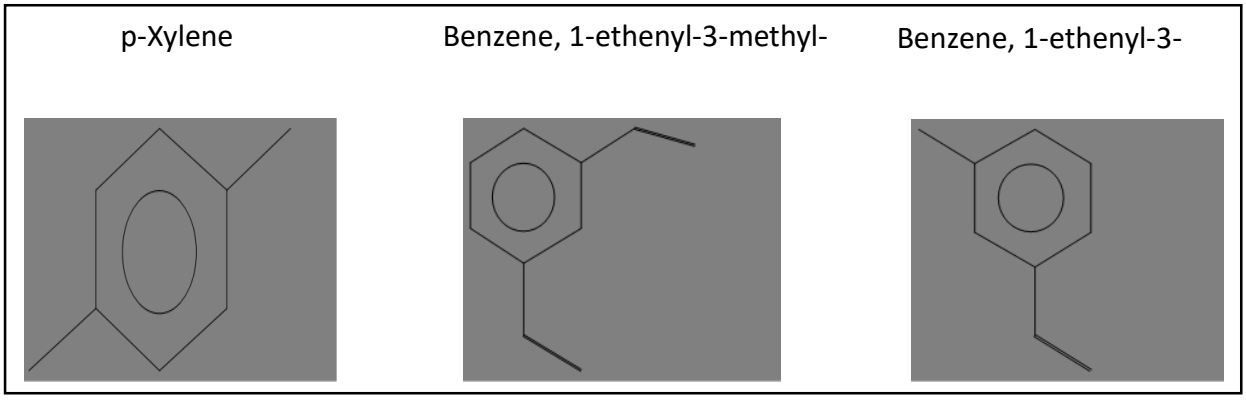

Figure 4.11: Chemical structure of some of the gases that evolved from resin pyrolysis

Needless to say, benzene is one of the commonly used carbon precursors for the synthesis of CNTs (Liu et al., 2011). Curved nanotubes are likely to be produced because according to (Khurshed and Bilal, 2016), linear hydrocarbons produce straight hollow CNTs while cyclic hydrocarbons produce curved CNTs. From research, aromatic compounds helped in the formation of CNTs as benzene follows the six membered ring base model. Therefore, as soon as benzene starts flowing into the reactor, a benzene layer forms on the catalyst surface and the C-H bonds are then broken due to reduction by the active catalyst. The hexagonal rings of carbon are then released, which become the basic building blocks of the CNTs. The catalyst used in the production of CNT from benzene is iron (Khurshed and Bilal, 2016; Mubarak et al., 2014). Some researchers have managed to synthesize CNT using benzene at temperature between 700 – 1100 °C, therefore, in this research the fixed synthesis temperature will be 800 °C as that is the temperature at which the highest concentration of

benzene had evolved from the resin pyrolysis. The effect of the carrier gas and the catalyst support was investigated for the synthesis of CNTs synthesized at 800 °C using an iron catalyst.

4.3.2 Carbon form analysis

In order to characterize the synthesized CNTs according to bonding structure of carbon nanomaterials, the Raman spectroscopy was employed. The spectrum gives information about CNTs as well as scattering at G-Band, D-Band, radial breathing mode (RBM) and G′ -Band. The G-band is the peak that is found at around 1575 - 1590 cm^{-1}, it is the graphitic band as it is associated with the vibration of carbon bonds in the graphitic planes. Another prominent and most common band is the D-band found at a peak of 1350 cm^{-1}. The D-band originates from a hybridized vibrational mode associated with graphene edges, this band indicates the presence of some disorder to the graphene structure. The G′-band occurs at a Raman shift of 2700 cm^{-1}. The MWCNTs Raman spectra is very similar to that of the SWCNTs, but the difference lies in the lack of RBM modes in the MWCNTs and much more prominent D-bands can be seen in the MWCNTs. The Figures 4.12 – 4.16 show the Raman spectra of the synthesized CNTs.

For the CNT synthesized using unsupported iron (Figure 4.12), it can be seen that there is no presence of the D, G or G′ bands, therefore, indicating the lack of crystalline carbon and armorphous carbon, thus no formation of CNTs was detected. This may be due to iron sintering occurring during the synthesis of the CNTs.

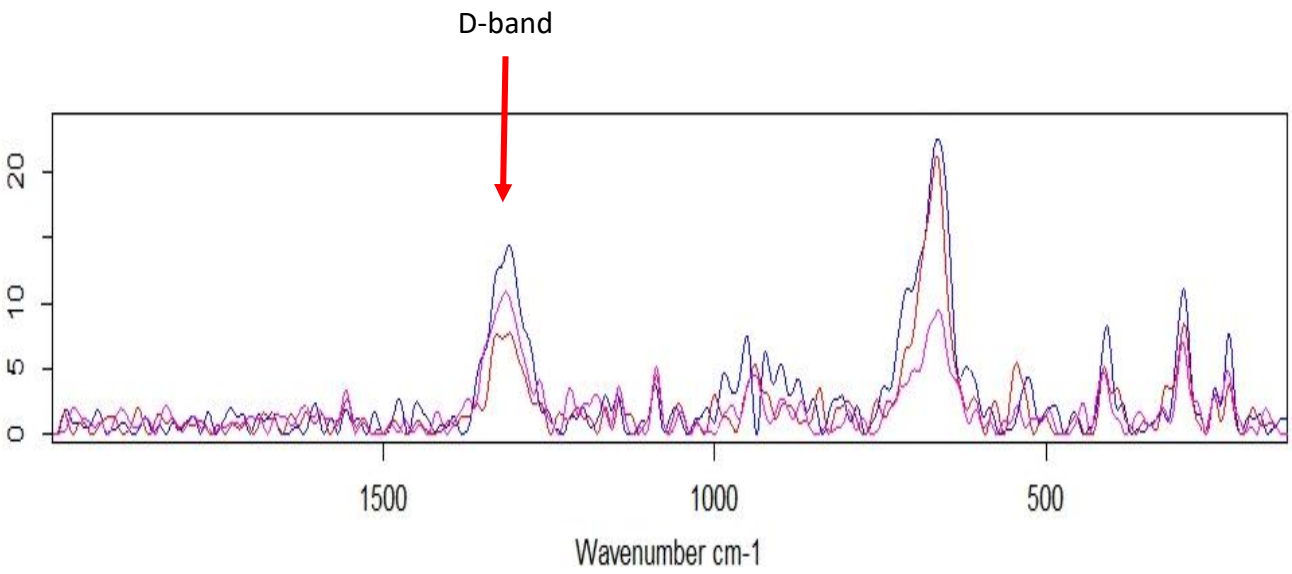

Figure 4.12: Raman spectroscopy of CNT synthesized at 800 °C for 30 minutes, using nitrogen as a carrier gas and unsupported Fe catalyst.

From Figure 4.13, the Raman spectra of iron supported on magnesium oxide, taken at 3 points on the sample. The D-band and G-band are present for the Raman spectra with the greatest intensity. However, it can also be seen that there are no RBM modes present, thus suggesting that the CNTs formed are MWCNTs.

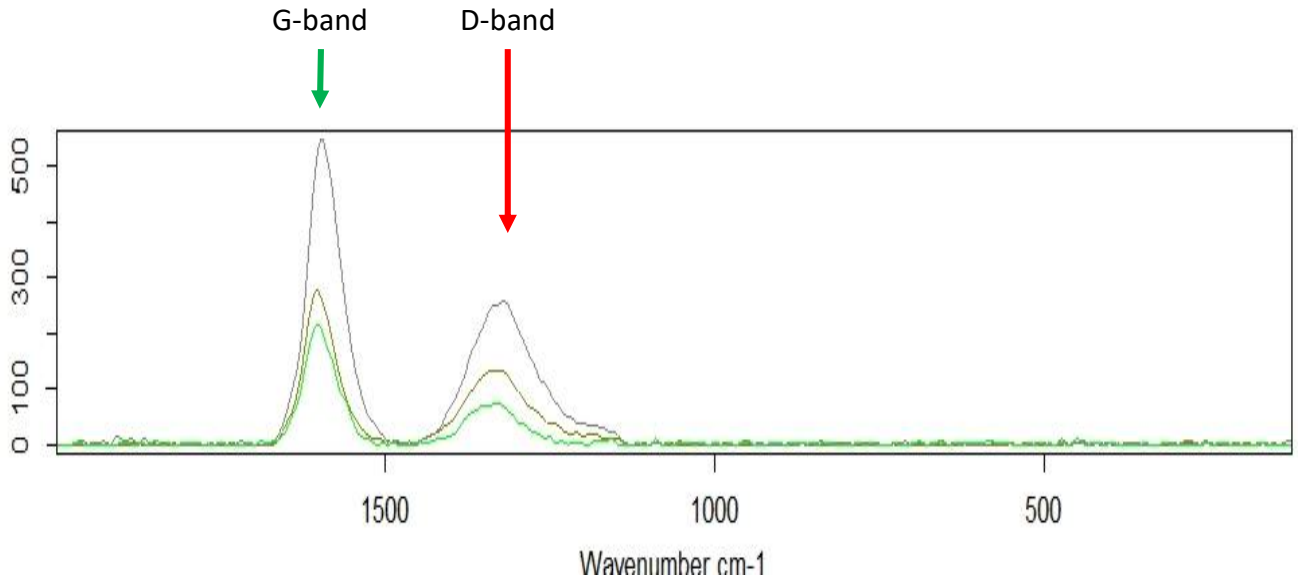

Figure 4.13: Raman spectroscopy of CNT synthesized at 800 °C for 30 minutes, using nitrogen as a carrier gas and Fe supported on MgO

From Figure 4.14, the presence of RBM modes indicates that SWCNTs were formed. The greater the D-band intensity, the more defect there is in the carbon present. The intensity of the D-band in Figure 4.13 (that of the MWCNTs) is approximately 260 a.u., thus being more prominent than that of the D-band found in Figure 4.14 (SWNTs), which is approximately at an intensity of 90 a.u.. It is expected for the D-band in MWCNTs to have a greater intensity than that of SWCNTs given that the MWCNTs have a multilayer in configuration and thus affinity for more disorder.

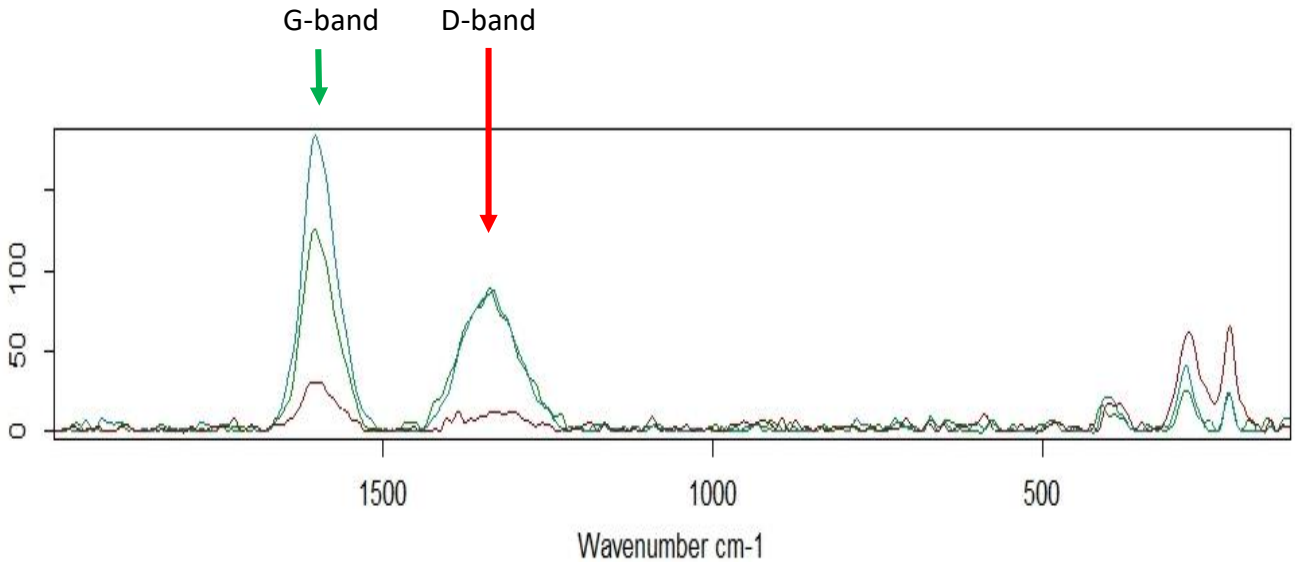

Figure 4.14: Raman spectroscopy of CNT synthesized at 800 °C for 30 minutes, using nitrogen as a carrier gas and Fe supported on Al_2O_3

Again, some RBM nodes can be viewed in Figure 4.15, indicating the presence of MWCNTs. However, the intensity of the D-band is relatively low – 100 a.u., in comparison to that of MWCNTs synthesized with iron supported on magnesium oxide - 260 (Figure 4.13). This suggests that there are less nanocrystalline structures formed of MWCNT, using iron supported on calcium carbonate as opposed to iron supported on magnesium. It may also indicate less walls being formed in the case of iron being supported on calcium carbonate.

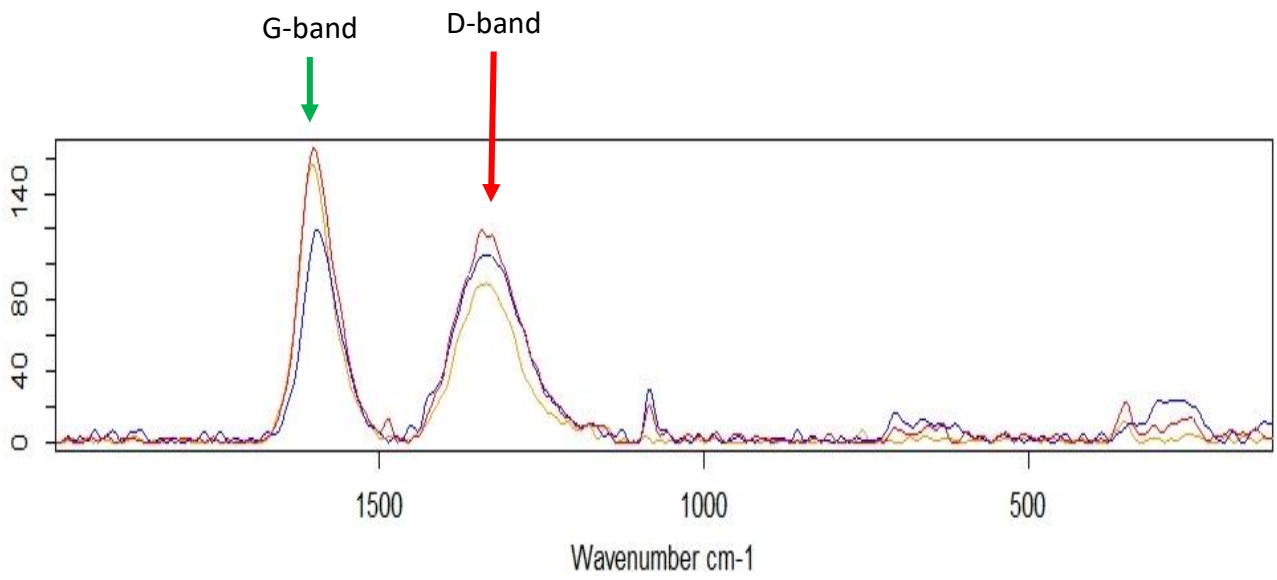

Figure 4.15: Raman spectroscopy of CNT synthesized at 800 °C for 30 minutes, using nitrogen as a carrier gas and Fe supported on $CaCO_3$

So far, the use of different metal supports has shown that different CNT forms can be produced. The use of iron supported on magnesium oxide and calcium carbonate yielded MWCNT, and the use of iron supported on aluminium oxide yielded SWCNTs. The effect of the carrier gas on the carbon form (Raman spec) of CNTs can be viewed in Figure 4.16, in which argon was used as a carrier gas, and the iron catalyst was supported by magnesium. Due to the lack of RBM nodes, as can be seen in Figure 4.16, it can be deduced that MWCNTs were formed, having the greatest G-band intensity of approximately 1050 a.u., thus suggesting a greater formation of armorphous structures (greater degree of graphitization) in comparison to the MWCNTs formed with nitrogen as a carried gas. The density of Nitrogen is 1.16 g/L and that of argon is 1.78 g/L. Due to argon being more dense than nitrogen, this creates a greater concentration gradient between the carbon source and metal catalyst in the reactor, and thus more nanotubes can be formed.

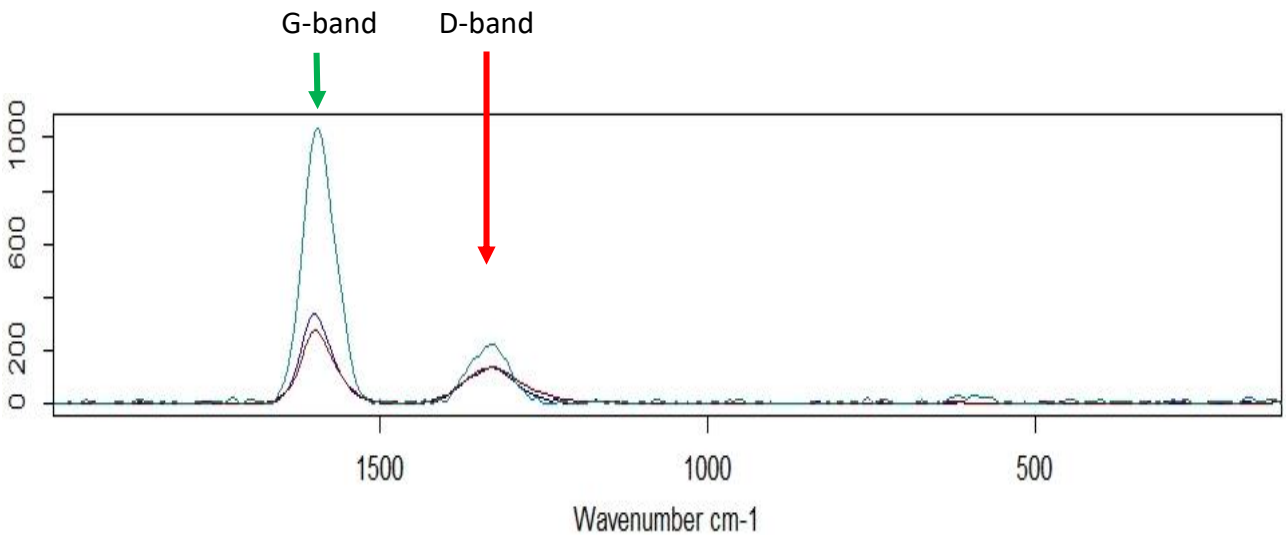

Figure 4.16: Raman spectroscopy of CNT synthesized at 800 °C for 30 minutes, using argon as a carrier gas and Fe supported on MgO

The degree of crystallinity and a measure of defects present on carbon nanomaterials can be calculated from the I_D/I_G ratio, this can be seen in Table 4.4. This ratio can be used as a measure of quality of the CNTs. The I_D/I_G ratio is the lowest for the CNT synthesized using argon as a carrier gas on iron supported by magnesium oxide, suggesting that there is the least amount of defective carbon, thus MWCNTs of a higher purity can be produced with argon as a carrier gas as opposed to using nitrogen. The greatest intensity ratio was that of iron supported on calcium carbonate, suggesting minimal graphitization and production of more nanocrystalline material.

Table 4.4: The intensity of the D and G band and the I_D/I_G ratio for synthesized CNTs.

	Support	I_G **(a.u.)**	I_D **(a.u.)**	I_D/I_G
N_2	Fe/MgO	580,00	260,00	0,45
N_2	Fe/Al_2O_3	180,00	90,00	0,50
N_2	$Fe/CaCO_3$	170,00	100,00	0,59
Ar	Fe/MgO	1050,00	200,00	0,19

4.3.3 Surface Topography and Morphological Analysis

The morphological analysis of the synthesized CNTs can be viewed from the SEM analysis in Figure 4.17. The SEM images presented in Figure 4.17 represents the different formation (or lack of) of the tubes for CNT produced with different catalyst support (unsupported Fe, Fe supported on MgO, Al_2O_3 and $CaCO_3$), and carrier gas (Fe supported on MgO using nitrogen and argon).

In Figure 4.17 (b), tube like structures can be seen where CNTs grown on iron supported by magnesium oxide. Figure 4.17 (c) shows CNTs grown on iron supported by aluminium oxide, and in Figure 4.17 (e) CNTs were grown on iron supported by magnesium oxide using argon as a carrier gas. The tube like structure is more defined for CNTs produced using argon as a carrier gas which correspond to the low Raman spectroscopy intensity ratio and results discussed above. There is less defective carbon, allowing for better definition and formation of tubes.

This is the case where no formation of D-bands and G-bands were present in the Raman spectroscopy (unsupported iron), suggesting lack of CNT formation. The SEM results confirm this as can be seen in Figures 4.17 (a) where structural view on the surface shows irregular ball/cube-like structures, which may be classified as nanospheres.

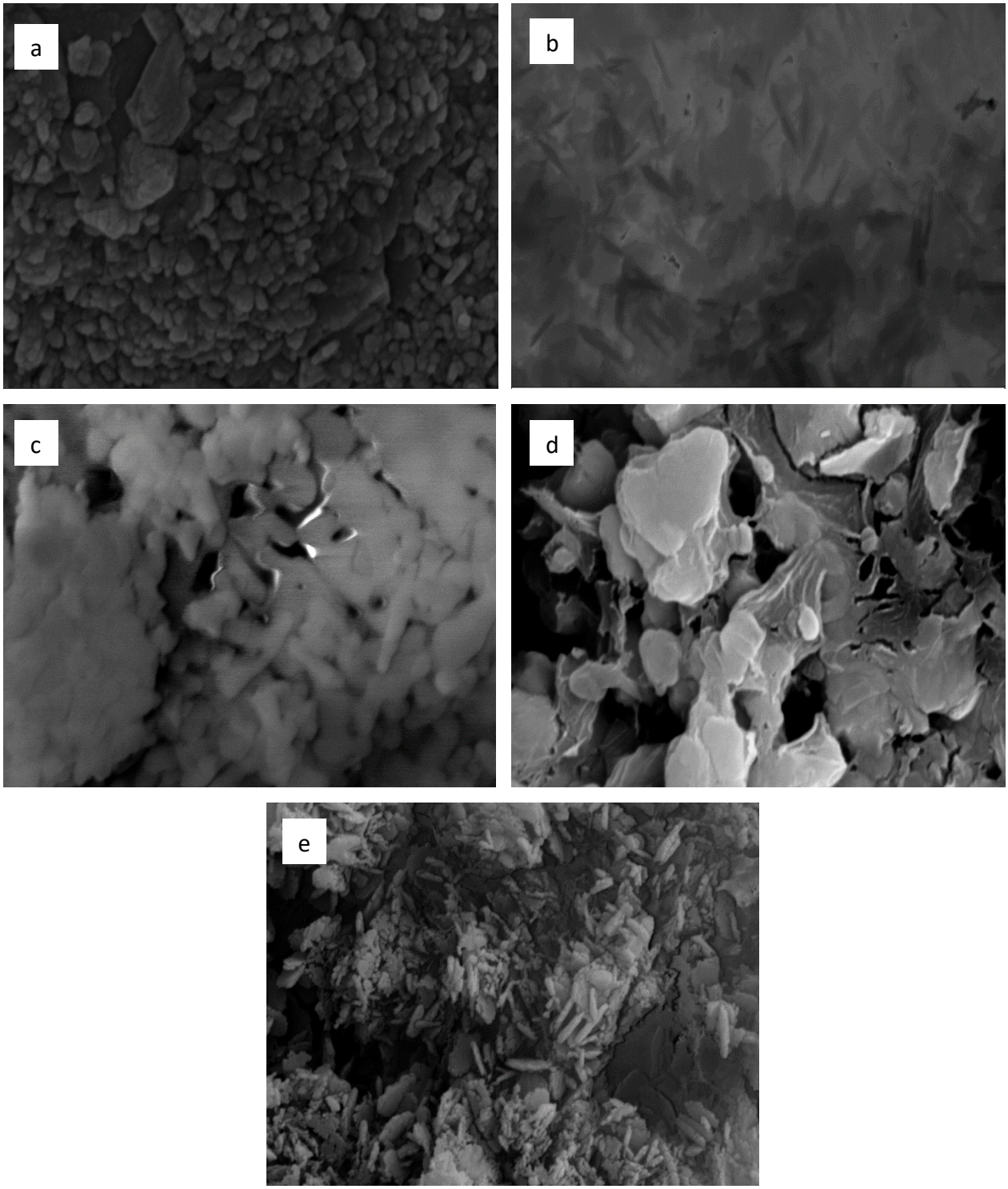

Figure 4.17: SEM images at a magnification of 50 000 x, of CNTs synthesized using nitrogen as a carrier gas at a reaction temperature of 800 ° C, for 30 minutes on; a) unsupported Fe; b) Fe/MgO; c) Fe/Al_2O_3 ; d) $Fe/CaCO_3$; and e) CNTs synthesized on Fe/MgO using argon as a carrier gas, at 800 ° C.

4.3.4 Surface Area and Pore Size Analysis

The single point surface area and the pore volume of the synthesized CNTs can be seen in Figure 4.18.

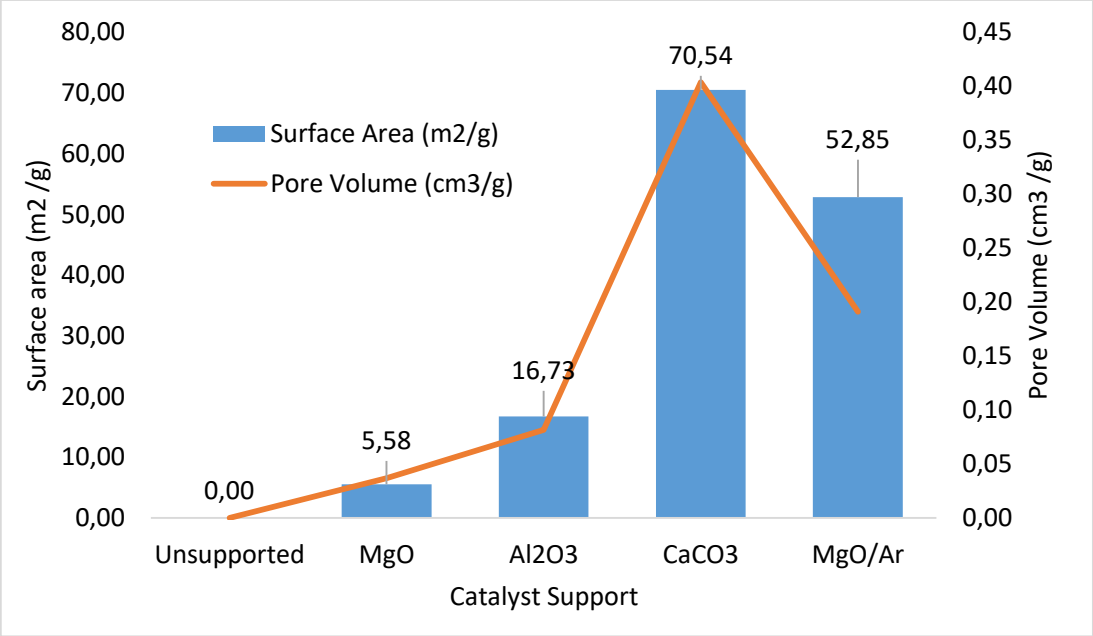

Figure 4.18: The surface area and pore volume analysis of the synthesized CNTs

The greatest surface area was achieved for the CNTs synthesized using iron supported on calcium carbonate (70.54 m^2/g). In the case of synthesizing CNTs from unsupported iron, the surface area was minimal, coinciding with the SEM results (suggesting no visible tubes being seen) and the Raman spectroscopy results (no formation of D and G band, therefore no tubes). The primary role of a catalyst support is to stabilize the metal catalyst, i.e. to prevent the metal particles from coalescing.

The single point surface area for the ACF synthesized at 800 °C can be seen in Figure 4.19, in order to compare the ACF produced at optimal temperature with the produced CNTs. It can therefore be seen that the surface area relationship to the pore volume, for both materials, are proportional. Increase in surface area results in an increase in pore volume. The greatest surface area achieved from all the materials that were synthesized was that of the ACF

synthesized at 800 °C, and because the synthesis of ACF material is more predictable and controllable, the ACF synthesized at 800 °C was the chosen adsorbent for the batch adsorptions of the platinum metal ion.

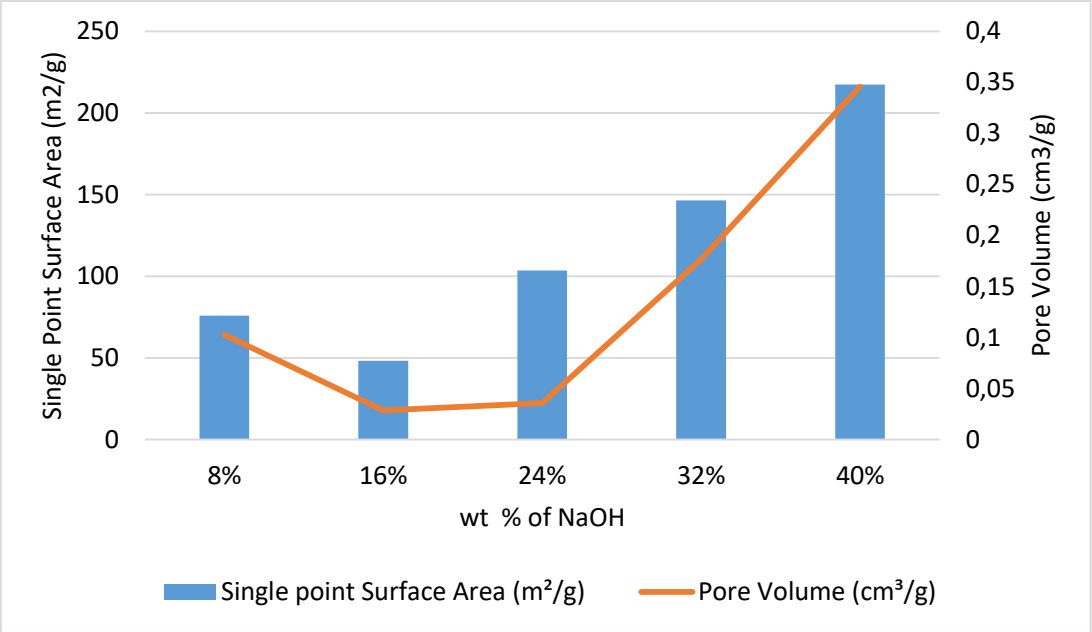

Figure 4.19: The surface are and pore volume analysis for the ACF synthesized at 800°C

It can be seen that the greatest pore size was that of MgO, refer to Table 4.5. The size of platinum ion is 0.18 nm which has a diameter less than that of the ACF pore size, therefore all the supported material are capable of adsorbing platinum ions within the pores. For the synthesized CNTs, it can be said that they are all mesoporous materials as they have a pore size range between 2 and 50 nm.

Table 4.5: Pore size of the synthesized CNTs

Support	**Pore Size (nm)**
Unsupported	0,00
MgO (N_2 – carrier gas)	32,60
Al_2O_3	19,52
$CaCO_3$	23,41
MgO (Ar – carrier gas)	14,52

4.3.5 Thermal stability and material purity analysis

The TGA was conducted in order to investigate the purity of the synthesized nanomaterials. This was achieved through observing the weight-loss curve and analyzing the initiation temperature, oxidation temperature and the residual mass.

The TGA graphs were obtained for the CNTs produced on unsupported iron, iron supported on magnesium oxide, aluminium oxide and calcium carbonate. These graphs are presented in Figure 4.20 and 4.21.

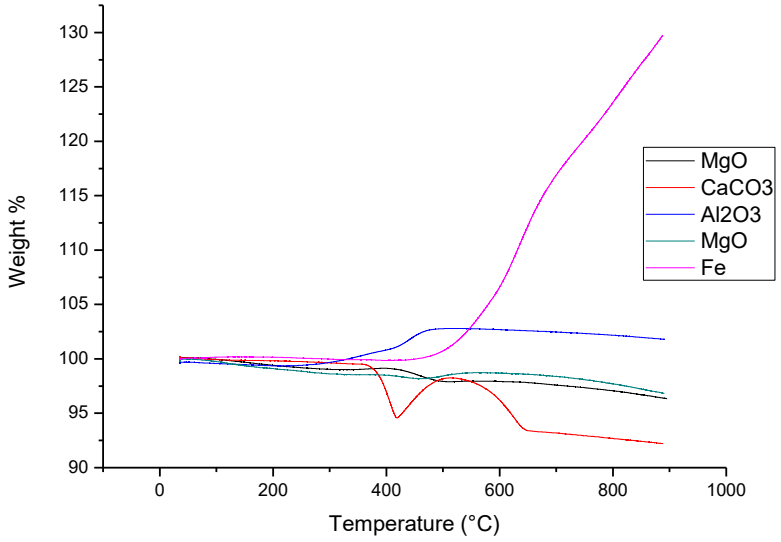

Figure 4.20: Shows the TGA graphs of CNTs synthesized with different support catalyst and un-supported iron catalyst

From the knowledge of oxidization of carbon materials with various micro structures, beginning at various specific temperatures, the TGA graphs help one to investigate the presence of CNTs. Due to the presence of catalyst present during the analysis, the weight loss/gain analysis during oxidation will not only be subjected to the oxidation of carbon. From Figure 4.20, it can be seen that the mass of the unsupported iron catalyst (graph Fe) increases with increase in temperature as there are copious amounts of iron present for oxidation to occur, and therefore, confirming that CNTs were not produced.

The CNTs produced with the iron catalyst supported on the aluminium oxide (TGA graph) indicates an increase in weight, this may be due to more iron particles present at the end of the experiment in comparison to the other supports used. From the Raman spectroscopy of iron supported by aluminium, SWCNTs were detected. The formation of MWCNTs, in comparison to that of SWCNTs, uses a greater amount of catalyst for the formation of tubes. Therefore, it can be expected that the residual amount of the iron catalyst can be greater in the case where SWCNTs were formed.

The TGA typical oxidation temperature for MWCNT, SWCNT and amorphous carbon are 400-650 °C, 350 - 500 °C and 200 - 300 °C, respectively (Shukrullah et al., 2016). The greatest weight loss occurred for the CNTs synthesized with iron supported on calcium carbonate. The TGA curve for $CaCO_3$ support in Figure 4.21 shows a two-step decomposition reaction. The first-step decomposition reaction has an oxidation initiation temperature of 364 °C and oxidation final temperature of 417 °C (MWCNTs). The second-step decomposition reaction starts from 529 °C and stops at 653 °C (SWCNTs). However, the weight loss for the first and second-step oxidation reaction is of 4.85 and 4.78 %, respectively. The slightly greater weight loss suggest a slightly greater production of MWCNTs than SWCNTs, hence from the Raman spectroscopy identified the synthesized material is MWCNTs. However, the weight loss was indeed minute, thus suggesting a very low concentration of CNTs produced, this coincides with the Raman and SEM results obtained in subsections above.

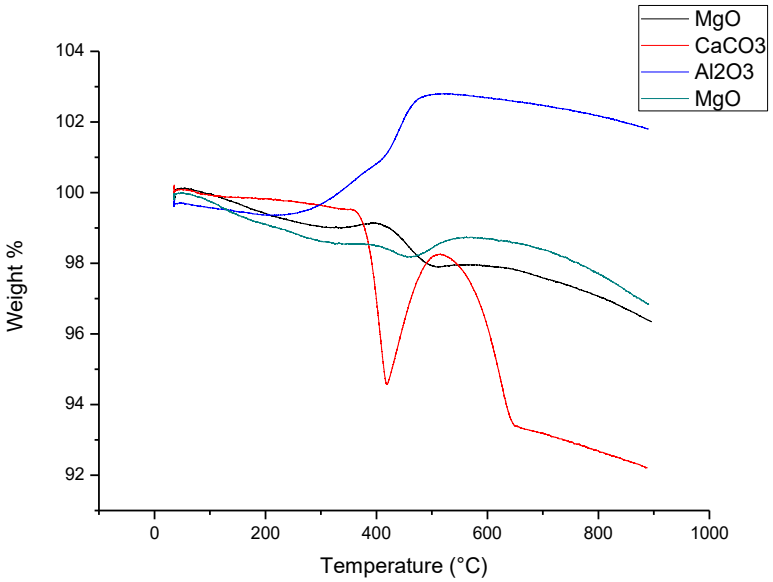

Figure 4.21: Shows the TGA graphs of of CNTs synthesized with different support catalyst

The graph (black MgO graph) indicates the synthesis of CNTs with iron supported by magnesium oxide using nitrogen as a carrier gas. From Figure 4.12, it can be seen that an oxidation reaction occurred between 383 – 466 °C indicating the formation of MWCNTs, however, the oxidation reaction resulted in a weight loss of 0.339% which means that the MWCNTs were in very small concentrations. This result corresponds to the results obtained from the Raman spectroscopy. From the Raman spectroscopies, it was also deduced that the CNTs synthesized with iron supported on magnesium, oxide using argon as a carrier gas, were MWCNTs of a greater intensity. Therefore, one can expect the weight loss on the TGA curve of magnesium oxide support with argon as a carrier gas (green graph) to have a greater weight loss, however, this is not true.

4.4 METAL ADSORPTION USING ACTIVATED CARBON FIBER

Batch adsorption experiments were conducted using ACF synthesized at 800 °C and 40 wt % NaOH, and varying concentration of platinum (100, 50 and 10 ppm), using potassium tetrchloroplatinate. The data used to plot the adsorption isotherms can be found in Appendix C of this report.

4.4.1 Effect of Contact Time and Initial Metal Ion Concentration

The effect of contact time is a vital parameter as it helps one to determine the adsorption kinetics of an adsorbate at any given initial concentration, therefore, the effect of contact time on the platinum metal ion adsorption by synthesized ACF from IER was investigated for 210 minutes (Figure 4.22).

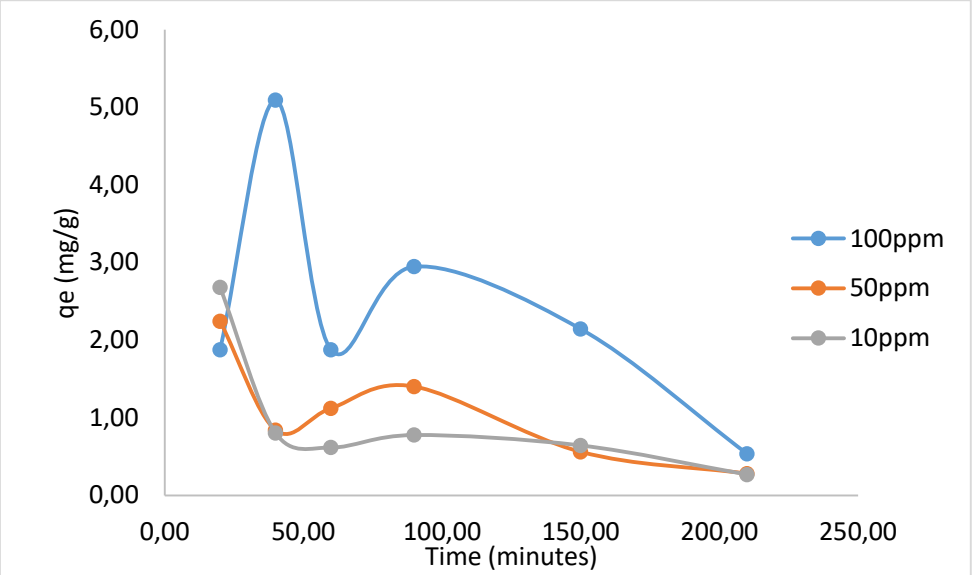

Figure 4.22: The effect of contact time on the initial platinum concentration

The kinetics studies were carried out at 30 ± 1 °C, at a pH of 2 and 100 rpm. Figure 4.22 shows the amount of platinum ion adsorbed onto the synthesized ACF as a function of time and concentration. It should be noted that the initial adsorbed concentrations are zero at the beginning. The greatest amount of metal ion adsorbed for the 50 ppm and 10 ppm solutions is at a time of 20 minutes, whereas for the 100ppm solution is at a time of 40 minutes. The greatest adsorption rate is from time 0 to 20 minutes for the 10 and 50 ppm solutions, and from time 0 to 40 minutes for the 100 ppm, as opposed to the adsorption rate later on in the experiment from time 60 to 90 minutes. This high adsorption rate can be attributed to the presence of a

large number of vacant adsorption sites leading to a large concentration gradient between the adsorbate in the solution (platinum) and the adsorbent (ACF).

It can be seen in Figure 4.23 that for a 50 ppm solution it took 20 minutes to adsorb 2.24 mg/g, and for the 100ppm solution it took 40 minutes to adsorb 5.09 mg/g, therefore, this indicates that doubling the initial concentration almost doubles the time it takes to reach the maximum amount of adsorbed metal ions. From this, one can deduce that the adsorption of platinum in dilute solutions (< 50ppm) using the synthesized ACF is more rapid than that of solutions with a higher concentration. In addition, with reference to research done by Mavhungu et al., 2016; on the recovery of platinum ions from activated grape stalk, at a time of 20 minutes, less than 2 mg/g of the platinum ions had been adsorbed, thus confirming that indeed the use of the synthesized ACF promotes rapid adsorption.

At a time of 40 minutes for the 50 and 10 ppm solutions, the platinum ions desorb back into the solution, a similar trend occurs for the 100 ppm solution at a time of 60minutes. For all three solutions, the metal ions adsorb, desorb then adsorb between experimental time of 0 to 100 minutes. However, from a time of 100 minutes only desorption takes place, and at a time of 210 minutes (end of the experiment), the amount of metal ions adsorbed is at its lowest, having less than 1 mg/g for all solutions. This may be an indication of weak forces between platinum and ACF, suggesting that physisorption took place, rather than chemisorption, as physisorption is the Van der Waals adsorption having weak forces of attraction, and adsorption being easily reversed.

4.4.2 Adsorption Isotherms

The Langmuir model was used to determine the maximum adsorption capacity which corresponds to the complete monolayer coverage on the surface of the ACF. Figure 4.23 shows the Langmuir adsorption isotherm for the platinum ions adsorption.

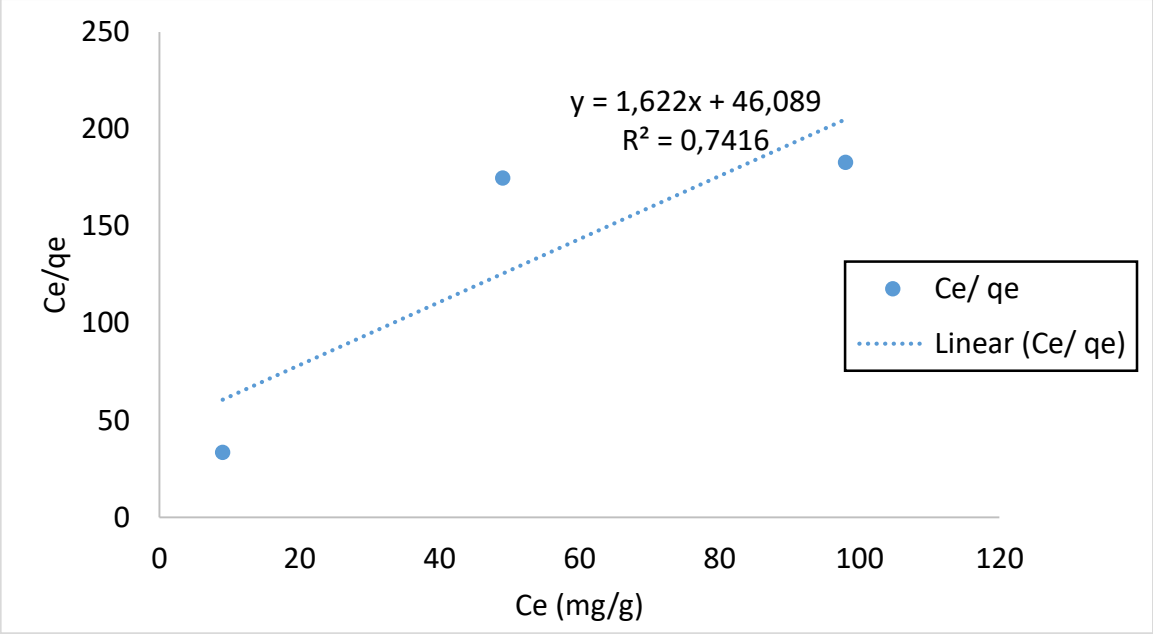

Figure 4.23: Langmuir adsorption isotherm for the adsorption of platinum ions using ACF synthesized at 800°C and 40 wt % NaOH

The linear isotherm parameters can be seen in Table 4.6, and the calculations for these parameters can be found in Appendix C. The parameter q_m in Table 4.6 represents the maximum amount of metal ion per unit mass of the ACF, which is 0.62 mg/g. Therefore, based on the Langmuir model, the theoretical saturation adsorption capacity of the monolayer is 0.62 mg/g. The value K_L represents the Langmuir constant (L/mg) relating to the affinity of binding sites. In this case, the K_L parameter is at a low of 0.04, suggesting a low affinity of platinum ions to the ACF binding sites. The parameter R^2 is a statistical parameter known as the coefficient of determination, it is used to determine fitness of the line of best fit of the data. The R^2 for the Langmuir isotherm is fairly decent, suggesting that the Langmuir isotherm model may be a reasonable representation of the adsorption that took place.

Table 4.6: Langmuir adsorption isotherm parameters

q_m (mg/g)	**0,62**
K_L (L/mg)	0,04
R^2	0,74

4.4.3 Freundlich Adsorption Isotherms

The Freundlich model was used to determine the adsorption intensity (1/n) of the sorbate (platinum) on the sorbent (ACF). The K_f value is the Freundlich constant related to the adsorption capacity of the adsorbent (Mavhungu et al., 2016). The calculations of these parameters can be found in Appendix C. In Figure 4.24, the Freundlich adsorption isotherm for the platinum ion adsorption can be seen.

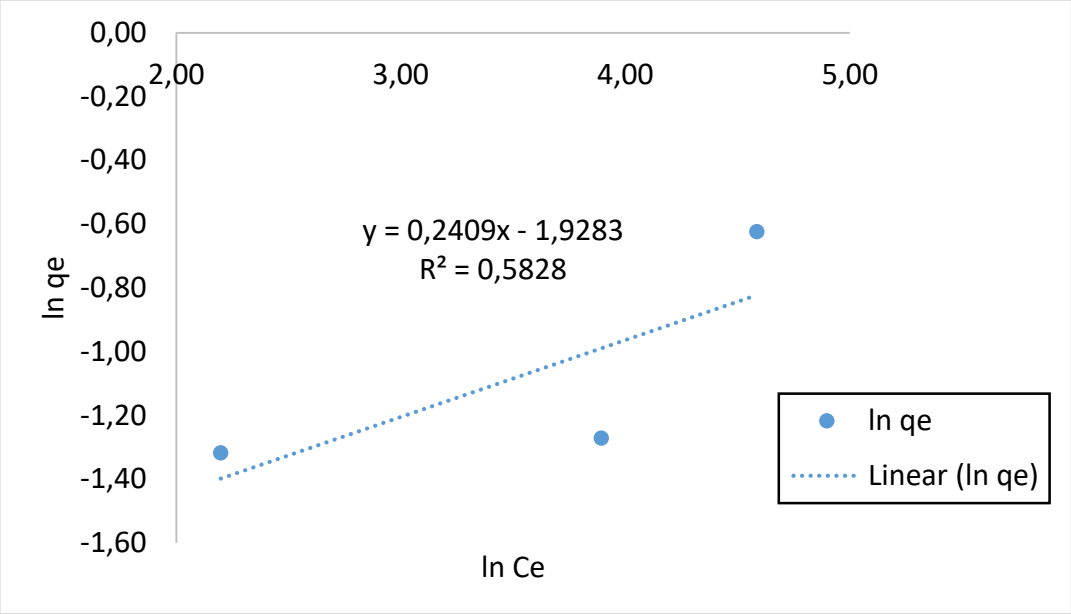

Figure 4.24: Freundlich adsorption isotherm for the adsorption of platinum ions from 100 ppm platinum solution using ACF synthesized at 800°C and 40 wt % NaOH

From Table 4.7, the K_f value was found to be 0.15 L/g, and the 1/n value (0.24) lies between 0 and 1, indicating that the adsorption was favourable at the studied conditions. The R^2 value obtained from the Freundlich isotherm was 0.58, which is less than that found for the Langmuir isotherm (0.74), suggesting that the Langmuir isotherm is a better model.

Table 4.7: Freundlich adsorption isotherm parameters

1/n	**0.24**
K_F (L/g)	0,15
R^2	0,58

The adsorption capacity of platinum on the synthesized ACF is compared to that of other adsorbents from literature in Table 4.8. According to the adsorption capacity obtained from the Langmuir isotherm (0.62 mg/g), it can be seen that this capacity is extremely low and doesn't compete well with other synthesized adsorbents.

Table 4.8: A comparison of adsorbent capacities for different adsorbents relative to the adsorption of platinum

	Adsorption capacity (mg/g)	
Adsorbent	**Pt (IV)**	**Reference**
Fe_3O_4 nanoparticles	13.27	(Zhou et al., 2009)
PA-lignin	104.57	(Ramesh et al., 2008; Zhou et al., 2009)
Amberlite IRC 718	42.93	(Zhou et al., 2009)
Poly(Vinylbenzylchloride-acrylonitrile-divinylbenzene) modified with tris(2-aminoethyl)amine	245	(Zhou et al., 2009)
TCS (Thiourea modified chitosan microspheres)	129.87	(Zhou et al., 2009)
Polystyrene supported 2,5 dimercapto-1,3,4-thiodiazole	6.44	(Ramesh et al., 2008)
2-Mercaptobenzothiazole-bonded silica gel	6.5	(Ramesh et al., 2008)
Crosslinked carboxymethyl chitosan hydrogels	1.16	(Ramesh et al., 2008)
lysine modified crosslinked chitosan	129.26	(Ramesh et al., 2008)
Glutaraldehyde crosslinked chitosan	300	(Ramesh et al., 2008)

From these results, it can be concluded that the synthesized ACF were able to adsorb platinum ions despite their low adsorption capacity. The following chapter will give a more detailed conclusion on the results obtained in this research.

4.5 REFERENCES

Abdallah, W., 2004. Production and Characterization of Activated Carbon from Sulphonated Styrene Divinylbenzene Copolymer (Thesis). Middle East Technical University, Ankara, Turkey.

Lenntech, 2003. AMBERLITE® XAD4 Industrial Grade Polymeric Adsorbent. [Online] p. 2 Available from: https://www.lenntech.com/Data-sheets/Amberlite-XAD4-L.pdf [Accessed: 20 October 2016]

Bhatia, G., Aggarwal, R.K., Punjabi, N., Bahl, O.P., 1997. Effect of sintering temperature on the characteristics of carbons based on mesocarbon microbeads. J. Mater. Sci. 32, 135–139.

Guo, J., Chong Lua, A., 1998. Characterization of chars pyrolyzed from oil palm stones for the preparation of activated carbons. J. Anal. Appl. Pyrolysis 46, 113–125.

Joshi, S., Pokharel, B.P., 2014. Preparation and Characterization of Activated Carbon from Lapsi (Choerospondias axillaris) Seed Stone by Chemical Activation with Potassium Hydroxide. J. Inst. Eng. 9, 79–88.

Khurshed, A.S., Bilal, A.T., 2016. Synthesis of carbon nanotubes by catalytic chemical vapour deposition:A review on carbon sources,catalysts and substrates. Mater. Sci. Semicond. Process. 1, 97–82.

Liu, W.-W., Aziz, A., Chai, S.-P., Mohamed, A.R., Tye, C.-T., 2011. The effect of carbon precursors (methane, benzene and camphor) on the quality of carbon nanotubes synthesised by the chemical vapour decomposition. Phys. E Low-Dimens. Syst. Nanostructures 43, 1535–1542.

Lowell, S., Shields, J.E., Thomas, M.A., Thommes, M., 2004. Characterization of Porous Solids and Powders: Surface Area, Pore Size and Density. Kluwer Academic Publishers, Netherlands.

Mavhungu, A., Mbaya, R.K.K., Moropeng, M.L., 2016. Recovery of Platinum and Palladium Ions from Aqueous Solution Using Grape Stalk Waste. Int. J. Chem. Eng. Appl. 4, 354–358.

Mubarak, N.M., Abdullah, E.C., Jayakumar, N.S., Sahu, J.N., 2014. An overview on methods for the production of carbon nanotubes. J. Ind. Eng. Chem. 20, 1186–1197.

Ramesh, A., Hasegawa, H., Sugimoto, W., Maki, T., Ueda, K., 2008. Adsorption of gold(III), platinum(IV) and palladium(II) onto glycine modified crosslinked chitosan resin. Bioresour. Technol. 99, 3801–3809.

Shah, K.A., Tali, B.A., 2015. Synthesis of carbon nanotubes by catalytic chemical vapour deposition: A review on carbon sources, catalysts and substrates. Mater. Sci. Semicond. Process. 41, 67–82.

Shukrullah, S., Mohamed, N.M., Shaharun, M.S., Naz, M.Y., 2016. Parametric study on vapor-solid growth mechanism of multiwalled carbon nanotubes. Mater. Chem. Phys. 176, 32 43.

Solomons, G.T.W., Fryhle, C.B., Snyder, 2011. Organic Chemistry, 10th ed. New Jersey, United States: John Wiley & Sons,

Zdravkov, B.D., Cermak, J.J., Sefara, M., Janku, J., 2007. Pore classification in the characterization of porous materials: A perspective. Cent. Eur. J. Chem. 5, 385–395.

Zhou, L., Liu, J., Liu, Z., 2009. Adsorption of platinum (IV) and palladium (II) from aqueous solution by thiourea-modified chitosan microspheres. J. Hazard. Mater. 172, 439-446.

5

CONCLUSION AND RECOMMENDATION

5.1 CONCLUSION

The aim of this research was to synthesize and characterize ACF and/or CNTs from IERs and subsequently use them for the adsorption of platinum ions from dilute solutions. Indeed both the proposed adsorbents were synthesized, characterized and only the ACF produced at 800 °C with 40 wt % NaOH was used for the adsorption as it yielded the greatest surface area.

5.1.1 Production of ACF

In this study, mesoporous ACFs (possessing pore sizes in the range of 2.29 to 20.06 nm) were produced from IER through chemical activation using NaOH as an activating agent. The study also showed that the activating temperature and concentration of the activating agent used both played a significant role in the production of ACFs and thus the surface area produced. When using a higher concentration, more pores are produced and there is also a higher probability of expanding the existing pores. In the case where the IER was activated with a high concentration of NaOH (i.e., 40 wt%), the carbonized residue yield was much higher than that for the samples

activated with lower concentrations of NaOH (i.e., 8 wt%). Therefore, it can be concluded that the ACF produced with 40 wt% NaOH was the most thermally stable product as it retained much of the weight at higher temperatures of 900 °C, during the analysis.

The results from the study showed that for a greater surface area to be achieved at higher temperatures, a relatively higher concentration of activating agent should be used. However, activation at extremely high temperatures such as 1000 °C resulted in fairly small surface area due to sintering/agglomeration of the finer particles at these conditions. Of the ACFs produced, the ACF produced at 800 °C with 40wt% NaOH solution possessed the greatest surface area of 217.41m^2/g, pore volume and pore size of 0.35cm^3/g and 6.72 nm, respectively, and had the greatest thermal stability when exposed to high temperatures of 900 °C.

5.1.2 Production of CNTs

For the production of CNTs from amberlite xad4 resin, the most prominent gas evolved from the resin pyrolysis was benzene at a temperature of 800 °C, for this reason, based on research, the choice in metal catalyst for CNT production was iron.

This study investigated the effect of catalyst support and carrier gas on the synthesis of the CNTs. The SWCNTs were only produced in the case where aluminium oxide was used as the iron metal catalyst support (Fe/Al_2O_3 and nitrogen as a carrier gas), the rest of the other material (Fe/MgO with nitrogen, $Fe/CaCO_3$ with nitrogen and Fe/MgO with argon) resulted in the production of MWCNTs. The use of argon as a carrier gas resulted in the greatest intensity of the G band from the Raman spectroscopy (1050.00 a.u.), thus signifying the greatest amount of amorphous carbon formed. Using argon resulted in the least I_D/I_G ratio obtained of 0.19, therefore the least defected material formed. The SEM images in the case when argon was used showed the most prominent fibril disk like structures (Figure 4.17).

However, the greatest surface area (70.54 m^2/g) was obtained from the CNTs synthesized using calcium carbonate as an iron catalyst support in which the greatest I_D /I_G ratio (0.59) was obtained, thus indicating a high degree of defected carbon. Therefore, it can be concluded that with greater defect, or rather greater intensity of the D band, a greater surface area can be formed. The use of iron supported on magnesium oxide with nitrogen as a carrier gas resulted in the least surface area (5.58 m^2/g) of the supported materials, however, when argon was employed as a carrier gas and MgO as a catalyst support the surface area was approximately 10 times more (52.85 m^2/g). It can therefore be concluded that argon as a carrier gas results in a greater surface area.

The TGA results confirm that any CNTs formed, were formed in very small quantities as the greatest amount of weight loss (4.78 wt %) was that of CNTs formed using calcium carbonate as a metal catalyst support (the case in which the most defective carbon was found). This suggests a greater need for a higher concentration of carbon source during the synthesis.

5.1.3 Adsorption of Platinum Ions

Adsorption experiments were conducted in order to assess the adsorption capacity and kinetics of the ACFs produced. As mentioned earlier, the choice in adsorbent was that of the adsorbent which yielded the greatest surface area, ACF produced at 800 °C and 40 wt % NaOH. It can be concluded that the synthesized ACF is able to adsorb platinum at low concentrations of 10 ppm. From observing the effect of contact time on the initial platinum concentrations, it can be concluded that the adsorption of platinum in dilute solutions (<50 ppm) is more rapid. In comparison to other adsorbents from literature, the ACF from IER has a greater adsorption rate yet a much smaller adsorption capacity. In addition to this, it can be concluded that physisorption took place, there were weak forces of attraction between the adsorbent and adsorbate as the adsorption process was easily reversed. Of the two adsorption isotherms

investigated (Langmuir and Freundlich), the Langmuir adsorption was a better fit of the data, and from this an adsorption capacity of 0.62 mg/g of the ACF, was found. From the Freundlich adsorption intensity parameter, it can be confirmed that the adsorption that took place was at favorable adsorption conditions as the 1/n value (0.24) lies between 0 and 1.

5.2 RECOMMENDATIONS

As mentioned above, this study has shown that it is possible to produce ACFs and CNTs from unused IER. Based on this, the main recommendation is to conduct further studies to assess the use of spent IER in the synthesis of these materials, in order to further determine if these materials would be a probable cost effective precursor which may contribute to the beneficiation of spent IERs, thus providing alternative means to dispose spent IER in an environmentally friendly manner. Other recommendations which would make this study more fruitful are listed below:

I. The use of the design of experiments (DOE) approach in the conduction of experiments would benefit in determining the precise and most optimum conditions of the synthesized materials, more specifically so the CNTs as they have many parameters affecting their synthesis. This would make for easier scale up of the synthesized CNTs and reproducibility of results, therefore, a comparison can be made between the synthesized ACF, CNTs and other adsorbents from literature.

II. For the synthesis of CNTs, the use of a double stage furnace can be used to have a better control over the resin pyrolysis temperatures and the synthesis temperatures.

III. The ACF can be functionalized in order to increase their affinity for the platinum ion uptake.

IV. It is also recommended to investigate the simultaneous production of ACF and CNTs. The gases emitted from the pyrolysis and carbonization of the ACF could be passed over the metal catalyst for the production of CNTs.

V. Another interesting investigation would be the use of the ACF synthesized from spent IER, which would then be used as a substrate for the growth of the CNTs, thus increasing the surface area, physical and chemical properties of the adsorbent.

VI. To use industrial solutions containing platinum ions in dilute solutions.

APPENDIX A: Activating agent solution preparation

A constant volume of 200 mL was used for all solutions.

A 40 wt % of NaOH contains 40 g of NaOH per 100 mL of solution (distilled water).

$\therefore m\ NaOH\ required\ = \frac{40}{100} \times 200 = 80\ g$

$\therefore 40g : 100\ mL = xg : 200mL$

Table A.2: Shows the mass used to create the various NaOH solutions with 200 mL of distilled water

NaOH WT %	Concentration (M)	Mass (g)
8,00	2,00	16,18
16,00	4,00	31,95
24,00	6,00	48,04
32,00	8,00	64,04
40,00	10,00	80,00

APPENDIX B: Catalyst Preparation

10g of each catalyst support ($CaCO_3$/ MgO/ Al_2O_3) was used to support 0.25 g of iron.

To confirm if there is enough Mg in 10g MgO to support 0.25g Fe:

$$Mass = n \times Mr \qquad \textit{Eqn B.1}$$

$$mass\ Mg : mass\ MgO$$

$$24\ g :\ 40\ g$$

$$1g\ Mg :\ 1.667g\ MgO$$

$$10g\ MgO = \frac{10}{1.667}\ g\ Mg$$

$$= 6\ g\ Mg$$

To confirm if there is enough Ca in 10g $CaCO_3$ to support 0.25g Fe:

$$mass\ Ca :\ mass\ CaCO_3$$

$$40.08g : 100.09g$$

$$1g\ Ca :\ 2.5g\ CaCO_3$$

$$10g\ CaCO_3 = \frac{10}{2.5}\ g\ Ca$$

$$= 4\ g\ Ca$$

To confirm if there is enough Al in 10g Al_2O_3 to support 0.25g Fe:

$$mass\ Al : mass\ Al_2O_3$$

$$26.98g \times 2mol\ :\ 1mol \times 101.96\ g$$

$$1g\ Al\ :\ 1.89\ g\ Al_2O_3$$

$$10g\ Al_2O_3 = \frac{10}{1.89}\ g\ Al$$

$$= 5.2\ g\ Al$$

Calculating the amount of iron salt that contains 0.25 g Fe:

$$mass\ Fe\ :\ mass\ of\ Fe\ (NO3)3.9H2O$$

$$n \times Mr \quad Fe\ :\ n \times Mr\ Fe\ (NO3)3.9H2O$$

$$1mol \times 55.845g/mol : 1mol \times 404g/mol$$

$$55.845g\ :\ 404g$$

APPENDIX

$1g\ Fe$: $7.234g\ Fe\ (NO3)3.9H2O$

$0.25\ g\ Fe\ = 7.234g\ \times\ 0.25$

$= 1.8\ g\ Fe\ (NO3)3.9H2O$

Volume of distilled water required to create a 10 % Fe solution:

$$n\ Fe\ = \frac{m}{Mr}$$

$$= \frac{0.25}{55.845}$$

$$= 0.00448$$

$$C\ = \frac{n}{V}$$

$$0.1\ = \frac{0.00448}{V}$$

$$V\ =\ 0.0447\ L$$

$$V\ =\ 44.7\ mL$$

APPENDIX C: Batch adsorption calculations

Calculations of the adsorption isotherm parameters

In order to determine the amount of metal adsorbed by the ACF, the following equation was used:

$$q_e = \frac{v(C_o - C_e)}{m} \qquad \textit{Eqn C.1}$$

Where:

$v = initial\ volume\ (L) = 0.03\ L$

$C_o = initial\ metal\ concentration\ in\ solution\ (mg/L)$

$C_e = metal\ concentration\ in\ solution\ at\ equilibrium\ (mg/L)$

$m = mass\ of\ the\ ACF\ (g)$

Example: for 100 ppm solution, using 0.112 g of ACF.

$$q_e = \frac{0.03(100 - 98)}{0.112} = 0.5357\ mg\ platinum/g\ ACF$$

Table C.1: Parameters used for Langmuir and Freundlich adsorption plots

Ppm	100	50	10
ACF (g)	0,112	0,107	0,112
C_e (mg/L)	98,000	49,000	9,000
q_e (mg/g)	0,536	0,280	0,268
C_e/ q_e	182,933	174,767	33,600
ln C_e	4,585	3,892	2,197
ln q_e	-0,624	-1,272	-1,317

APPENDIX C

Calculations for the Langmuir adsorption isotherms parameters

As previously mentioned, the Langmuir adsorption isotherm can be represented by the following equation:

$$\frac{C_e}{q_e} = \frac{1}{q_m K_L} + \frac{C_e}{q_m} \qquad \textit{Eqn C.2}$$

Where $\frac{1}{q_m}$ is the gradient and $\frac{\mathbf{1}}{\boldsymbol{q_m K_L}}$ is the y-intercept**.** From this the value of q_m was found, then that of $\boldsymbol{K_L}$

The Langmuir adsorption isotherm equation found was:

$$y = 1.622x - 46.089 \qquad \textit{Eqn C.3}$$

From the equation, $\frac{1}{\mathrm{q_m}} = 1.622$

$$\therefore \mathrm{q_m} = \frac{1}{1.622} = 0.617\ mg/g$$

$$\frac{1}{q_m K_L} = y - intercept = -46.089$$

$$\therefore K_L = \frac{1}{q_m \times y - intercept} = \frac{1}{0.617 \times -46.089} = 0.035$$

Table C.2: The Langmuir adsorption isotherms parameters

y-intercept	46.089
$\mathbf{1/q_m}$	1.622
$\mathbf{q_m}$ **(mg/g)**	0.617
$\boldsymbol{K_L}$	0.035
$\mathbf{R^2}$	0.742

Calculations for the Freundlich adsorption isotherms parameters

As previously mentioned, the Freundlich adsorption isotherm can be represented by the following equation:

$$Ln\ q_e = Ln\ K_f + \frac{1}{n} Ln\ C_e \qquad \textit{Eqn C.4}$$

Where $\frac{1}{n}$ is the gradient and $\boldsymbol{Ln\ K_f}$ is the y-intercept**.** From this the value of n was found, then that of K_f**.**

The Freundlich adsorption isotherm equation for the 100 ppm solution:

$y = 0.241x - 1.928$ *Eqn C.5*

From the equation, $\frac{1}{\mathrm{n}} = 0.241$

$\therefore n = \frac{1}{0.241} = 4.151$

$\ln K_f = y - intercept = -1.928$

$\therefore\ K_f = e^{-1.928} = 0.145$

Table C.3: The Freundlich adsorption isotherms parameters

1/n	0.241
n	4.151
ln K_f	-1.928
K_f	0.145
R^2	0.583